

IDENTIFICATION OF NOVEL INTERACTING PROTEINS OF  
FOUR AND A HALF LIM DOMAINS PROTEIN 1 FROM HUMAN  
EMBRYONIC KIDNEY 293 CELLS

By

Thiruchelvi Shathasivam

A thesis submitted in conformity with the requirements for the degree of Masters of Science  
Graduated Department of Physiology  
University of Toronto

© Copyright by Thiruchelvi Shathasivam (2009)



Library and Archives  
Canada

Published Heritage  
Branch

395 Wellington Street  
Ottawa ON K1A 0N4  
Canada

Bibliothèque et  
Archives Canada

Direction du  
Patrimoine de l'édition

395, rue Wellington  
Ottawa ON K1A 0N4  
Canada

*Your file Votre référence*  
ISBN: 978-0-494-59584-8  
*Our file Notre référence*  
ISBN: 978-0-494-59584-8

#### NOTICE:

The author has granted a non-exclusive license allowing Library and Archives Canada to reproduce, publish, archive, preserve, conserve, communicate to the public by telecommunication or on the Internet, loan, distribute and sell theses worldwide, for commercial or non-commercial purposes, in microform, paper, electronic and/or any other formats.

The author retains copyright ownership and moral rights in this thesis. Neither the thesis nor substantial extracts from it may be printed or otherwise reproduced without the author's permission.

#### AVIS:

L'auteur a accordé une licence non exclusive permettant à la Bibliothèque et Archives Canada de reproduire, publier, archiver, sauvegarder, conserver, transmettre au public par télécommunication ou par l'Internet, prêter, distribuer et vendre des thèses partout dans le monde, à des fins commerciales ou autres, sur support microforme, papier, électronique et/ou autres formats.

L'auteur conserve la propriété du droit d'auteur et des droits moraux qui protègent cette thèse. Ni la thèse ni des extraits substantiels de celle-ci ne doivent être imprimés ou autrement reproduits sans son autorisation.

---

In compliance with the Canadian Privacy Act some supporting forms may have been removed from this thesis.

While these forms may be included in the document page count, their removal does not represent any loss of content from the thesis.

Conformément à la loi canadienne sur la protection de la vie privée, quelques formulaires secondaires ont été enlevés de cette thèse.

Bien que ces formulaires aient inclus dans la pagination, il n'y aura aucun contenu manquant.

  
**Canada**

# Identification of Novel Interacting Proteins of Four and a Half LIM Domains Protein 1 from Human Embryonic Kidney 293 Cells

Thiruchelvi Shathasivam

Masters of Science

Graduated Department of Physiology

University of Toronto

2009

## ABSTRACT

Four and a half LIM domains protein 1 (FHL1), consisting of 4.5 protein interaction mediating LIM domains, is a predominantly skeletal muscle protein that has consistently been upregulated in a variety of cardiovascular diseases. Since proteins mediate their functions in conjunction with other proteins, it was considered that delineation of interactions would provide insight into FHL1's regulation and regulatory functions. We performed tandem affinity purification (TAP) from human embryonic kidney 293 (HEK-293) cells to purify tagged FHL1 and interacting proteins. Samples were analyzed using gel-free liquid chromatography mass spectrometry (LC-MS). 61 high confidence potential interactors were identified from multiple experiments. Validation of interactions was then performed by co-immunoprecipitation (co-IP) or streptavidin bead pull down, and supported by immunofluorescent colocalization studies. FHL1 interactions could thus be supported for four novel candidates: non-muscle  $\alpha$ -actinin 1 (ACTN1), PDZ and LIM domain protein 1 (PDLIM1), cytoplasmic gelsolin (GSN), and ryanodine receptor 1 (RYR1).

## **ACKNOWLEDGMENTS**

I would like to express my sincere gratitude to those who have made this work possible. I would like to thank first and foremost my supervisor, Dr. Anthony Gramolini, for his guidance and valuable insight. I have learned so much from you during my studies. Many thanks as well to Dr. Parveen Sharma for her continued support and patience. Thank you for teaching me the technical and biochemical skills I needed to pursue this project, and for letting me bounce endless ideas off of you. Additionally, I would like to acknowledge the support of Dr. Thomas Kislinger, for his mass spectrometry expertise and participation as a committee member. To my labmates and friends, thank you for your support and encouragement, for keeping my spirits high. Special thanks to my parents and sisters for their love and support, especially nearing the conclusion of my studies. Thank you for believing in me.

Permission was granted from Molecular and Cellular Proteomics for the use of copyrighted images in Figure 6.

# TABLE OF CONTENTS

<b>ABSTRACT</b>	<b>II</b>
<b>ACKNOWLEDGMENTS</b>	<b>III</b>
<b>LIST OF TABLES</b>	<b>VII</b>
<b>LIST OF FIGURES</b>	<b>VIII</b>
<b>LIST OF COMMON ABBREVIATIONS</b>	<b>IX</b>
<b>CHAPTER ONE: INTRODUCTION</b>	<b>1</b>
<b>I. FOUR AND A HALF LIM DOMAINS PROTEIN 1</b>	<b>1</b>
I.A The LIM Domain	1
I.B FHL Family of Proteins	2
I.C FHL1 Isoforms	6
I.D FHL1 Functions	10
I.E FHL1 and Skeletal Muscle Myopathies	14
<b>II. PROTEIN-PROTEIN INTERACTIONS</b>	<b>16</b>
II.A General Introduction	16
II.B Yeast Two-Hybrid	19
II.C Protein Array	19
II.D Tandem Affinity Purification	20
<b>III. HEART FAILURE</b>	<b>21</b>
III.A General Introduction	21
III.B Pathophysiology of Heart Failure	21
<b>IV. PHOSPHOLAMBAN</b>	<b>24</b>
IV.A Overview of Phospholamban	24
IV.B Mutations in Human Phospholamban and Cardiomyopathy	25
<b>V. STATEMENT OF INTENT</b>	<b>28</b>
<b>CHAPTER TWO: MATERIALS AND METHODS</b>	<b>29</b>
<b>I. DUAL AFFINITY TAGGING OF FHL1</b>	<b>29</b>
I.A Preparation of Origene Clones	29
I.B Insertion into TOPO Vectors	30
I.C Insertion into pCTAP Vectors	32
<b>II. TANDEM AFFINITY PURIFICATION</b>	<b>34</b>
II.A Tissue Culturing	34
II.B Tandem Affinity Purification	34
<b>III. SDS-POLYACRYLAMIDE GEL ANALYSIS</b>	<b>35</b>
III.A Polyacrylamide Gel Electrophoresis	36
III.B Coomassie Blue Staining of Proteins	36

III.C Immunoblot Detection of Proteins	36
III.D Silver Staining of Proteins	37
<b>IV. MASS SPECTROMETRY ANALYSIS</b>	<b>37</b>
IV.A Preparation of Samples	37
IV.B Mass Spectrometry	39
<b>V. IN VITRO FHL1 PULL DOWN ASSAYS FROM MICE VENTRICULAR LYSATES</b>	<b>40</b>
V.A Preparation of FHL1 Containing Protein Lysate from HEK-293 Cells	40
V.B Immobilization of FHL1 onto TALON® Metal Affinity Resin	40
V.C Preparation of Protein Lysate from Mice Ventricular Tissue	40
V.D Formation of FHL1 Interactions <i>In Vitro</i>	41
<b>VI. ALTERNATIVE DUAL TAGGING OF BAIT cDNAS</b>	<b>41</b>
VI.A Amplification of Destination Vector	41
VI.B Amplification of ORFeome Clones	42
VI.C ORFeome Cloning	42
<b>VII. IN-VIVO CO-IMMUNOPRECIPITATION FROM HEK-293 CELLS AND Tg-PLN R9C MICE</b>	<b>43</b>
VII.A Preparation of Protein Extracts from HEK-293 Cells and Tg-PLN R9C Mice	43
VII.B Co-Immunoprecipitation	43
<b>VIII. CO-IMMUNOFLUORESCENT SUBCELLULAR CO-LOCALIZATION ANALYSIS</b>	<b>44</b>
VIII.A Slide Preparations of Fixed Cultured Cells	44
VIII.B Slide Preparations of Fixed Isolated Skeletal Soleus Muscle Fibers	45
VIII.C Co-Immunofluorescent Staining of Fixed Tissue	45
<b>CHAPTER THREE: RESULTS</b>	<b>47</b>
<b>I. PURIFICATION OF FHL1 CONTAINING PROTEIN COMPLEXES</b>	<b>47</b>
I.A Generation of FHL1-SBP/CBP Expression Constructs	47
I.B Expression and Purification of Tagged Bait and Co-Purification of Potential Interactors	48
I.C Co-Purification of Additional Proteins with FHL1	49
<b>II. IDENTIFICATION OF POTENTIAL FHL1 INTERACTING PROTEINS</b>	<b>50</b>
II.A Proteins Identified from FHL1 Purifications by Mass Spectrometry	50
II.B Filtering and Comparing Subsets of Proteins Identified from Purifications	51
II.C Prioritization of Potential Interactors	56
II.D Screening for Known FHL1 Interacting Proteins	56
<b>III. CHARACTERIZATION OF THE 61 POTENTIAL FHL1 INTERACTING PROTEINS</b>	<b>56</b>
III.A Analysis of Overrepresented GO-Terms	56
III.B Identification of Known Interactions	58
<b>IV. ASSOCIATION WITH DISEASE</b>	<b>60</b>
IV.A Lysate Differences	60
IV.B Microarray Study	62
<b>V. VALIDATION OF INTERACTIONS</b>	<b>65</b>
V.A In HEK-293 Cells	65
V.B In Diseased Hearts	69
<b>VI. SUBCELLULAR LOCALIZATION</b>	<b>73</b>
VI.A HEK-293 Cells	73
VI.B Skeletal Muscle	78

<b>CHAPTER FOUR: CONCLUSIONS</b>	<b>83</b>
<b>CHAPTER FIVE: DISCUSSION</b>	<b>84</b>
<b>I. PURIFYING PROTEIN COMPLEXES</b>	<b>84</b>
<b>II. ASSOCIATION WITH HEART FAILURE</b>	<b>87</b>
II.A Validity of Studying the Tg-PLN R9C Model	87
II.B Reliability of the Profiling Studies of the Tg-PLN R9C Model	87
II.C Four and a half LIM domain protein 1	88
II.D $\alpha$ -Actinin-1	89
II.E Gelsolin	89
II.F PDZ-LIM Protein 1	90
II.G Ryanodine Receptor 1	90
<b>III. INTERACTIONS WITH FHL1</b>	<b>90</b>
III.A $\alpha$ -Actinin-1	90
III.B Gelsolin	91
III.C PDZ-LIM Protein 1	92
III.D Ryanodine Receptor 1	93
<b>CHAPTER SIX: LIMITATIONS</b>	<b>95</b>
<b>CHAPTER SEVEN: FUTURE DIRECTIONS</b>	<b>96</b>
<b>REFERENCES</b>	<b>97</b>

## LIST OF TABLES

Table 1. FHL1 Isoform Specific Interactions .....	17
Table 2. Known FHL1 Interactions .....	18
Table 3. Putative FHL1 Interactions.....	19
Table 4. List of Primers Used For Cloning.....	31
Table 5. 61 Potential FHL1 Interactors Found in Repetitive Experiments.....	55

## LIST OF FIGURES

Figure 1. General Secondary Structure of Four and a Half LIM Domain Proteins .....	1
Figure 2. Domain Features of FHL1 and Spliced Variants .....	6
Figure 3. FHL1 and Notch Signaling.....	9
Figure 4. FHL1 and Anchorage Independence .....	13
Figure 5. FHL1 Inhibition of Tumour Cell Growth by Interaction with Smad Proteins .....	14
Figure 6. Significantly upregulated proteins in PLN R9C mice .....	27
Figure 7. Tandem Affinity Purification and Mass Spectrometry .....	46
Figure 8. Generation of FHL1-SBP/CBP Expression Constructs .....	48
Figure 9. Tandem Affinity Purification of SBP/CBP Tagged Proteins from HEK-293 Cells ...	49
Figure 10. Recovering Interacting Proteins with Purification of FHL1-SBP/CBP .....	50
Figure 11. Mass Spectrometry Detection of FHL1 (Isoform 1) .....	52
Figure 12. Filtering and Comparing Mass Spectrometry Purification Data .....	53
Figure 13. Proteins Identified by Mass Spectrometry from FHL1-SBP/CBP Purifications.....	54
Figure 14. Analysis of Overrepresented Molecular Functions Found Within the 61 Potential FHL1 Interactors .....	57
Figure 15. Analysis of Overrepresented Biological Processes Found Within the 61 Potential FHL1 Interactors .....	58
Figure 16. Known Interactions Amongst FHL1 and the 61 Potential Interactors .....	59
Figure 17. Differences in Pull-Down Assays from Wild Type and PLN R9C mice .....	61
Figure 18. Correlations in mRNA Transcript Levels of FHL1 and Potential Interactors in Tg-PLN R9C Mice .....	63
Figure 19. Co-immunoprecipitation Validation of FHL1 Interactions from HEK-293 Cells ....	67
Figure 20. Mass Spectrometry Detection of Ryanodine Receptor 1 .....	68
Figure 21. Validation of Interactions by Streptavidin Affinity Purification from HEK-293 Cells .....	69
Figure 22. Co-immunoprecipitation Validation of FHL1 Interactions from PLN R9C Mice Ventricles .....	70
Figure 23. Mass Spectrometry Detection of Gelsolin.....	71
Figure 24. Mass Spectrometry Detection of Alpha Actinin 1 (Isoform 1) .....	72
Figure 25. Subcellular Co-localization of FHL1 and PDLIM1 in HEK-293 Cells .....	74
Figure 26. Subcellular Co-localization of FHL1 and GSN in HEK-293 Cells.....	75
Figure 27. Subcellular Co-localization of FHL1 and ACTN1 in HEK-293 Cells.....	76
Figure 28. Subcellular Co-localization of FHL1 and RYR1 in HEK-293 Cells .....	77
Figure 29. Subcellular Co-localization of FHL1 and GSN in Skeletal Muscle.....	79
Figure 30. Subcellular Co-localization of FHL1 and ACTN1 in Skeletal Muscle.....	80
Figure 31. Subcellular Co-localization of FHL1 and RYR1 in Skeletal Muscle.....	81
Figure 32. Subcellular Co-localization of FHL1 and PDLIM1 in C2C12 Myoblasts.....	82

## LIST OF COMMON ABBREVIATIONS

ACT	activator of CREM in testis
ACTN1	$\alpha$ -actinin 1
ANF	atrial natriuretic factor
BMP	bone morphogenetic protein
CBP	calmodulin binding peptide
co-IP	co-immunoprecipitation
CREM	cAMP-responsive element modulator
CRP	cysteine-rich proteins
DCM	dilated cardiomyopathy
DPYSL3	dihydropyrimidinase-like 3
ERK2	extracellular signal-regulated kinase 2
ET-1	endothelin-1
FHL1	four and a half LIM domains protein 1
GOFFA	Gene Ontology for Functional Analysis
GSN	cytoplasmic gelsolin
Hes	hairy enhancer of split
His	histidine
HPC2	polycomb 2 homolog
LC-MS	liquid chromatography mass spectrometry
MyBP-C	myosin binding protein C
NFATc1	nuclear factor of activated T cells cytoplasmic component 1
NIC	notch intracellular domain
NLS	nuclear localization signal
PcG	polycomp group
PDLIM1	PDZ and LIM domain protein 1
PIAS1	protein inhibitor of activated STAT 1
PLN	phospholamban
PLN R9C	Arg-9 to Cys mutation in PLN gene
RBP1	cellular retinol-binding protein 1
RBP-J	J-recombination signal protein
RYR	ryanodine receptor
RYR1	ryanodine receptor 1
SBP	streptavidin binding peptide
SMAD	Sma- and Mad-related protein
SR	sarcoplasmic reticulum
STAT1	signal transducer and activator of transcription-1
SUMO	small ubiquitin-related modifier
TAP	tandem affinity purification
TGF	transforming growth factor
Tg-PLN R9C	transgenic PLN R9C murine model
TNF- $\alpha$	tumor necrosis factor- $\alpha$
Y2H	yeast-two hybrid

# CHAPTER ONE: INTRODUCTION

## I. FOUR AND A HALF LIM DOMAINS PROTEIN 1

### I.A The LIM Domain

**I.A.1 Structure:** FHL1 belongs to the family of FHL proteins characterized by the presence of four and a half LIM domains [1, 2]. The acronym LIM was derived from the first letter of three homeodomain transcription factors from which the domain was first discovered: 1) Lin-11 promotes asymmetric cell divisions in *Caenorhabditis elegans* during vulval development and regulates vulval morphogenesis [3, 4]; 2) Isl-1 participates in murine motor neuron generation and development [5]; and 3) Mec-3 regulates the differentiation of mechanosensory neurons in *C. elegans* [6].

The LIM domain is a highly conserved double zinc-finger motif separated by two amino acids, and composed of approximately 55 amino acids with 8 highly conserved residues. The consensus amino acid sequence of LIM domains has been defined as Cys-X<sub>2</sub>-Cys-X<sub>16-23</sub>-His-X<sub>2</sub>-Cys-X<sub>2</sub>-Cys-X<sub>2</sub>-Cys-X<sub>16-21</sub>-Cys-X<sub>2</sub>-Cys/His/Asp, where X represents any amino acid [7-9]. The Cys and His residues coordinate the binding of two Zn<sup>2+</sup> for every LIM domain, contributing to the stabilization of the secondary and tertiary structure of the protein (Figure 1) [1, 9].

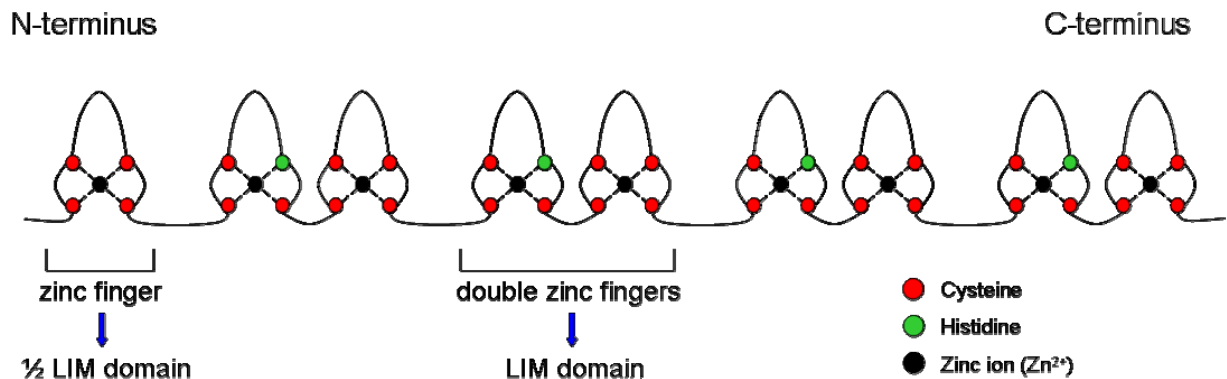


**Figure 1. General Secondary Structure of Four and a Half LIM Domain Proteins**

Schematic of the secondary structural features common to all members of the FHL family of proteins. There are four complete LIM domains, each with the capacity to bind two Zn<sup>2+</sup> molecules. At the N-terminus of the protein exists a single zinc finger domain, equivalent to the C-terminal half of a LIM domain.

**I.A.2 Binding Functions:** The LIM domains have been proposed to function as modular protein-protein binding interfaces upon which the coordinated assembly of multimeric protein complexes occurs [9, 10]. These scaffold proteins are capable of interacting with other LIM domain containing proteins, forming homo- or heterodimers [11]. Furthermore, LIM domains often associate with tyrosine-containing motifs, PDZ domains, ankyrin repeats, and helix-loop-helix domains [11]. Nonetheless, multiple efforts to identify conserved preferences for discrete binding sequences have not been successful [9]. Multidimensional NMR spectroscopy and x-ray crystallography structural analysis studies have revealed a resemblance between the C-terminal zinc finger of LIM domains and the DNA-binding zinc finger of the GATA and steroid-hormone-receptor classes of transcription factors [8, 9]. However, there is no evidence to date that LIM domains directly bind DNA [9, 10].

**I.A.3 Biological Processes:** The presence of a LIM domain was recently recognized as a potential hallmark of proteins associating with both the actin cytoskeleton and transcriptional machinery [9, 12]. For instance, the cysteine-rich proteins (CRP) 1 and 2, each containing two LIM domains, interact with zyxin and alpha-actinin in the cytoplasm and participate in cytoskeletal remodeling [13, 14]. In addition, they translocate to the nucleus and act as bridging molecules interacting with both serum response factors (SRF) and GATA proteins. In smooth muscle cells, this tetrameric complex activates gene targets and facilitates differentiation [15]. However, the physiological processes responsible for regulating the shuttling of LIM domain proteins between the cytoplasm and nucleus have yet to be elucidated [10].

## **I.B FHL Family of Proteins**

**I.B.1 Structure:** In humans, the FHL LIM-only protein family is composed of four members, designated FHL1, FHL2, FHL3, and activator of CREM in testis (ACT), also referred to as FHL5 [1, 2, 16, 17]. The FHL family of proteins is defined by a particular secondary structural arrangement of LIM domains (Figure 1). All members are comprised of four complete LIM domains arranged in tandem and separated by eight amino acid residues. In addition, there is an N-terminal single zinc finger domain with a consensus sequence equivalent to the C-terminal half of a LIM-domain motif, and hence the name four and a half LIM domain proteins [17].

**I.B.2 Tissue Expression Patterns:** In general, FHL proteins are expressed primarily in striated muscle, with the exception of ACT. Though numerous groups have undertaken to

characterize the tissue distribution for different FHL proteins, and aside from their agreement on the prominence in striated muscle or testis, the findings have not been consistent [1, 2, 11, 17-19]. The discrepancies in the observed expressions may be attributable to the different detection methods or organisms used. In addition, variations in the gender or age of the subjects tissues were obtained from could have contributed to the inconsistencies. Fimia and colleagues performed RNA analysis for each FHL family member from various tissues harvested from mice [20]. FHL2 was most abundant in the heart, with low expression detected from the ovary and adrenal gland. In contrast, FHL3 was exclusively expressed in skeletal muscle, which correlated well with previous findings. FHL1 was the only member to demonstrate a broader range of expression. Though predominantly a skeletal muscle protein, FHL1 transcripts were also found at high levels in the heart, ovary, kidney, and lung. Lower expressions were detected from the testis and pituitary gland [20].

Unlike the other FHL proteins, ACT is a testis specific protein, expressed in spermatids of adult testis [17, 20]. In mouse, there exists another FHL family member, FHL4, which is also exclusively expressed in the testis, though not as abundantly as ACT [20, 21]. FHL4 mRNA detection was restricted to cells of the seminiferous tubules associated with spermatogenesis [20, 21]. To date, however, the human equivalent of murine FHL4 has not been identified, nor has translation of the murine FHL4 mRNA been validated [21].

### **I.B.3 Functions:**

I.B.3.i *Four and a Half LIM Domains Protein 2*: The FHL2 protein is the best studied member of the FHL family of proteins. Over 50 different protein interactions have been identified to date, belonging to a broad spectrum of functional categories, including receptors, signal transducers, structural proteins, splicing factors, metabolic enzymes, transcription factors and cofactors, and DNA replication and repair enzymes [18]. In accordance with this, FHL2 has been implicated in a number of physiological processes, including regulation of signal transduction, gene expression, cytoskeleton modulation, cell adhesion, survival and mobility [22].

In the embryonic heart, FHL2 was enriched in the ventricular septum and regions adjacent to the atrio-ventricular ring [23]. Expression was also detected in the developing vasculature [23, 24]. Though the expression patterns are suggestive of a role in the development of the cardiac septa and circulatory system, *fhl2* null mice were viable and displayed no detectable abnormalities in the cardiac phenotype [23-25]. However, an exaggerated

hypertrophic response was elicited from *fhl2* null mice, compared to wild-type mice, with sustained  $\beta$ -adrenergic stimulation [24]. This may, in part, be attributable to greater extracellular signal-regulated kinase 2 (ERK2) activity, a signal transducer of the hypertrophic growth response which can normally be antagonized by FHL2 [26]. Furthermore, FHL2 may also be involved in repolarization of cardiac cells via its interaction with the  $\beta$ -subunit minK of voltage-gated  $K^+$  channels encoding the delayed rectifier current  $I_{Ks}$  [27]. FHL2 may mediate a structural connection between minK and the cytoskeleton [27]. Similarly, FHL2 is considered to function as an adaptor molecule coupling metabolic enzymes to titin, such as MM-creatine kinase, adenylate cyclase, and phosphofructokinase [28]. Titin is a protein vital to the assembly of the sarcomere, force transmission, and maintenance of resting tension [29]. Thus, FHL2 aids in recruiting metabolic enzymes to a site of high energy consumption [28, 29].

Within the cell, FHL2 has been identified in both the cytoplasm, in association with the cytoskeleton, and the nucleus [18]. Consistent with its presence in the nucleus, FHL2 also functions as a transcriptional cofactor for various transcription factors. For instance, in pulmonary artery smooth muscle cells FHL2 translocates into the nucleus upon stimulation with bone morphogenetic protein (BMP) 4 and inhibits transcriptional activation of vascular smooth muscle cell specific genes mediated by the BMP signaling pathway [30]. FHL2 directly binds SRF, and whilst not inhibiting the recruitment of SRF's cofactor myocardin-related transcription factor A (MRTF-A), it does antagonize the recruitment of components of the SWI/SNF chromatin remodeling complex essential for transcriptional activation, such as Brg1 and RNA polymerase II [30, 31]. In contrast, FHL2 directly interacts with myocardin, and MRTF-A, in smooth muscle cells and enhances their transactivation of smooth muscle cell specific promoters. FHL2 possibly confers protection from proteasome-mediated degradation, thus stabilizing myocardin and MRTF-A [32]. Thus, FHL2 is a multi-functional protein involved in broad array of activities in both the cytoplasmic and nuclear compartments of the cell.

**I.B.3.ii *Four and a Half LIM Domains Protein 3*:** The predominantly skeletal muscle protein FHL3 is differentially expressed during myogenesis, with alterations in subcellular localization [2, 33]. These findings were suggestive of an involvement in muscle cell differentiation and development. In C2C12 myoblasts, FHL3 is expressed in the nucleus and cytoplasm, specifically at focal adhesion sites and actin stress fibers [33, 34]. In myotubes, however, FHL3 is absent from the nucleus [33]. When FHL3 was overexpressed in myoblasts though, a more diffuse cytoplasmic expression was observed, in parallel with a diffuse cytoplasmic phalloidin

staining [34]. Disassembly of the actin cytoskeleton in myoblasts was mediated by inhibition of  $\alpha$ -actinin's actin crosslinking function [34]. In accordance with this, FHL3 expression was upregulated in C2C12 cells migrating into a wound edge. Rapid restructuring of the actin stress fibers is characteristic of migrating cells [34]. In addition, overexpression of FHL3 retards C2C12 differentiation, where as siRNA mediated knockdown accelerates differentiation [35].

Consistent with its nuclear localization, and like FHL2, FHL3 participates in both activation and repression of different transcription factors. For instance, Sox15 recruits FHL3 to synergistically coactivate the *forkhead/winged helix 1* (Foxk1) gene, which is expressed in undifferentiated myogenic progenitor cells (MPCs) residing in adult skeletal muscle [36]. This interaction and subsequent regulation of Foxk1 could induce quiescent MPCs to reenter the cell cycle and regenerate injured skeletal muscle [36]. In contrast, FHL3 interacts with MyoD to suppress MyoD-dependent transcription, such as the myogenin gene, thereby negatively regulating myotube formation [35]. Since FHL3 behaves as both a co-activator and co-repressor, it likely functions as an adaptor molecule important in the assembly and stabilization of large transcriptional complexes [37, 38]. Thus, the findings from both the cytoplasmic and nuclear regions support a role for FHL3 in differentiation and development.

**I.B.3.iii Activator of CREM in Testis:** The most recently identified member of the FHL family, ACT is expressed exclusively in the testis [20, 39]. Within the testis, it is detected specifically within the nucleus of spermatids, where it colocalizes with cAMP-responsive element modulator (CREM) [39]. As interacting proteins, ACT and CREM display coordinated expression during testis development [20, 39]. Furthermore, ACT is capable of transactivating CREM-mediated transcription [39]. Coactivation by ACT is also independent of CREB binding protein and TBP-associated factor 130 involvements and phosphorylation of Ser117 in CREM. These are all components of the classical view of CREM-mediated transcription. Thus, ACT provides an alternative pathway, functioning in a signaling-independent manner [40, 41]. The transactivation function of ACT is dependent on the specific arrangement of the LIM domains, as determined by 1) the assessment of the transactivation properties of ACT with deletion of various combinations of LIM domains, and 2) the differential activation potentials of the various FHL proteins [20]. Thus, ACT possesses a more defined expression pattern and function compared to the other FHL proteins.

## I.C FHL1 Isoforms

**I.C.1 Structure:** Although FHL1 is classified as a LIM-only protein, spliced variants have been identified containing additional domains resulting in differential localization patterns and functions. Similar to full-length FHL1 (isoform FHL1A), two additional isoforms (FHL1C and FHL1B) were initially identified from murine studies and referred to as KyoT2 and KyoT3 respectively (Figure 2) [11, 42-45].

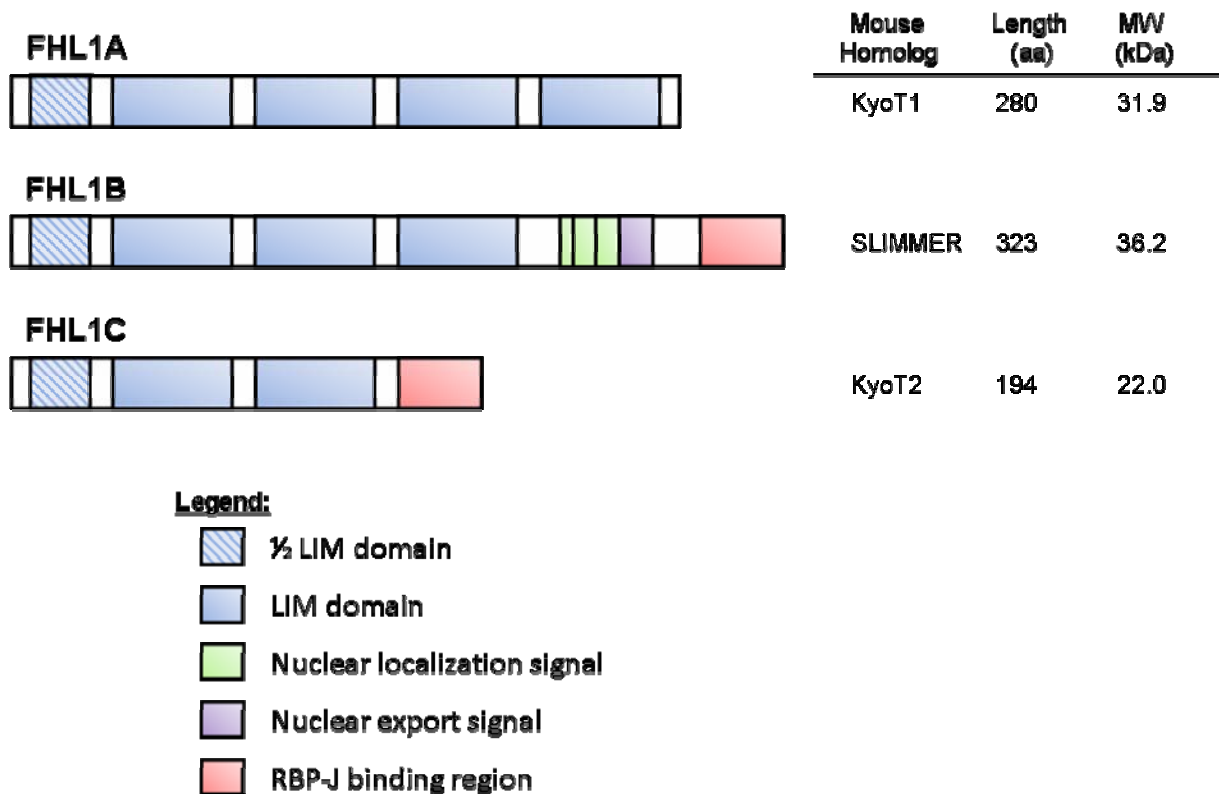


**Figure 2. Domain Features of FHL1 and Spliced Variants**

Schematic representation of the domain structures present in each of the three isoforms of FHL1.

I.C.1.i *FHL1C/KyoT2*: FHL1C (KyoT2) is the shorter isoform of FHL1, encoding for a 22.0 kDa protein sharing the N-terminal two and a half LIM domains with FHL1. However, alternative splicing of exon 5 results in a frameshift in translation, producing a 27 amino acid putative J-recombination signal protein (RBP-J) binding region at the C-terminus [42, 44]. In addition, similar to FHL1, within the cell the isoform is distributed diffusely in the cytoplasm and nucleus, as determined from GFP-fusion protein expression from C2C12 myoblasts and HepG2 hepatocells [44]. Since FHL1C lacks any typical nuclear localization signal, its translocation to the nucleus may be mediated by particular protein modifications and/or protein interactions [44].

Northern blot and RT-PCR tissue distribution analysis revealed FHL1C is expressed specifically in testis, skeletal muscle, and the heart, albeit at lower levels than FHL1 [44]. In the human heart, FHL1C transcript expression was more precisely localized in the left and right ventricles, with lower expression detected in the aorta and left atrium [44]. In contrast, murine KyoT2 exhibits a broader distribution, with transcripts expressed at relatively higher levels in skeletal muscle, brain, lung, kidney, and genital organs with lower detection from the thymus, lymph nodes, and liver [42, 44]. The disparities in tissue distribution between FHL1C and KyoT2 could be attributable to functional differences in human and mouse or due to the age and sex of subjects used in the studies.

I.C.1.ii FHL1B/SLIMMER/KyoT3: Although FHL1B (KyoT3) is the larger isoform, encoding for a 34 kDa protein, it contains only the first three and a half LIM domains found in FHL1 [11]. The occurrence of a 200 bp insertion at position 741 results in the generation of three tandem putative bipartite nuclear localization signal (NLS) motifs, followed by a nuclear export sequence and the identical putative RBP-J binding region found in FHL1C [11, 43]. Unlike FHL1C however, FHL1B is predominantly distributed in the nucleus of C2C12 myoblasts and HepG2 hepatocells, mainly attributable to the first bipartite NLS [11, 43]. Interestingly, in differentiated myotubes, it is localized exclusively in the cytosol, similar to FHL1 [11]. Northern blot and RT-PCR tissue distribution analysis revealed relatively greater abundance of FHL1B in skeletal muscle compared to heart, colon, prostate, and small intestine. In addition to these tissues, murine KyoT3 mRNA was also detected in spleen, thymus, testis, ovary, brain, placenta, lung, liver, kidney, and pancreatic tissue [11, 43].

**I.C.2 Notch Signaling:** The Notch signaling pathway is an evolutionarily conserved pathway participating in the control of a broad range of developmental processes, including cell fate determination, differentiation, proliferation, and apoptosis through local cell-cell interaction [46]. Mammals express four members of the Notch family of receptors, all designated a type 1 transmembrane receptor with a total of five ligands. The ligands too are single-pass transmembrane proteins, categorized into two families (delta-like 1,3,4 and jagged 1,2), that allow for Notch signaling between neighbouring cells [46, 47]. Direct interaction of the ligand with the Notch receptor triggers proteolytic cleavage of the Notch receptor by  $\gamma$ -secretase-like protease, releasing the Notch intracellular domain (NIC) into the cytoplasm. NIC translocates into the nucleus and serves as a transcriptional activator of the DNA binding protein RBP-J, in

combination with other co-activators [46, 47]. In the absence of transcriptional activators, RBP-J is capable of suppressing transcription of Notch target genes by binding several co-repressor proteins (Figure 3) [46, 47]. Numerous Notch transcriptional targets have been described, but the hairy enhancer of split (Hes) and Hes-related families of transcriptional regulators are some of the best defined. These targets function as transcriptional repressors mediating downstream responses of Notch signaling [46, 47].

**I.C.3 KyoT2/3 and Notch Signaling:** KyoT2 was discovered during yeast two hybrid (Y2H) screenings of mouse embryonic and HeLa cell cDNA libraries using RBP-J as the bait, and the interaction was subsequently verified in mammalian cell systems [42]. Since their binding regions on RBP-J overlap, KyoT2 competes with NIC for binding [42]. In contrast to NIC, KyoT2 interacts with RBP-J to suppress transcription, in a concentration-dependent manner [42, 47]. Furthermore, electrophoretic mobility shift assays revealed that while KyoT2 is capable of interacting with the RBP-J-DNA complex, it mostly displaces RBP-J from DNA, thus contributing to its repressional activities [42]. Subsequently, KyoT2 was found to interact with RING1 via its LIM domains [47]. RING1 belongs to the polycomb group (PcG) proteins which function as transcription suppressors [47]. In co-transfected HEK-293 and COS7 cells, RING1 was shown to form a multimeric complex with KyoT2 and RBP-J, contributing to the repression of RBP-J mediated transactivation. These effects could be abrogated by human immunodeficiency virus type I enhancer binding protein 3, which competes with RING1 to bind KyoT2 at both LIM domains [47]. Similar patterns were also observed for Polycomb 2 homolog (HPC2), another PcG protein interactor of KyoT2 (Figure 3) [48]. These findings suggest there may be two approaches for the KyoT2-mediated suppression of RBP-J. First, KyoT2 could compete with transactivators for binding sites on RBP-J. In addition, it could recruit co-suppressors such as RING1 and/or HPC2. PcG proteins, including HPC2, have been known to form large complexes on promoters to suppress transcription [42, 47, 48].

Similar to KyoT2, KyoT3 was recently demonstrated to compete with NIC for binding RBP-J and repressing transactivation of RBP-J dependent promoters [45]. However, RT-PCR analysis of Hes-1 mRNA levels revealed KyoT3 mediated repression occurred only in the presence of NIC. In the absence of NIC, elevated Hes-1 mRNA was detected in the presence of KyoT3 [45]. It is plausible KyoT3 recruits other molecules to any of its LIM domains to transactivate the Hes-1 promoter or antagonize the repression of RBP-J activity [45].

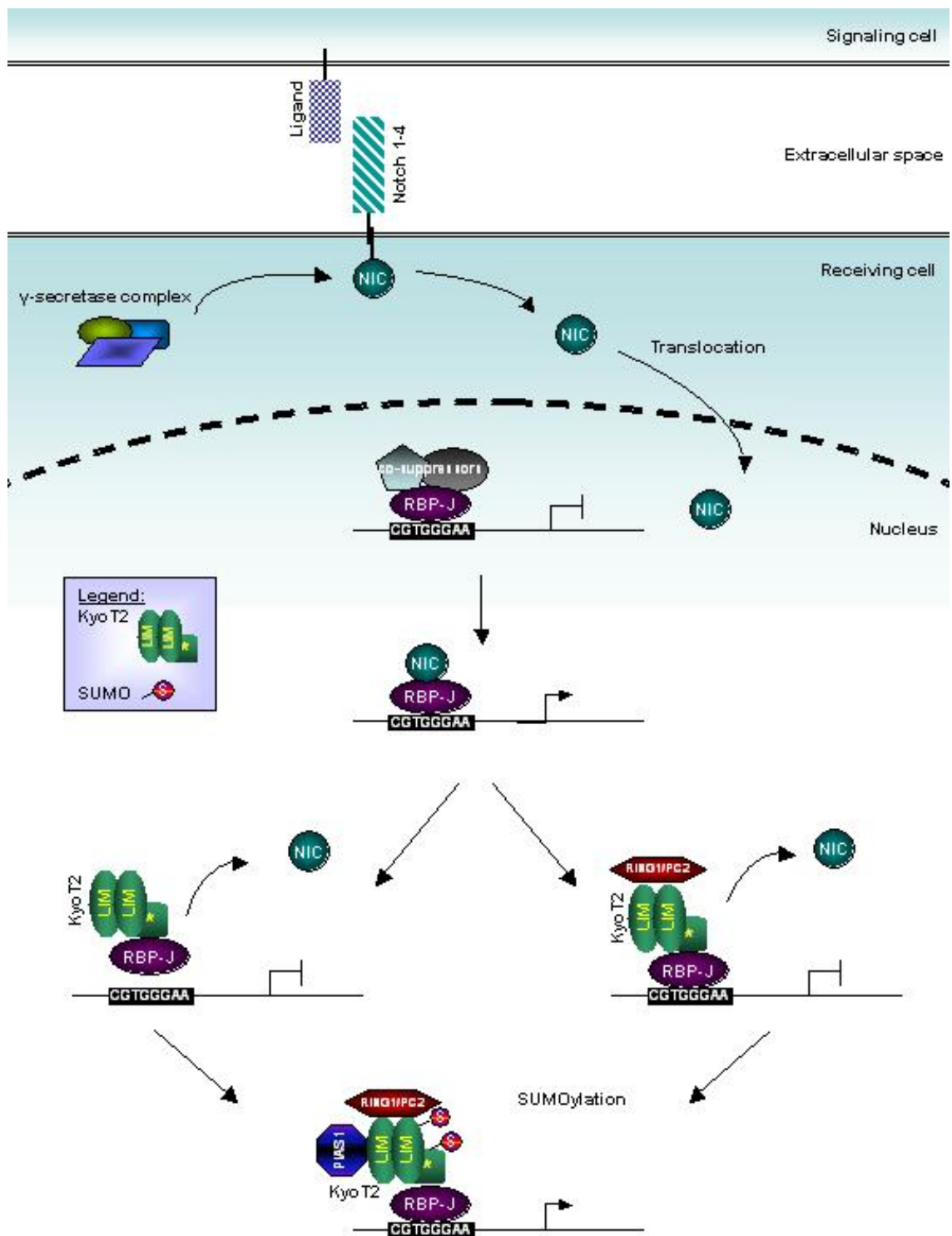


**Figure 3. FHL1 and Notch Signaling**

In mouse, the Notch signaling pathway is activated by proteolytic cleavage of the Notch receptor by  $\gamma$ -secretase-like protease, releasing the Notch intracellular domain (NIC). NIC translocates into the nucleus and transactivates RBP-J. KyoT2 can disrupt this interaction via its RBP-J binding domain and subsequently suppress transcription by displacing RBP-J from DNA and/or recruiting co-suppressors (ie. RING1 and/or HPC2). Furthermore, sumoylation by PIAS1 antagonizes KyoT2's repressor activity.

**I.C.4 KyoT2 and Sumoylation:** Post-translational modification is a common regulatory mechanism of many signaling pathways and transcription factors. KyoT2 repression of Notch signaling in cells via interaction with RBP-J can be modulated by protein inhibitor of activated STAT 1 (PIAS1), promoting transactivation of RBP-J [49]. Considering KyoT2 interacts with two small ubiquitin-related modifier (SUMO) modification E3 ligases (HPC2 and PIAS1), KyoT2 was suggested to be a substrate for SUMOylation [48, 49]. This was verified when the effects of PIAS1 were neutralized in the presence of Sentrin/SUMO-specific protease SENP2, a SUMO hydrolase [49]. PIAS1 promotes SUMOylation of KyoT2 at two sites, K144 in the second LIM domain, and K171 near the RBP-J binding motif, which antagonizes KyoT2's repressor activity (Figure 3). In particular, modification of the K171 site most counteracted the repression. Unlike PIAS1, overexpression of HPC2 did not enhance SUMOylation of KyoT2 beyond basal levels [49]. In general, SUMOylation can alter the stability, localization, and biological activities of modified proteins [49]. In the case of KyoT2, no effects on its subcellular localization or interaction with RBP-J were detected [49].

## **I.D FHL1 Functions**

The predominance of FHL1 in skeletal muscle and its expression pattern during development are suggestive of a functional role for FHL1 in muscle. For instance, in skeletal muscle of embryonic sheep, an increase in FHL1 mRNA level was evident from 120 days, when fiber hypertrophy predominates, to birth. FHL1 mRNA levels continued to increase postnatally, associated with skeletal muscle growth [7].

Considering that, FHL1 has been associated with numerous functions in muscle cells, although the precise mechanisms have yet to be elucidated. Furthermore, the capacity of FHL1 to function as a transcriptional regulator has been demonstrated, similar to other members of the FHL family.

### **I.D.1 Striated Muscle Functions**

**I.D.1.i Integrin Mediated Effects:** Activation of cell-surface integrins results in reorganization of the actin cytoskeleton, with the formation of focal adhesion complexes and stress fibers. In myoblasts, integrin activation also causes for dual localization of FHL1 in the nucleus and the cytoplasm, specifically at focal adhesions and along stress fibers [50]. In activated and transfected myoblasts, FHL1 was discovered to inhibit cell adhesion whilst promoting cell spreading and migration, mediated specifically by  $\alpha 5\beta 1$ -integrin [50]. However,

overexpression of FHL1 in myoblast cells subjected to differentiation conditions promotes alignment and fusion of cells to form multinucleated myotubes [51]. Two distinct phenotypes evident in differentiated cells was significant branching, with multiple major cytoplasmic protrusions from the cell body, and hyperelongation of mononucleated myotubes [51]. Both phenotypes are indicative of cytoskeletal remodeling, induced by FHL1 overexpression and integrin activation. Integrin-matrix interactions were sufficient for induction of the branched phenotype, whilst hyperelongation was dependent specifically on ligand-binding to the  $\alpha 5\beta 1$ -integrin [51].

I.D.1.ii **Myosin Thick Filament and Sarcomere Assembly:** Characterization of the FHL1 interaction with myosin binding protein C (MyBP-C) revealed a role in myosin filament formation and sarcomere assembly [52]. FHL1 competes with myosin for binding MyBP-C, since they share a common binding region, thus impairing MyBP-C from binding to myosin filaments. When FHL1 was overexpressed in differentiating skeletal muscle cells, disruptions in the formation of the Z-line of the sarcomere and assembly of the myosin thick filament were evident [52]. Similarly, myosin thick filament formation was also inhibited by RNAi mediated knockdown of FHL1. The knockdown also impeded the incorporation of MyBP-C into the sarcomere, with the formation of dense MyBP-C aggregates instead. Thus, FHL1 regulates myosin filament and sarcomere formation, with consequences for altering the MyBP-C to myosin ratio [52].

I.D.1.iii **Biomechanical Stress Sensor and Response:** FHL1 also mediates hypertrophic biomechanical stress responses in mice, upon detection of stretch or agonists induced by G protein coupled receptor signaling [53]. FHL1 was identified as a component of the stress sensor complex at the sarcomeric I-band, where it interacts with the MAPK cascade components, Raf1, MEK2, and ERK2, at the N2B region of titin in cardiomyocytes. Though the precise mechanisms are not known, FHL1 mediates communication between the stretch sensor complex and downstream responses by titin and MAPK components [53]. For instance, in papillary muscles isolated from FHL1 knockout mice and subjected to stretch ( $L_{max}$ ), there was a loss of stretch-induced hypertrophic signaling responses. This was measured by quantitative PCR of ELK1 and atrial natriuretic factor (ANF), a transcriptional target of ERK1/2 and marker of hypertrophy respectively [53]. A specific role for FHL1 in diastolic tension was also suggested when the stretched papillary muscle displayed reduced diastolic stress and increased

compliance [53]. Furthermore, the N2B element of titin is a component of the extensible region of titin which contributes to the myofibrillar passive tension generated upon stretch [53].

I.D.1.iv **Regulator of Muscle Mass:** Similarly, FHL1 transgenic mice revealed FHL1 functions to increase skeletal muscle mass and strength, with reduced susceptibility to fatigue [54]. The skeletal muscle hypertrophy observed was caused by increased muscle fiber dimensions, associated with a conversion to oxidative fiber, rather than hyperplasia. Hypertrophy and fiber type switching were reminiscent of nuclear factor of activated T cells cytoplasmic component 1 (NFATc1) involvement, which lead to the discovery of an interaction between FHL1 and NFATc1 [54]. Furthermore, FHL1 functions as a transactivator of NFATc1 mediated transcription [54].

I.D.1.v **Electrophysiology:** In addition to these described functions, FHL1 also has the capacity for a role in electrophysiology. Yang *et al.* identified FHL1 as an interacting partner of the Shaker-related voltage-gated K<sup>+</sup> channel KCNA5 alpha-subunit in human atrium, and characterized the interaction in CHO cells [55]. As evidenced from patch clamp recordings of K<sup>+</sup> current, FHL1 was capable of modulating KCNA5 activity, by increasing K<sup>+</sup> current density, altering channel gating, and enhancing slow inactivation [55].

**I.D.2 Transcriptional Regulation Functions:** FHL1 has repeatedly been detected downregulated in a variety of cancers, during comparative microarray profiling studies and immunohistochemical analysis of human clinical samples. Reduced expression has been identified in lung, prostate, breast, ovarian, colon, thyroid, brain, renal, liver, gastric, and skin cancers and melanomas [56-60]. In primary gastric cancer patients, a significantly shorter survival was observed from patients with relatively lower FHL1 expression levels [60]. Furthermore, FHL1 suppression appeared greatest in widely invasive and metastatic cases [58-61]. FHL1 levels significantly correlated with deeper tumour invasion of the serosal layer and the incidence of distant metastasis in primary gastric cancer [60].

Analogous to these findings, FHL1 was identified as a tumour suppressor gene which acts to inhibit non-anchored cell growth and migration [59]. In transformed cells however, Src tyrosine kinase phosphorylated Crk-associated substrate (CAS), a focal adhesion adaptor protein, to suppress FHL1 expression and promote non-anchored tumour cell growth and migration (Figure 4) [59]. FHL1 gene silencing was induced by methylation of the promoter

region [62]. Thus, diminished FHL1 expression likely attributes to poorer survival via heightened biological aggressiveness of the tumour [60].

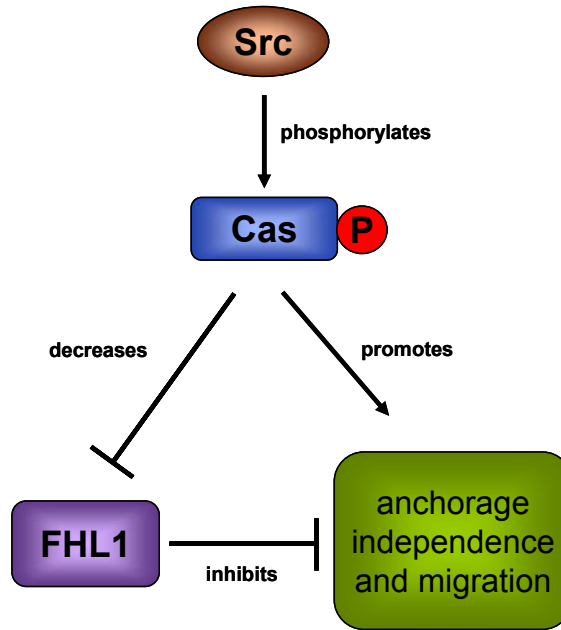


**Figure 4. FHL1 and Anchorage Independence**

Src requires Cas to suppress FHL1 expression to promote non-anchored tumour cell growth and migration, which would otherwise be inhibited by FHL1.

However, in human hepatocellular liver carcinoma cells cultured *in vitro* or injected into nude mice, expression of FHL1 decreased cancer cell growth via interaction with Sma- and Mad-related (SMAD) proteins for a transforming growth factor (TGF)  $\beta$  like response (Figure 5) [63]. FHL1 interacted with SMAD2 and SMAD3 in the cytoplasm, and enhanced phosphorylation of the SMAD proteins through casein kinase 1 delta (CK1 $\delta$ ). Furthermore, FHL1 promoted interaction with SMAD4 and translocation into the nucleus, where it stimulated expression of growth inhibitor genes, such as the CDK inhibitor p21, and suppression of the growth promoting gene c-myc [63]. Although FHL1 modulated TGF- $\beta$  responsive transcription, it actually functions independent of TGF- $\beta$  and the TGF- $\beta$  receptor. Since it mediated differential phosphorylation of the Smad3 protein, FHL1 may regulate additional targets not affected by TGF- $\beta$  [63].

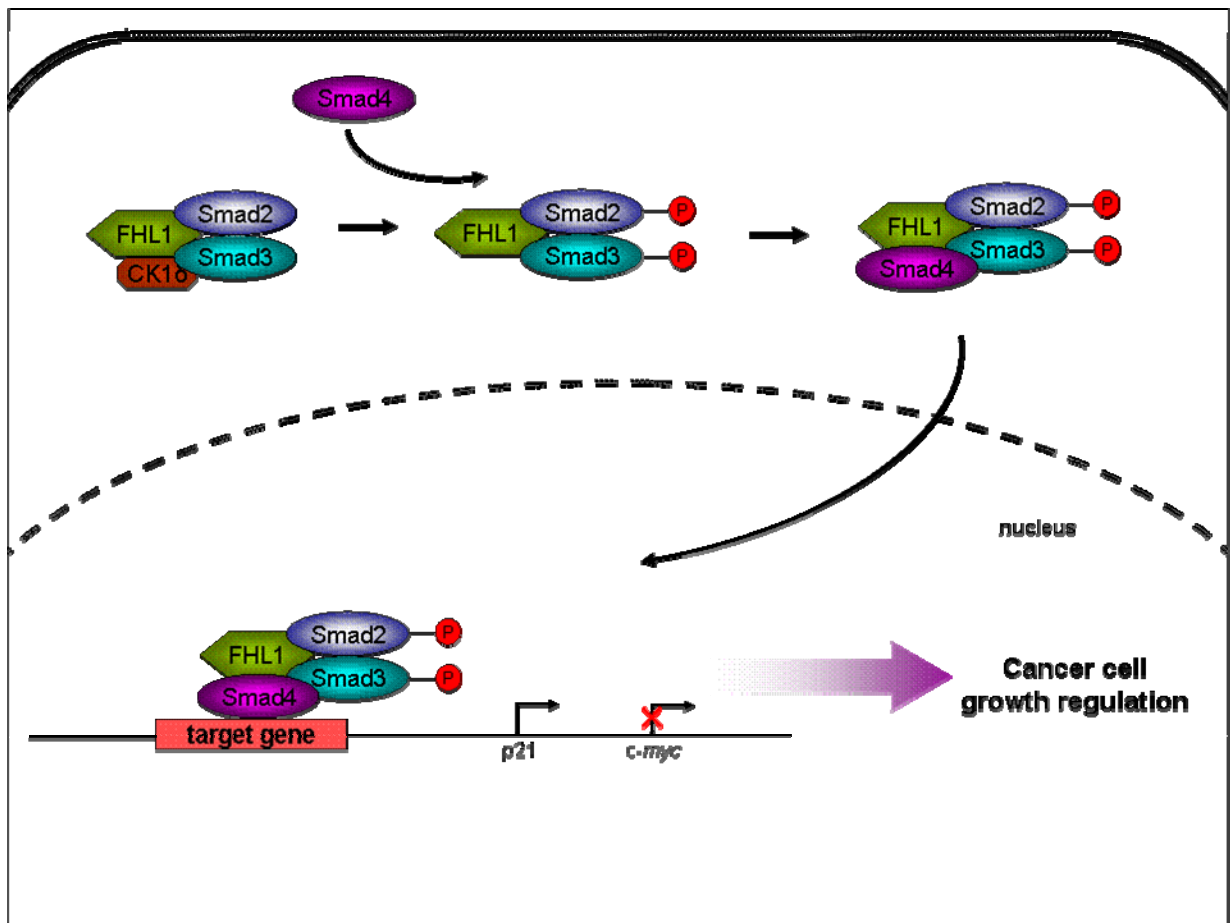


**Figure 5. FHL1 Inhibition of Tumour Cell Growth by Interaction with Smad Proteins**

FHL1 inhibits tumour cell growth by transcriptional regulation of TGF- $\beta$ -responsive genes, though independent of TGF- $\beta$  and TGF- $\beta$  receptor. FHL1 phosphorylates cytoplasmic Smad2 and Smad3 through interaction with CK1 $\delta$ , and facilitates interaction with Smad4. Nuclear translocation occurs, where the Smad proteins in complex with FHL1 regulate TGF- $\beta$ -responsive gene transcription.

Modified from: [63].

### I.E FHL1 and Skeletal Muscle Myopathies

FHL1 was recently identified as the causal gene for three different X-linked myopathies, in accordance with its gene localization on the X-chromosome [1]. One of the first mutations identified in the human FHL1 gene was also responsible for the first known X-linked dominantly inherited form of scapuloperoneal myopathy (XSPM), identified in a large Italian-American family [64]. XSPM is a neuromuscular disorder characterized by progressive muscular atrophy, initiated in the lower legs and extending to the shoulders and arms with scapular winging, possibly with impaired sensory functions. These phenotypes were attributed to a Trp-122 to Ser substitution, occurring in the second LIM domain. Quantification

experiments revealed an inverse relationship between the FHL1 protein level and the duration since symptom onset [64].

Another two FHL1 mutations were discovered to be causal for a novel recessive muscular disorder. X-linked myopathy with postural muscle atrophy (XMPMA) was clinically characterized by weakness and atrophy of postural muscles while alternative muscle groups were hypertrophic [65]. In general, muscle groups composed predominantly of type I fibers were atrophic, while those primarily comprised of type II fibers were hypertrophic. These symptoms were usually noted at about 30 years of age. Furthermore, affected individuals typically died of heart failure, suspected to be caused by HCM [65]. The original mutation, discovered in a large Austrian family, was a Cys-224 to Trp substitution located in the fourth LIM domain. In a British family, an isoleucine insertion mutation in the second LIM domain was also found. Immunoblot analysis revealed almost complete absence of FHL1 protein from affected individuals [65].

To date however, the greatest number of FHL1 mutations has been associated with X-linked reducing body myopathy (XRBM), with all ten known amino acid substitution mutations occurring in the second LIM domain [66-68]. Clinically XRBM is a rare muscular disorder causing progressive muscular weakness, generally affecting proximal muscles. Histopathological analysis, however, is required to identify the presence of characteristic intracytoplasmic aggregates [66-68]. Furthermore, unlike XSPM and XMPMA, FHL1 is more abundantly expressed in the diseased state, particularly enriched in the intracytoplasmic inclusion bodies. In addition to both wild type and mutant FHL1, these aggregates also sequester interacting partners, such as MyBP-C and NFATc1 [66].

Rigid spine was identified as a common clinical feature among patients afflicted with any of the three x-linked myopathies [69]. In accordance with this, an in-frame nine base pair deletion mutation, corresponding to the second LIM domain, was identified in a patient diagnosed with rigid spine syndrome. The patient presented with early scoliosis and wide spread muscular atrophy, with mildly impaired respiratory functions. Furthermore, intracytoplasmic inclusion bodies were also detected from biopsied muscle samples [69].

In general, each of the described human FHL1 mutations were localized within a LIM domain, affecting highly conserved residues. For instance, the Cys-to-Ser mutation causing XMPMA involved a Cys necessary for  $Zn^{2+}$  binding [65]. NMR spectroscopy also predicted complete disruption of the  $Zn^{2+}$  binding sites in two severe cases of XRBM, where the mutations were localized to invariant consensus residues involved in coordinating  $Zn^{2+}$  binding

[66]. Metal ions can contribute to the stabilization of a protein's tertiary structure, as is the case with  $Zn^{2+}$  ions and LIM domains. Thus, mutations disrupting these properties can have deleterious effects on protein structure and stability [66].

## **II. PROTEIN-PROTEIN INTERACTIONS**

### **II.A General Introduction**

Within the cell, proteins contribute to the control and execution of cellular activities. One important level of functional organization of the corresponding complex proteome is the establishment of multimeric protein complexes [70]. Furthermore, protein interactions and the formation of complexes are governed in a time- and space-dependent manner [70]. Within a complex, each component contributes to the overall function, which can further be regulated by neighbouring proteins and complexes [70]. Studying protein interactions thus provides an opportunity to gain insight into the functional roles of poorly characterized proteins. Since proteins involved in the same cellular processes often interact, functional associations can be predicted by elucidation of interactions with better annotated proteins, in addition to characterizing the subcellular distribution patterns [70-72].

The protein interactions initially identified for FHL1 were specific for the two alternatively spliced variants from mice. Table 1 lists the known isoform specific interactions. Their involvement in the Notch signaling pathways was originally suggested by Y2H screening of various libraries using RBP-J as the bait protein [42]. Similarly, most of the known protein interactions involving FHL1A were also discovered by the Y2H method, and subsequently validated (Table 2). In contrast, several putative FHL1 interactions also exist, which were not further validated (Table 3). Ewing and colleagues attempted to build a large human protein-protein interaction network, using 338 FLAG tagged bait proteins which were co-IPed from HEK-393 cells and analyzed via MS. FHL1 was identified in the co-IPs of five different proteins [73].

Several different techniques are thus available for the discovery of novel protein interactions, such as the widely accepted Y2H screening method. Another screening method developed more recently is the protein microarray. In contrast to these, TAP coupled to MS analysis offers an alternative method whereby protein complexes can be purified from cells and identified [71, 72].

**Table 1. FHL1 Isoform Specific Interactions**

This table outlines all the known protein interactions for the two alternative spliced variants of FHL1, with a description of the interaction identification and validation methods used. The databases searched for identifying the interactions are also listed.

GENE	PROTEIN	ISOFORM SPECIFICITY	INTERACTION DETECTION	DATABAS E	REF.
HIVEP3	Human immunodeficiency virus type I enhancer binding protein 3	KyoT2	<i>In vivo</i> tag co-IP; <i>in vivo</i> mammalian two hybrid assay (luciferase reporter)	HPRD, I2D, PubMed	[47]
RBPJ	J kappa-recombination signal binding protein	KyoT1 (weak); KyoT2, KyoT3 *interaction via RBP-J-binding motif	KyoT1/2: Y2H screen of mouse 9.5-dpc embryos and HeLa cells (RBP-J=bait); <i>in vitro</i> GST-pull down; EMSA; <i>in vivo</i> tag co-IP from COS-7 cells KyoT3: <i>in vivo</i> tag co-IP from HeLa cells	HPRD, I2D, PubMed	[42, 45]
RING1	Ring finger protein 1	KyoT1 (Y2H); KyoT2 *interaction via LIM domains	Y2H screen of human lymph node cDNA library (KyoT2=bait); Y2H assay; <i>in vitro</i> GST-pull down; <i>in vivo</i> tag co-IP from HEK-293 cells; <i>in vivo</i> mammalian two hybrid assay (luciferase reporter) from HEK-293 cells	HPRD, I2D, PubMed	[47]
CBX4	PC2 (Chromobox protein homolog 4)	KyoT1 (Y2H); KyoT2 *interaction via LIM domains	Y2H screen of human lymph node cDNA library (KyoT2=bait); <i>in vitro</i> GST-pull down; <i>in vivo</i> tag co-IP from HEK-293 cells; <i>in vivo</i> mammalian two hybrid assay (luciferase reporter) from HEK-293 cells	HPRD, I2D, PubMed	[48]
PIAS1	Protein inhibitor of activated STAT-1 (Signal transducer and activator of transcription-1)	KyoT2	Y2H screen of human lymph node cDNA library (KyoT2=bait); <i>in vitro</i> GST-pull down; <i>in vivo</i> tag co-IP from HEK-293 cells; <i>in vivo</i> mammalian two hybrid assay (luciferase reporter) from HEK-293 cells	PubMed	[49]

**Table 2. Known FHL1 Interactions**

This table outlines all the known FHL1 protein interactions to date, with a description of the identification and validation methods used and, when known, the specific LIM domains involved. The databases searched for identifying the interactions are also listed.

GENE	PROTEIN	DOMAIN SPECIFICITY	INTERACTION DETECTION	DATABAS E	REF.
MYBPC 1 (cardiac and slow type)	Myosin binding protein C, slow type		Y2H screen of human skeletal muscle library (FHL1=bait); <i>in vitro</i> GST-pull down; <i>in vivo</i> tag co-IP from COS-1 cells; <i>in vivo</i> FHL1 co-IP from murine Sol8 skeletal myotubes; immunofluorescence co-localization in murine soleus muscle	HPRD, I2D, PubMed	[52]
SRF	Serum response factor	via LIM domains	<i>In vitro</i> GST-pull down	HPRD, I2D, PubMed	[31]
FHL2	Four and a half LIM domains protein 2 (Skeletal muscle LIM protein 3)		Immunofluorescence colocalization in cotransfected rat cardiomyocytes; <i>in vitro</i> GST-pull down	HPRD, I2D, PubMed	[74]
KCNA5	Voltage-gated potassium channel subunit Kv1.5		GST-pull down (KCNA5=bait) of human atrial lysate, followed by MS; <i>in vivo</i> KCNA5 co-IP from human atrium, cotransfected CHO cells; immunofluorescence colocalization in cotransfected CHO cells	PubMed	[55]
NFATC1	Nuclear factor of activated T-cells, cytosolic component 1		GST-tagged FHL1 purification from cotransformed (with His-NFATc1) E. coli; GST-pull down (KCNA5=bait) of murine skeletal muscle lysate; immunofluorescence colocalization in cotransfected C2C12 cells, with wild-type and RBM mutant FHL1	PubMed	[54]
TLN1	Talin 1		<i>In vivo</i> FHL1-myc co-IP from mouse embryonic fibroblast cells (NIH 3T3), followed by in-gel digestion and MS; FHL1-myc co-IP from human PSMCs; immunofluorescence colocalization in human PSMCs and human lung tissue	PubMed	[75]
RAF1	raf proto-oncogene serine/threonine protein kinase	first 2 LIM domains essential	Y2H assay; Raf1 co-IP from murine cardiac muscle; immunofluorescence colocalization in adult cardiomyocytes	PubMed	[53]
MEK2	Mitogen-Activated Protein Kinase Kinase 2	first 2 LIM domains essential	Y2H assay; MEK1/2 co-IP from murine cardiac muscle; immunofluorescence colocalization in adult cardiomyocytes	PubMed	[53]
ERK2		first 2 LIM domains essential	Y2H assay; ERK2 co-IP from murine cardiac muscle; immunofluorescence colocalization in adult cardiomyocytes	PubMed	[53]
ERK2 (TYDD)	Constitutively phosphorylated mutant of ERK2	first 2 LIM domains essential	Y2H assay; co-IP from murine cardiac muscle;	PubMed	[53]
TTN	Human cardiac Titin N2B → N2B element of titin		<i>In vivo</i> co-IP of HA-FHL1 from COS cells (cotransfected with GFP-titin N2B); immunofluorescence colocalization in adult cardiomyocytes	PubMed	[53]
SMAD2	Mothers against decapentaplegic homolog 2 (Sma- and Mad-related protein 2)		<i>In vitro</i> GST-pull down; <i>in vivo</i> co-IP from cotransfected HEK-293 cells; co-IP from human hepatoma HepG2 cells (endogenous)	PubMed	[63]
SMAD3	Mothers against decapentaplegic homolog 3		<i>In vitro</i> GST-pull down; <i>in vivo</i> co-IP from cotransfected HEK-293 cells; co-IP from human hepatoma HepG2 cells (endogenous)	PubMed	[63]
SMAD4	Mothers against decapentaplegic homolog 4		<i>In vitro</i> GST-pull down; <i>in vivo</i> co-IP from cotransfected HEK-293 cells; co-IP from human hepatoma HepG2 cells (endogenous)	PubMed	[63]
CSNK1 D	Casein kinase 1, delta		<i>In vitro</i> GST-pull down; <i>in vivo</i> co-IP from cotransfected HEK-293 cells; co-IP from human hepatoma HepG2 and SMMC7721 cells (endogenous)	PubMed	[63]

**Table 3. Putative FHL1 Interactions**

This table outlines the putative FHL1 interactions, with a description of the identification and validation methods used and the organism the interaction was detected from. The databases searched for identifying the interactions are also listed.

GENE	PROTEIN	SPECIES	INTERACTION DETECTION	DATABASE	REF.
EPB41	Protein 4.1 ( Band 4.1)	Human	Co-IP of Flag-EBP41 from HEK-293 cells, followed by MS	IntAct, I2D	[73]
MCC	Colorectal mutant cancer protein (Protein MCC)	Human	Co-IP of Flag-MCC from HEK-293 cells, followed by MS	IntAct, I2D	[73]
HLA-B	HLA class I histocompatibility antigen, B-42 alpha chain	Human	Co-IP of Flag-HLA-B from HEK-293 cells, followed by MS	IntAct, I2D	[73]
IKBKE	Inhibitor of nuclear factor kappa-B kinase subunit epsilon (I kappa-B kinase epsilon)	Human	Co-IP of Flag-IKBKE from HEK-293 cells, followed by MS	IntAct, I2D	[73]
PRKAB1	5'-AMP-activated protein kinase subunit beta-1	Human	Co-IP of Flag-PRKAB1 from HEK-293 cells, followed by MS	IntAct, I2D	[73]
Slc2a4	Solute carrier family 2, facilitated glucose transporter member 4 (Glucose transporter type 4, insulin-responsive; GLUT-4)	Rat	Co-IP of Myc-GLUT4 from rat L6 myoblast cells, followed by MS	IntAct, I2D	[76]

## II.B Yeast Two-Hybrid

The basic premise of an Y2H system is that a reporter protein can be fragmented into two halves, abolishing its general activity. However, when the fragments are co-expressed as fusion proteins of two interacting proteins, their function can be restored upon physical association mediated by interaction between the fusion proteins [71, 72, 77]. The most commonly used reporter proteins are transcription factors, with cleavage separating the activation and binding domains. Upon physical reconstitution, the transcription factor activates a reporter gene, usually generating a colorimetric or fluorescent readout [77]. Based on the yeast expression system, automation allows for high throughput screening of cDNA libraries. Goehler *et al.* applied this method to generate a protein-protein interaction network for Huntington's disease. Using a matrix comprised of cDNAs associated with the huntingtin aggregation process, 186 protein interactions were identified among 35 bait and 51 prey proteins. Literature review revealed greater than 89% of these interactions were previously unknown [78].

## II.C Protein Array

An analogue of the DNA microarray, protein microarrays are in the relatively early stages of development [72, 77]. Functional protein microarray technology is based on protein chips consisting of arrayed, immobilized full-length proteins or protein domains [79], which allows for studying various protein interactions, including protein-protein, protein-DNA, and protein-small molecule interactions [79]. When designing protein chips, the chosen slide

surface must be appropriate for the immobilization of the selected proteins, maintenance of protein conformation and function, desired protein orientation (random or uniform), and maximizes the binding capacity [79].

Ramachandran *et al.* designed a nucleic acid programmable protein array, utilizing a cell-free system for the transcription and translation of recombinant proteins [80]. First, plasmid DNA was cross-linked to the slide surface, along with anti-GST capture antibody. In situ expression was achieved by incubation with a rabbit lysate with T7 polymerase, and the resulting epitope tagged proteins were captured and antibody-bound to the array [80]. They applied this technique to study the human DNA replication complex, whereby 29 DNA replication proteins were expressed and immobilized. As a result, 110 interactions were identified, of which 63 were previously unknown [80].

## II.D Tandem Affinity Purification

Originally developed in yeast, TAP allows for the purification of endogenously assembled protein complexes under native conditions [81]. The method depends on the expression of a recombinant protein of interest with dual affinity tags. Used in various combinations, the tags are usually short hydrophilic peptides or small proteins [82]. The general procedure consists of affinity capturing of a desired protein in combination with its interacting partners. Nonspecific proteins are removed with multiple gentle washes and the remaining complexes eluted. Using the eluted complexes, a second affinity purification is performed utilizing the alternative tag. Sub-optimal enrichment of bait and interacting proteins compared to background signal, with single-step purifications, necessitates performing a second purification step [83]. To identify the copurified proteins, the method is often coupled to MS analysis [71, 83].

Since its conception in yeast, TAP has been extended to other organisms, such as *Drosophila* and the *Arabidopsis thaliana* plant [84, 85]. Although the methodology has been successfully applied to studying protein interactions from mammalian cells, certain limitations were evident, particularly an overall low yield of bait and specific interacting proteins [83, 86, 87]. To resolve this issue, several groups have attempted to determine the ideal dual-tagging system. For instance, Burckstummer and colleagues tested four combinations of affinity tags using I $\kappa$ B kinase  $\gamma$ , purified from HEK-293 cells, and proclaimed a 10-fold improvement in yield of bait recovery using a protein G and streptavidin binding peptide combination [87]. Similarly, Giannone and colleagues compared the purification efficiency of the human telomeric

repeat binding factor 2, using five different tag combinations. Furthermore, they demonstrated a potential for regulating expression levels by induction, using tetracycline for example [83].

### **III. HEART FAILURE**

#### **III.A General Introduction**

The human heart is a dynamic organ, functioning as a muscular, mechanical pump responsible for generating an appropriate cardiac output and pressure to meet the metabolic needs of the body and maintain homeostasis. When the heart deteriorates in function, heart failure ensues. Heart failure is a severe and progressive cardiac disorder, and credited as the leading cause of morbidity and mortality worldwide [88]. In the United States alone, there are an estimated 5200000 afflicted individuals, with 550000 new cases diagnosed each year. This translates into a prevalence of 1-2 % with an incidence rate of 5-10 per 1000 persons per year [88, 89]. Cardiovascular disease accounts for more deaths annually than cancer, chronic lower respiratory disease, accidents, and diabetes mellitus combined [88].

#### **III.B Pathophysiology of Heart Failure**

##### **III.B.1 Structural Remodeling**

III.B.1.i *Myocardial Hypertrophy*: Cardiac hypertrophy is defined as an increase in heart muscle mass due to an increase in the size of constituent myocytes [90]. Hypertrophy is a physiological compensatory response of the heart in response to an increase in stress, induced by exercise or pregnancy for example. It is also an ubiquitous component of various cardiovascular diseases leading to heart failure, such as hypertension, valvular disease, and cardiomyopathies [91]. In heart failure, hypertrophy is initially an adaptive response that normalizes wall stress to preserve and enhance cardiac output. Myocardial hypertrophy is characterized by an increase in cardiomyocyte size, increased protein synthesis, reduced rates of protein degradation, and changes in gene expression, including re-expression of fetal genes such as  $\beta$ -myosin heavy chain and ANF [92]. The most prominent stimuli for induction of hypertrophy include biomechanical and stretch factors, and neurohumoral factors, such as the hormones, cytokines, chemokines, and growth factors. However, with prolonged exposure to stress, compensatory hypertrophy eventually devolves into myocardial dysfunction [90, 91].

III.B.1.ii *Hypertrophic Signaling Pathways*: The molecular mechanisms underlying the deterioration of compensatory hypertrophy to pathological hypertrophy are poorly understood. However, several signaling pathways are known to be induced in the diseased state, especially via mechanical stretch and neurohumoral receptor stimulation [93].

*Angiotensin II*: Mechanical stretch stimulates the secretion of angiotensin II (Ang II) from cardiac myocytes, which then binds Ang II type I (AT1) receptors to initiate intracellular protein kinase cascades, for instance, leading to the synthesis of endothelin-1 (ET-1) and TGF-1 [90, 94]. In hypertrophied hearts, AT1 and AT2 receptors even display increased expression [94]. Ang II is also associated with the increased cardiac fibrosis observed during cardiac remodeling and hypertrophy. It is capable of inducing growth and collagen synthesis in cardiac fibroblast growth via Ang II receptors [90, 94]. Excessive Ang II also results in a negative contractile response by cardiomyocytes, which prolonged exposure reducing their mechanical performance. Though the complete mechanism of Ang II in hypertrophy has not been fully elucidated, its physiological relevance can be demonstrated through angiotensin converting enzyme (ACE) inhibitor therapy, which has been successful in resolving hypertrophy [90, 94, 95].

*Endothelin-1*: Endothelins are a family of vasoconstrictor peptides produced predominantly by vascular endothelial cells. In heart failure, ET-1 levels are increased in myocardial tissue by cardiomyocytes and fibroblasts stimulated by several factors, including Ang II and TGF- $\beta$  [96]. In turn, ET-1 also stimulates hypertrophy by binding endothelin-1 type A (ETA) receptors on cardiac myocytes. The signal transduction pathway results in the production of diacylglycerol (DAG) and inositol 1,4,5-triphosphate (InsP3) [96, 97]. Sustained release of DAG prolongs activation of protein kinase C (PKC), which has been implicated in the hypertrophic response of the myocardium. In pathological cardiac conditions, expression of ETA and ETB receptors are also upregulated [96, 97]. In neonatal rat cardiomyocytes, exposure to ET-1 was shown to mediate a hypertrophic effect, which could be attenuated by ETA receptor blockade with BQ-123 treatment. In transgenic mice with cardiac-specific overexpression of ET-1, cardiac hypertrophy was evident, with rapid deterioration of cardiac function and progression to death. An increased expression of inflammatory cytokines was also present [96]. ET-1 mediated cardiac remodeling is also associated with reactivation of fetal genes, including B-MHC and ANF [97]. Furthermore, it is involved with cardiac fibrosis by stimulating the increased production and deposition of collagen and osteopontin [96].

**Tumor Necrosis Factor- $\alpha$  (TNF- $\alpha$ ):** More recently, a strong association between inflammation and cardiac disease has been established. Elevated plasma levels of pro-inflammatory cytokines such as IL-6, IL-8, and TNF- $\alpha$  have been demonstrated to predict heart failure [98]. In rats subjected to a continuous infusion of circulating TNF- $\alpha$ , a time-dependent depression in LV function was observed, with stimulation of the hypertrophic growth response in adult cardiac myocytes [99]. Similarly, transgenic mice with cardiac specific overexpression of TNF- $\alpha$  developed DCM [100]. In patients with heart failure and severe mitral regurgitation, mitral valve repair reverses the abnormal expression of TNF- $\alpha$  and reduces the severity of LV remodeling [101].

**III.B.2 Electrical Remodeling:** Another feature of the failing heart is electrical remodeling, which also leaves the heart vulnerable to ventricular arrhythmias leading to sudden cardiac death. Ion channel dysfunction is a hallmark of heart failure, and the leading contributor to the electrical remodeling processes [102, 103].

III.B.2.i **Potassium Channel Remodeling:** The transient outward K<sup>+</sup> current ( $I_{to}$ ) is activated following the onset of an action potential and accounts for the brief interval of early repolarization (phase I) following the rapid depolarization (phase 0) [104]. A reduced  $I_{to}$  density has consistently been observed in numerous animal models of cardiac hypertrophy and failure. In humans, the downregulation of  $I_{to}$  in turn reduces calcium entry through the L-type calcium channel and shortens the duration of the action potential. In contrast, in rodent models, the action potential is prolonged with a reduction of  $I_{to}$  [104]. The pore-forming alpha subunit of cardiac  $I_{to}$  is encoded by the potassium voltage-gated channel, Shal-related subfamily, member 3 (Kv4.3), which is also reduced at the mRNA level in human heart failure. In rats, gene transfer of Kv4.3 could effectively reverse  $I_{to}$  downregulation and attenuate the hypertrophic response initiated by aortic stenosis [104]. The inward rectifier K<sup>+</sup> current ( $I_{K1}$ ) maintains the resting membrane potential and participates in the terminal repolarization stage. In diseased conditions, the  $I_{K1}$  channel density is reduced, which contributes to the prolonged action potential and also increases the susceptibility to spontaneous membrane depolarizations [104].

III.B.2.ii **Calcium Channel Remodeling:** In heart failure, there is clear evidence that the Ca<sup>2+</sup> transient is prolonged and Ca<sup>2+</sup> reuptake is reduced. These changes are manifested by defective sequestration of Ca<sup>2+</sup> by the sarcoplasmic reticulum (SR), resulting from a down-regulation of

the SR ATPase mRNA and activity [105]. In isolated cardiomyocytes from failing human hearts, calcium handling and contractile dysfunction could be improved by transfection with the sarco/endoplasmic reticulum  $\text{Ca}^{2+}$  ATPase (SERCA) 2a gene. In addition, SERCA2a activity is highly modulated by phospholamban (PLN), a transmembrane phosphoprotein of the SR [105, 106]. PLN inhibits SERCA2a function during its unphosphorylated state. In isolated human cardiomyocytes from failing hearts, inhibition of PLN also enhanced SERCA2a activity and improved cell contractility [106].

The ryanodine receptor (RYR) 2 of the SR is also downregulated in the failing ventricular myocardium at both the mRNA and protein levels [105]. In addition, hyperphosphorylation of RYR2 causes for the dissociation of FKBP12.6, an accessory protein necessary for RYR2 function. This produces a diastolic calcium leak and increased calcium waves [105, 107]. Recently, A. R. Marks identified a small class of molecules capable of enhancing the FKBP12.6 binding affinity to RYR2, which reduces the diastolic calcium leak responsible for delayed after depolarizations [107].

III.B.2.iii ***Sodium Channel Remodeling:*** In heart failure, there are also alterations in the  $\text{Na}^+$  transport mechanism. For instance, the  $\text{Na}^+/\text{K}^+$  ATPase of the plasma membrane exchanges 2 extracellular  $\text{K}^+$  for 3 intracellular  $\text{Na}^+$ , establishing a net outward repolarizing current [103]. In the diseased heart though, the expression and function of the  $\text{Na}^+/\text{K}^+$  ATPase is reduced, contributing to a prolonged action potential. In ventricular hypertrophy and heart failure the intracellular  $\text{Na}^+$  concentration is increased approximately 2-3 fold [103].

## **IV. PHOSPHOLAMBAN**

### **IV.A Overview of Phospholamban**

PLN is an integral membrane phosphoprotein of the SR. Though it is mainly expressed in cardiac muscle, PLN expression is also present in slow-twitch skeletal muscle, smooth muscle, and endothelial cells [106]. This 6.1 kDa phosphoprotein is composed of a highly conserved sequence of 52 amino acids consisting of three structural domains. Domain IA (amino acids 1-20) consists of a highly charged helical structure with two regulatory phosphorylation sites. Ser-16 is phosphorylated by cAMP-dependent protein kinase, whilst Thr-17 is phosphorylated by  $\text{Ca}^{2+}$ /calmodulin-dependent protein kinase. Domain IB (amino acids

21-30) contains a polar B-hairpin structure. The third domain, domain II (amino acids 31-52) is composed of a hydrophobic neutral transmembrane helix [108]. In the SR membrane, PLN exists as a homo pentamer in equilibrium with the monomer. However, it is monomeric PLN that is the active form, capable of binding and regulating SERCA. The presence of increasing amounts of monomeric PLN actually heightens SERCA inhibition. Recall that dephosphorylated phospholamban acts as an inhibitor of SERCA while phosphorylation relieves this inhibition [106].

#### **IV.B Mutations in Human Phospholamban and Cardiomyopathy**

A causal role for PLN in cardiomyopathies was established when 4 inheritable mutations were identified during genetic screening of the human PLN gene in individuals with familial cardiomyopathies. The first human PLN mutation identified was a single nucleotide transition, 77A→G, in a highly conserved region of the promoter [109]. The affected individual was heterozygous for the mutation, presenting with familial late onset type of hypertrophic cardiomyopathy. Luciferase assay performed with transfected neonatal rat cardiomyocytes revealed the mutation increased the PLN promoter activity by 1.5-fold [109]. This may be suggestive of an important role for the mutation in depressing calcium cycling by induction of PLN expression, leading to hypertrophy [109].

Next, the first mutation in the coding region of PLN was identified. Haghghi *et al.* discovered a T-to-G transversion mutation at nucleic acid 116 in two large Greek families, which converts codon Leu-39 to a premature stop codon (PLN-Leu39Stop) [110]. This translates into an incomplete penetrance of a cardiomyopathic phenotype, with early onset DCM and heart failure in homozygous individuals, and a more variable clinical phenotype in heterozygotes. Analysis of a homozygous explanted heart indicated the absence of detectable PLN protein, analogous to a PLN null condition [110]. More recently, Haghghi *et al.* described an Arg 14 deletion mutation in the PLN protein (PLN R14Del), resulting in lethal, hereditary DCM [111]. A transgenic mouse model of the PLN R14Del mutation recapitulated the human phenotype, exhibiting premature death and an enlarged myocardium, with ventricular dilation, myocyte disarray, and myocardial fibrosis [111]. During *in vitro* and *in vivo* studies, the mutant PLN was revealed to exert a dominant negative effect on wild-type PLN, resulting in superinhibition of Ca<sup>2+</sup> affinity for SERCA2a and cardiac contractility. The mechanisms by which the mutant PLN mediates its effects are likely related to its structure, which is predominantly monomeric due to a destabilized pentameric structure [111]. Furthermore, Arg 14 is a highly conserved

amino acid in PLN, and fulfills the requirement for basic amino acids upstream of the Ser 16 for protein kinase A (PKA) mediated phosphorylation. An enhanced association between mutant PLN and SERCA is suggestive of an inability of phosphorylation by PKA to relieve the inhibitory effects. Thus, increased inhibition of SERCA and prolonged SR Ca<sup>2+</sup> cycling disturbance could lead to ventricular remodeling, which progresses to ventricular failure [111].

Previously in our group, another mutation was also identified in the PLN gene, whereby a C-to-T missense mutation at nucleotide 25 encodes for the conversion of Arg-9 to Cys (PLN R9C) in the cytoplasmic domain [112]. Clinical and pedigree evaluations of the large American family revealed an autosomal dominant inheritance pattern of early onset DCM. In affected individuals, progression to heart failure ensued within 5-10 years of symptom onset, resulting in an approximate average age of death of 25 years [112]. Evaluation of the mutation in cultured HEK-293 cells revealed PLN R9C prevented phosphorylation of wild type PLN by trapping and inactivating PKA, thereby resulting in chronic SERCA2A inhibition. Thus, a dominant diseased phenotype is mediated by the capacity of mutant PLN R9C to inhibit phosphorylation of wild type PLN R9C present in heterozygotes [112].

A transgenic mouse model of this mutation (Tg-PLN R9C) exhibited a comparable cardiac phenotype as its human counterparts, with early onset DCM characterized by increased chamber dimensions and decreased contractility, and rapid progression to heart failure [112, 113]. To better understand the key molecular players and mechanisms responsible for the development of heart failure in this mouse model, a large scale comparative proteomic profiling of ventricular muscle tissue from wild type and Tg-PLN R9C mice was performed during the progression of disease. 593 proteins were identified as significantly differentially expressed in the diseased state, of which the majority (467) were upregulated [113]. These proteins were mapped bioinformatically to several different biological pathways, predominantly including ER-stress response, cytoskeletal remodeling, Ca<sup>2+</sup> signaling responses, and apoptosis. FHL1 was identified among the subset of 40 proteins deemed to be the most differentially expressed (Figure 6A), which was further verified by immunoblot and northern blot analysis (Figure 6B and C) [113]. Thus, Tg-PLN R9C mice recapitulated the human disease phenotype extremely well, proving to be a good model for studying heart failure resulting primarily from disturbances in myocellular calcium.

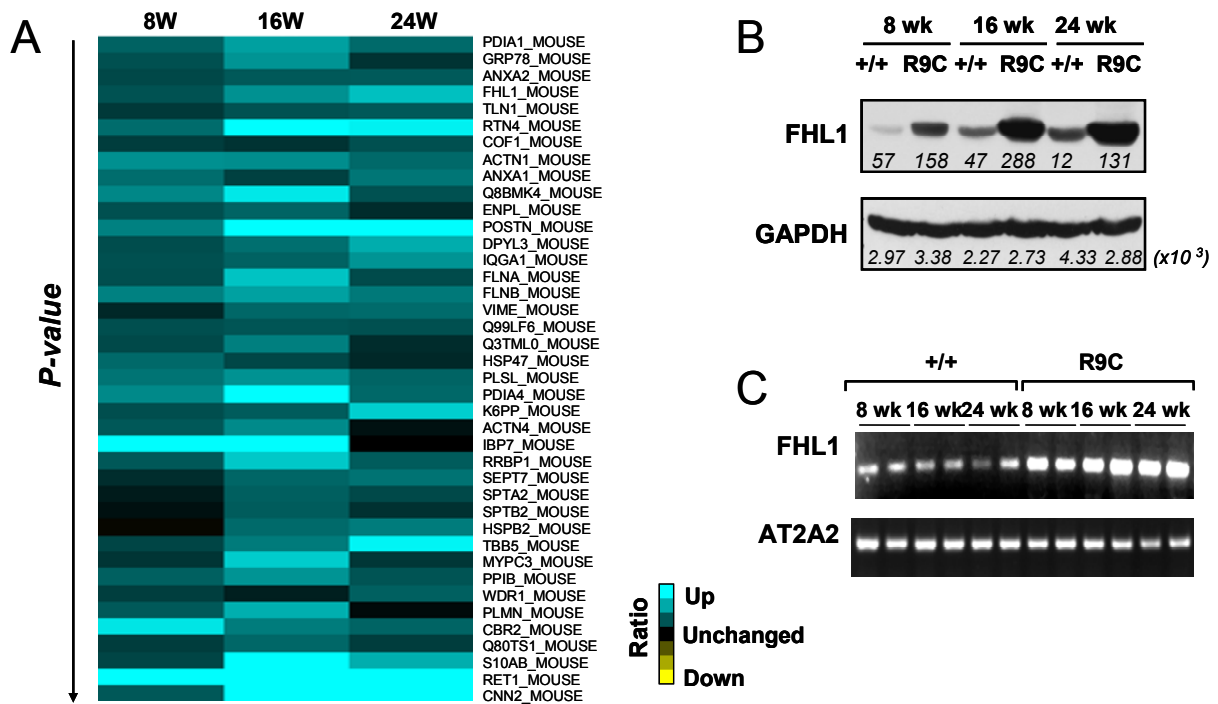


**Figure 6. Significantly upregulated proteins in PLN R9C mice**

**(A)** Hierarchical clusters of the 40 most up-regulated proteins detected in transgenic PLN R9C mice ventricles by MS. Heatmap depicts ratios of spectral counts in PLN R9C:wildtype at 8, 16, and 24 weeks of age. **(B)** Immunoblot analysis of FHL1 protein levels in wildtype and PLN R9C mice cardiac tissue throughout disease progression. GAPDH was used as a control. Spectral counts are shown below. **(C)** RT-PCR analysis of FHL1 transcript level in wildtype and PLN R9C mice at 8, 16, and 24 weeks. AT2A2 served as a control. Modified data from Gramolini, A.O., *et al.* Mol Cell Proteomics, 2008. 7(3): p. 519-33.

## **V. STATEMENT OF INTENT**

FHL1 is the most broadly expressed member of the family of FHL proteins, and likewise implicated in a broad array of biological processes. Furthermore, in several disease conditions where FHL1 is differential expressed, FHL2 and FHL3 expression levels have remained unaltered. Thus, considering the diversity of its associations, FHL1 likely mediates its biological functions in conjunction with other proteins. Theoretically, thus, identifying interacting partners of FHL1 would provide insight into its regulation and regulatory functions.

*The overall objectives of this thesis project are to:*

- I. Identify FHL1 protein complexes using affinity tagged fusion proteins, protein biochemistry, and mass spectrometry;**
- II. Identify any correlations between FHL and interacting candidates in the Tg-PLN R9C model of DCM using pull-down assays and data-mining of the previously performed microarray study;**
- III. Validate protein interactions with FHL1;**
- IV. Identify subcellular distribution patterns of protein interactors.**

## CHAPTER TWO: MATERIALS AND METHODS

### I. DUAL AFFINITY TAGGING OF FHL1

#### I.A Preparation of Origene Clones

**I.A.1 Resuspension of OriGene Clones:** The cDNA clones for FHL1, dihydropyrimidinase-like 3 (DPYSL3), and cellular retinol-binding protein 1 (RBP1) were purchased from OriGene (catalog numbers TC119225, TC119256, and TC30328 respectively) and provided as a lyophilized product. cDNAs were resuspended in 15  $\mu\text{L}$  of water in their original tubes and left at room temperature for 10 minutes before being vortexed for 10 seconds. Their resulting concentrations were 66  $\mu\text{g}/\mu\text{L}$ . DPYSL3 and RBP1 were to serve as tag controls.

**I.A.2 Chemical Transformation of DH5- $\alpha$  cells:** The cDNA vectors were then introduced into *Escherichia coli* strain DH5- $\alpha$  cells by chemical transformation. Briefly, 3  $\mu\text{L}$  of plasmid DNA was added to 50  $\mu\text{L}$  of DH5- $\alpha$  cells and incubated on ice for 30 minutes and then heat shocked for 45 seconds at 42°C. The cells were then shaken for 1 hour at 37°C with 950  $\mu\text{L}$  of SOC media (Sigma). Finally, the transformed cells were pelleted by centrifugation (10000 rpm, 1 minute), resuspended in 150  $\mu\text{L}$  of SOC media, and spread onto LB agar plates with ampicillin resistance (50  $\mu\text{g}/\text{mL}$ ) under sterile conditions. The plates were incubated overnight at 37°C.

**I.A.3 Amplification and Maxi Preparations of DNA:** To amplify the cDNA, 250 mL of sterile 2x YT liquid culture (BioShop) with ampicillin (50  $\mu\text{g}/\text{mL}$ ) was inoculated with a sample of DH5- $\alpha$  cells picked from an individual colony from the LB agar plates. The cultures were shaken overnight at 37°C. To isolate the plasmid DNA, the maxi preparation method was performed using Qiagen's Plasmid Maxi Kit. Approximately after 16-18 hours of shaking, the bacterial culture was centrifuged at 4100 rpm for 15 minutes at 4°C and the supernatant discarded. The pellet was completely resuspended in 10 mL of cold P1 Resuspension Buffer containing RNase, with vortexing. 10 mL of P2 Lysis Buffer was then added and thoroughly mixed by gently inverting the tube several times. Immediately after, the reaction was terminated with the addition of 10 mL of P3 Neutralization Buffer and mixing by inverting. The samples were incubated on ice for 20 minutes and then centrifuged at 4100 rpm for 20 minutes at 4°C.

The resulting supernatant was applied to a QIAGEN-tip 500 column, which was already equilibrated by allowing 20 mL of Buffer QBT to drain through by gravity flow. Three successive washes were performed with 30 mL of Buffer QC to remove all contaminants. 15 mL of Buffer QF was then added to elute the bound DNA and collected in a centrifuge tube. To precipitate the DNA, 10.5 mL of isopropanol was added and mixed by inverting and centrifuged immediately at 12000 rpm for 30 minutes at 4°C. The supernatant was discarded slowly and the DNA pellet was washed by adding 20 mL of 70% ethanol and centrifuging at 12000 rpm for 15 minutes at 4°C. The supernatant was again removed slowly and the pellet was allowed to air-dry to remove all traces of ethanol. Finally, the pellet was dissolved in 1 mL of TE Buffer and the resulting DNA concentration was determined using a Ultrospec™ 2100 *pro* UV/Visible Spectrophotometer (GE Healthcare).

## **I.B Insertion into TOPO Vectors**

### **I.B.1 Polymerase Chain Reaction (PCR) to Remove Stop Codons and Add Restriction Sites:**

The cDNA clones purchased from OriGene contained stop codons. Since the proteins of interest were to be C-terminally tagged, PCR reactions were performed to 1) amplify the full length cDNA of interest without the stop codon, and 2) introduce novel restriction enzyme recognition sequences. For all three cDNAs of interest, an EcoRI restriction site was to be introduced at the 5' end of the sequence and a SalI restriction site at the 3' end. This would later allow for the full length cDNA to be restriction enzyme digested and subsequently ligated into Stratagene's pCTAP vector in-frame with dual affinity tags. Primers were designed using an on-line program (<http://www.yeastgenome.org/cgi-bin/web-primer>) and ordered from Sigma-Genosys Canada. Table 4 lists the primers used. PCR reactions consisted of 5µL of Taq Buffer (Fermentas), 1µL of dNTP Mix (Fermentas), 2µl Forward Primer, 2µl Reverse Primer, 0.5µl Taq Polymerase (Fermentas), 4µl MgCl<sub>2</sub> (Fermentas), 1µl DNA template (50ng/µL), and 34.5µl water. PCR was performed using the Primus 96 Plus Thermal Cycler (MWG-Biotech). The amplification cycle of the specific cDNA consisted of 3 sequential steps repeated 45 times: 1) denaturation at 95°C for 30 seconds; 2) annealing at 53°C for 1 minute; and 3) extension at 70°C for 2 minutes. To ensure that all PCR products were fully extended, a 7 minutes extension at 72°C was included after the last cycle.

**Table 4. List of Primers Used For Cloning**

CDNA	INSERT	FORWARD PRIMER	REVERSE PRIMER
FHL1	842 bp	AAGAATTCTGGGCACCATGGCGGAGAAG	GTCGACCAGCTTTTTGGCACAGTC
DPYSL3	1712 bp	AAGAATTCCACCGCCACCATGTCCTACC	GTCGACACTCAGAGATGTGATATTAGAAC
RBPI	407 bp	AAGAATTCCCGAAATGCCAGTCGACTTC	GTCGACCTGCACCTTCTTGAATACTTGC

**I.B.2 DNA Agarose Gel Electrophoresis:** To analyze the PCR products, agarose gel electrophoresis was performed. 2  $\mu$ L of 6x DNA Loading Dye (Fermentas) was added to 10  $\mu$ L of sample and loaded onto a 1% DNA agarose gel and electrophoresed for 20 minutes at 100 V in 1x TAE buffer (40 mM Tris-acetate, 1mM EDTA). Gels were prepared by dissolving 1 g of Ultra Pure™ Agarose (Invitrogen) in 100mL of 1x TAE, with heating in a microwave. 1  $\mu$ L of ethidium bromide (EMD Chemicals Inc.) was added to the solution just prior to casting. GeneRuler™ DNA Ladder Mix (Fermentas) was used to gauge molecular weights, whilst viewed on a UV light box.

**I.B.3 TOPO Cloning:** To insert the amplified PCR products into pCR®2.1-TOPO® vectors, TOPO cloning reactions were performed using Invitrogen's TOPO TA Cloning® product. Briefly, 2  $\mu$ L of fresh PCR product was mixed with 1  $\mu$ L of Salt Solution and 3  $\mu$ L of sterile water, and incubated at room temperature for 30 minutes. DH5- $\alpha$  cells were transformed with the cloned products and plated onto ampicillin (50  $\mu$ g/mL) LB agar plates.

**I.B.4 Minipreparation of DNA:** To identify individual colonies of cells containing pCR®2.1-TOPO® vectors with the cDNA inserts, restriction enzyme digestion, DNA agarose gel electrophoresis, and nucleotide sequencing needed to be performed. First, for smaller scale amplification of the plasmid DNA, 2 mL of sterile 2x YT liquid culture with ampicillin was inoculated with a sample of DH5- $\alpha$  cells picked from an individual colony from the LB agar plates. The cultures were shaken overnight at 37°C. To isolate the amplified plasmids, the minipreparation method was performed using buffers from the QIAprep Spin Miniprep Kit (Qiagen). Approximately after 16-18 hours of shaking, the bacterial culture was centrifuged at 14000 rpm for 30 seconds at room temperature and the supernatant discarded. The pellet was completely resuspended in 100  $\mu$ L of ice-cold P1 Resuspension Buffer containing RNase, with vortexing. 100  $\mu$ L of P2 Lysis Buffer was then added and mixed gently by inverting. Immediately after, the reaction was terminated with the addition of 100  $\mu$ L of P3 Neutralization Buffer and mixing by inverting. The samples were then centrifuged (10 minutes, 14000 rpm,

room temperature) and the resulting supernatant, containing the plasmid DNA, was transferred to a new microcentrifuge tube. 1 mL of 100% ethanol was added to the supernatant and incubated on ice for 2-5 minutes before centrifugation (2 minutes, 14000 rpm, room temperature). The supernatant was discarded and the plasmid DNA pellet was air dried to remove all traces of ethanol (~ 30 minutes). Finally, the pellet was dissolved in 50  $\mu$ L of EB buffer.

#### **I.B.4 Validation by Restriction Enzyme Digestion and Sequencing of Plasmid**

**DNA:** To confirm insertion of the cDNA into the vector, 3  $\mu$ L of DNA was digested with 0.5  $\mu$ L of EcoRI (Fermentas) and 0.5  $\mu$ L of Sall (Fermentas) in 1  $\mu$ L of Buffer 3 (Fermentas), 4  $\mu$ L of water, and 1  $\mu$ L of 10x BSA (Fermentas). The reactions were incubated at 37°C for 1 hour. To analyze the digestion products, agarose gel electrophoresis was performed with 10  $\mu$ L of sample. Samples which appeared to contain the cDNA insert were subsequently submitted for nucleotide sequencing at Sigma Genosys Canada. The generic M13 Forward and Reverse Primers were used to verify cDNA insertion.

### **I.C Insertion into pCTAP Vectors**

**I.C.1 Preparation of pCTAP Vector:** For additional purification experiments, proteins were fused with streptavidin binding peptide (SBP) and calmodulin binding peptide (CBP) affinity tags. For C-terminal tagging, the pCTAP vector was purchased from Stratagene. Prior to use, the vector was amplified in 250 mL of sterile 2x YT growth media containing kanamycin (10  $\mu$ g/mL) resistance and subsequently recovered using Qiagen's maxi preparation kit.

**I.C.2 Digestion Reactions to Recover cDNA Inserts:** Since the cDNAs of interest were inserted into the pCR<sup>®</sup>2.1-TOPO<sup>®</sup> vector with novel restriction enzymes sites compatible with the pCTAP vector, restriction enzyme digestion was performed to recover the cDNA inserts, using 25  $\mu$ L of cDNA containing pCR<sup>®</sup>2.1-TOPO<sup>®</sup> vectors and EcoRI and Sall restriction enzymes. Simultaneously, 10  $\mu$ L of pCTAP vector was similarly digested. Both reactions were performed at 37°C for 1 hour, before addition of 2  $\mu$ L of shrimp alkaline phosphatase (Fermentas) to the pCTAP digestion reaction and incubation at 37°C for 30 minutes.

**I.C.3 DNA Gel Electrophoresis and Gel Extraction:** DNA gel electrophoresis was then performed with 50  $\mu$ L of the pCR<sup>®</sup>2.1-TOPO<sup>®</sup> vector digestion reaction samples upon termination. While viewing the DNA agarose gel on an UV light box, the band corresponding to the cDNA of interest was excised from the gel using a blade or scalpel and placed into a microcentrifuge tube. Recovery of DNA from agarose gels was performed using Qiagen's

QIAquick Gel Extraction Kit. 500  $\mu$ L of Buffer QC was added to the microcentrifuge tube and incubated at 50°C until the gel had completely dissolved (approximately 10 minutes), occasionally vortexing. 200  $\mu$ L of isopropanol was then added to the sample and mixed. To remove the DNA from the solution, the sample was added to a QIAquick spin column placed in a 2 mL collection tube and centrifuged for 1 minute at 5000 rpm. The collection tube, containing the flowthrough, was emptied and replaced onto the spin column. 750  $\mu$ L of Buffer PE was then added to the column and, after 2-5 minutes of incubation at room temperature, was centrifuged for 1 minute at 5000 rpm. Once again, the collection tube was emptied of the flowthrough and replaced on the spin column for an additional spin at 14000 rpm for 30 seconds to ensure removal of any residual ethanol. The spin column was then placed in a new 1.5 mL microcentrifuge tube and the bound DNA eluted by the addition of 50  $\mu$ L of Buffer EB to the membrane and centrifuged for 5 minutes at 14000 rpm.

**I.C.4 Ligation Reactions and Amplification of DNA:** Next, ligation reactions were performed overnight at 4°C, with varying insert to vector volume ratios. In general, a 2:1 ligation reaction consisted of 1  $\mu$ L of vector, 2  $\mu$ L of cDNA insert, 1  $\mu$ L of T4 DNA Ligase (Fermentas), 1  $\mu$ L T4 DNA Ligase Buffer (Fermentas), and 5  $\mu$ L of water. DH5- $\alpha$  cells were then transformed with 3  $\mu$ L of ligation samples by chemical transformation, and plated overnight onto LB agar plates with kanamycin (10  $\mu$ g/mL) resistance. To identify individual colonies of cells containing pCTAP vectors with the cDNA inserts, transformed DH5- $\alpha$  cells were grown in 2 mL of sterile 2x YT liquid culture with kanamycin (10  $\mu$ g/mL) and the plasmids isolated by the minipreparation method.

**I.C.5 Validation by Restriction Enzyme Digestion and Sequencing of Plasmid DNA:** To confirm insertion of the cDNA, 3  $\mu$ L of plasmid DNA was digested as previously described, using EcoRI and Sall enzymes. To analyze the digestion products, agarose gel electrophoresis was performed with 10  $\mu$ L of sample. Plasmid samples which appeared to contain the cDNA insert were subsequently submitted for nucleotide sequencing at ACGT Corporation. The generic T3 Reverse and T7 Forward Primers were used to verify cDNA insertion into the pCTAP vectors.

## **II. TANDEM AFFINITY PURIFICATION**

### **II.A Tissue Culturing**

**II.A.1 Culturing HEK-293 Cells:** HEK-293 cells were used for the expression and affinity purification of SBP/CBP tagged proteins. HEK-293 cells were cultured in Dulbecco's Modified Eagle's Medium (DMEM) H21 (Tissue Culture Media Facility at University Health Network, Toronto) in a 37°C, 5% CO<sub>2</sub>, humidified incubator. The DMEM H21 media was supplemented with 10% fetal bovine serum (Gibco), 1x MEM Non-Essential Amino Acids Solution (Gibco), and 2.5µg/mL amphotericin-β (Sigma-Aldrich). Stock cultures were maintained in 75 cm<sup>2</sup> cell culture flasks (BD Falcon), in 12 mL of media. Confluent (80-100%) flasks of HEK-293 cells were plated at a dilution of 1 into 5 to ensure 50-70% confluency of cells the next day for transfection. For affinity purification, ten 100 mm plates of cells were plated in 10 mL of media.

**II.A.2 Transfection of Cells:** Transfection of cells was performed the next day using the calcium phosphate transfection method. For 10 plates of HEK-293 cells, at 50-70% confluency, a 5 mL solution was prepared with 620 µL of 2M CaCl<sub>2</sub>, 100 µg of DNA, and 4.3 mL of sterilized water. The solution was lightly mixed before being added drop wise to 5 mL of 2x HEPES (274 mM NaCl, 1.4 mM Na<sub>2</sub>HPO<sub>4</sub>·7H<sub>2</sub>O, 54 mM HEPES) and let stand 20 minutes at room temperature. 1 mL of the final solution was then added drop wise to each plate. The cells received fresh media 18-24 hours later.

### **II.B Tandem Affinity Purification**

**II.B.1 Harvesting HEK-293 Cells and Preparing the Protein Extract:** 40-48 hours following calcium phosphate transfection, cells were harvested from their plates with an ice cold solution of 1x PBS (137 mM NaCl, 10 mM Phosphate, 2.7 mM KCl, pH of 7.4) with 5 mM EDTA. The cells were then pelleted by centrifugation (4100 rpm, 5 minutes, 4°C) and washed in ice cold 1x PBS. For TAP, Stratagene's InterPlay® Mammalian TAP Purification Kit was used (Figure 7). Following centrifugation (4100 rpm, 5 minutes, 4°C) and removal of the supernatant, the cells were resuspended in 2 mL of Lysis Buffer supplemented with 1 mM PMSF and 1x protease inhibitor. The cells were then subjected to three successive rounds of freeze-thawing by incubation in dry ice for 10 minutes followed by cold water for 10 minutes. Furthermore, the cells were homogenized on ice in a Dounce homogenizer (30 strokes with a loose pestle) and then incubated on ice for 1 hour, with occasional vortexing. To remove the

cell debris, the lysate was then centrifuged at 8000 rpm for 20 min at 4°C. The resulting supernatant, the protein extract, was supplemented with 10 mM  $\beta$ -mercaptoethanol and 2 mM EDTA.

**II.B.2 Purifying the Protein Complexes Using Streptavidin Resin:** While preparing the protein extract, 50  $\mu$ L of a 50% streptavidin resin slurry was prepared by washing twice with 1 mL of ice cold Streptavidin Binding Buffer (SBB) with centrifugation (3800 rpm, 5 minutes, 4°C). The SBB was supplemented with 10 mM  $\beta$ -mercaptoethanol, 1 mM PMSF, and 1x protease inhibitor prior to use. These washes were essential to remove any trace of ethanol present in the resin slurry storage buffer. The protein extract was then added to the washed resin and rotated for 2 hours at 4°C to allow the tagged proteins to bind streptavidin via the SBP tag. Protein bound to the streptavidin resin were then separated from the flowthrough by centrifugation (3800 rpm, 5 minutes, 4°C) and washed thrice in 1 mL of supplemented SBB by rotating for 5 minutes at 4°C followed by centrifugation (3800 rpm, 5 minutes, 4°C). Next, bound protein were eluted twice with 100  $\mu$ L for 1 hour with ice cold Streptavidin Elution Buffer with 10 mM  $\beta$ -mercaptoethanol, 1 mM PMSF, and 1x protease inhibitor.

**II.B.3 Purifying the Protein Complexes Using Calmodulin Resin:** To further purify the tagged protein complexes, the streptavidin eluted samples were allowed to bind calmodulin resin via their CBP tag. First, similar to streptavidin resin, 25  $\mu$ L of a 50% calmodulin resin slurry was prepared by washing twice with 1 mL of ice cold Calmodulin Binding Buffer (CBB) with centrifugation (3800 rpm, 5 minutes, 4°C). The CBB was first treated with 10 mM  $\beta$ -mercaptoethanol, 1 mM PMSF, and 1x protease inhibitor. The streptavidin elutions were then pooled and treated with 4  $\mu$ L of Streptavidin Supernatant Supplement and 800  $\mu$ L of CBB before rotating at 4°C overnight. The next day, calmodulin bound protein were separated from the flowthrough by centrifugation (3800 rpm, 5 minutes, 4°C) and washed twice in 1 mL of supplemented CBB by rotating for 10 minutes at 4°C followed by centrifugation (3800 rpm, 5 minutes, 4°C), and washed once in CBB with only 10 mM  $\beta$ -mercaptoethanol. To elute the purified proteins, two successive 1 hour elutions were performed at 4°C on a rotator with 100  $\mu$ L of ice cold Calmodulin Elution Buffer.

### **III. SDS-POLYACRYLAMIDE GEL ANALYSIS**

Following purification, protein samples could be resolved on a gel via sodium dodecyl sulfate polyacrylamide gel electrophoresis (SDS-PAGE) and analyzed by a variety of methods.

To detect all proteins present, coomassie blue staining and silver staining was used, whereas immunoblot was used to detect the presence of specific proteins of interest.

### **III.A Polyacrylamide Gel Electrophoresis**

First, 10% SDS-polyacrylamide gels were prepared by the addition of resolving gel solution (water, 37.5:1 Acrylamide/Bis Mix (BIO-RAD), 1.5 M Tris (pH 8.8), 10% SDS (EMD), 10% Ammonium Persulfate (VWR International), TEMED (EMD)) and allowed to solidify. Stacking gel solution (water, 37.5:1 Acrylamide/Bis Mix, 1.5 M Tris (pH 6.8), 10% SDS, 10% Ammonium Persulfate, TEMED) was then added and allowed to solidify. Next, samples to be resolved were denatured by the addition of 6x Protein Loading Dye and boiling for 10 minutes before being loaded onto gels and resolved by electrophoresis. PageRuler™ Prestained Protein Ladder (Fermentas) was used as a protein standard to gauge molecular weights.

### **III.B Coomassie Blue Staining of Proteins**

To non-specifically stain proteins present in SDS-PAGE gels, resolved gels were transferred to clean dish and incubated overnight on a shaker with Coomassie Blue Stain (BioRad). The next day, excess dye was removed by incubating in water, on a rocker. Finally, gels could be viewed on a white light transilluminator.

### **III.C Immunoblot Detection of Proteins**

For immunoblotting, proteins were first transferred from the polyacrylamide gel to a nitrocellulose membrane. The blots were then blocked in 1x PBS with 0.2% Tween 20 (Sigma) (PBS-T) and 5% fat free milk for 1 hour at room temperature and incubated with primary antibody diluted in 5% milk-PBS-T solution overnight at 4°C, both on a shaker. Three 15 minutes washes with PBS-T were performed the next day, followed by incubation with HRP-conjugated secondary antibody diluted in 5% milk-PBS-T solution for 1 hour at room temperature with shaking. Following three 15 minutes washes with PBS-T, blots were treated with SuperSignal West Pico Chemiluminescent Substrates (Pierce) for 5 minute and then exposed to film in a dark room setting, which was subsequently developed. Dilutions for the various commercially available antibodies used for immunoblotting are as such: anti-CBP tag (1:500; Santa Cruz), anti-V5 tag (1:2000; Invitrogen), anti-FHL1 (1:5000, Imgenex), anti-GSN (1:3000; BD Bioscience), anti-ACTN1 (1:1000; Santa Cruz), anti-RYR1 (1:2500; ABR). All

HRP-conjugated secondary antibodies, anti-mouse (Promega) and anti-goat (Santa Cruz), were diluted at 1:2500.

### **III.D Silver Staining of Proteins**

For silver staining, the resolved polyacrylamide gel was placed in a clean dish and all subsequent steps were performed at room temperature, with 50 mL of freshly prepared solutions, with gentle rocking. First, the gel was fixed with Solution A (50% methanol, 10% acetic acid) for 30 minutes. Next, it was incubated in Solution B (50% methanol) for 15 minutes followed by three 5 minute washes performed with milli-Q water. The gel was then incubated with Solution C (0.2g/L of sodiumthiosulphate) for two minutes before subjected to three additional washes with milli-Q water, 30 seconds each. The gel was then treated with chilled Solution D (2g/L of silver nitrate) for 25 minutes, followed by three 1 minute washes performed with milli-Q water. To develop the gel, Solution E (30g/L of sodium carbonate, 0.5mL/L of 37% formaldehyde, and 20mL/L of Solution C) was used. This step was monitored to gauge optimal staining (usually 3-5 minutes). Once sufficient staining was achieved, developing was terminated by treatment with Solution F (14g/L of EDTA) for 10 minutes. Finally, the gel was washed and stored in milli-Q water.

## **IV. MASS SPECTROMETRY ANALYSIS**

### **IV.A Preparation of Samples**

**IV.A.1 Tryptic Digestion:** Once the protein complexes were purified on the calmodulin resin, several different tryptic digest methods were applied to prepare the sample for subsequent mass spectrometry analysis (Figure 7), specifically in-solution digestion, on-bead digestion, and in-gel digestion methods. Both in-solution and on-bead digestions were performed with non-denatured protein structures, while denatured proteins are trypsin digested with the in-gel digestion method.

**IV.A.1.i In-Solution Tryptic Digestion:** Trypsin digestion was performed of eluates from calmodulin resin by the addition of 25 ng/uL of trypsin (Promega) and 27 mM of CaCl<sub>2</sub>. Excess CaCl<sub>2</sub> was necessary to quench the EDTA used in calmodulin elutions.

IV.A.1.ii *On-Bead Tryptic Digestion*: Instead of eluting off calmodulin beads, on-bead digestion was also performed. Following the third wash with CBB, Trypsin Digestion Buffer (50 mM  $\text{NH}_4\text{HCO}_3$  (pH 8.0), 1mM  $\text{CaCl}_2$ , 25 ng/uL Trypsin) was added to the beads and rotated overnight at 37°C.

IV.A.1.iii *In-Gel Tryptic Digestion*: Purified samples were also denatured from calmodulin beads by boiling in 6x Protein Loading Buffer and subjected to SDS-PAGE followed by silver staining. In-gel tryptic digest was performed to generate and extract digested peptides [114]. First, each lane was divided into multiple blocks with a clean scalpel or razor blade, and each block was subsequently diced into ~9 pieces and transferred into a clean 1.5mL microcentrifuge tube. To each block of gel pieces, 500uL of acetonitrile was added and incubated at room temperature, with occasional vortexing. When the gel pieces had shrunk and turned white in colour, the acetonitrile was removed and 100 uL of a 100mM ammonium bicarbonate with 10 mM DTT solution was added and incubated at 56°C for 30 minutes. The samples were then equilibrated with room temperature before adding 500uL of acetonitrile for 10 minutes. Next, the acetonitrile was replaced with approximately 100 uL of freshly prepared 55mM iodoacetamide in 100mM ammonium bicarbonate to completely cover the gel pieces and incubated at room temperature in the dark for 20 minutes. The pieces were shrunk again with the addition of 500uL of acetonitrile for 10 minutes. Then, to saturate the gel pieces with trypsin, they were completely submerged in Trypsin Buffer (10mM ammonium bicarbonate, 10% acetonitrile, 13 ng/uL Trypsin) and incubated on ice for 90 minutes. When required, 10mM ammonium bicarbonate buffer was used to replenish the buffer volume. The samples were then incubated at 37°C overnight on a rotator. The next day, the samples were removed to RT and the peptide containing supernatant was transferred to a new tube. Approximately 100uL Extraction Buffer (1:2 ratio of 5% Formic Acid:Acetonitrile) was added to the gel pieces, vortexed, and incubated at 37°C for 15 minutes on the rotator. This step was repeated once more. All peptide extraction solutions were pooled together and vacuum-dried at 45°C to approximately 10 uL. A final volume of about 50 uL was established with the addition of Buffer A (5% acetonitrile, 0.1% Formic Acid in HPLC-grade water).

**IV.A.2 Solid-Phase Extraction of Tryptic Peptides:** Prior to subjecting trypsin digested samples to mass spectrometry analysis, solid-phase extraction was performed using OMIX C-18 pipette tips (Varian Inc.) to purify the peptides from potential contaminants. First, to condition

the OMIX C-18 pipette tip, 110uL of Solution 1 (50% Acetonitrile) was passed through the tip twice. The column was then equilibrated twice with 110uL of Solution 2/3 (0.1% TFA). The tryptic digest samples, with 40 uL of added 2.5% TFA, was then added to the column and let drain slowly through to allow the peptides to bind the column. The pass-through was collected and reapplied to the column. This step was repeated a total of four times. Next, the tryptic peptide bound column was washed once with 110uL of Solution 2/3 and then eluted twice with 110 uL of Solution 4 (70% Acetonitrile, 0.1% TFA). To concentrate the pooled eluate to about 30 uL, speed vacuum was performed at 45°C.

## **IV.B Mass Spectrometry**

**IV.B.1 Sample Preparation and LC-MS Analysis:** Speed vacuum concentrated samples were resuspended in 20 µL of Solution 1 (50% Acetonitrile) and acidified by the addition of 5% formic acid. Following this, LC-MS was performed on tryptic peptides by Thomas Kislinger, at the University of Toronto (Figure 7). First, microcapillary fused silica columns with an internal diameter of 75 µm were pulled to a fine tip using a P-2000 laser puller (Sutter Instruments) and packed with 7 cm of Magic C18 100 Å reversed phase resin (Michrom Bioresources). Prepared samples were loaded manually onto columns using an in-house pressure vessel. The columns were aligned with an LTQ linear ion trap mass spectrometer (Thermo Scientific) equipped with a nano-electrospray source (Proxeon Biosystems). The bound peptides were eluted using a conventional water/acetonitrile gradient, over a period of 2 hours, and transferred via electrospray ionization directly into the mass spectrometer.

**IV.B.2 Protein Identification:** Raw files were converted to m/zXML using the ReAdW algorithm and searched by X! Tandem (<http://www.ebi.ac.uk/IPI>) against the human IPI (International Protein Index) protein sequence database. To address and minimize the false positive rate in the database search, all fragment spectra were searched against the IPI human reversed database [115, 116]. The false discovery rate was set to 0.5 % at the protein level [115, 116]. Only peptides matching these criteria were accepted to generate the final list of identified proteins, with further consideration given only to proteins identified with a minimum of two unique peptides.

## **V. IN VITRO FHL1 PULL DOWN ASSAYS FROM MICE VENTRICULAR LYSATES**

### **V.A Preparation of FHL1 Containing Protein Lysate from HEK-293 Cells**

HEK-293 cells were cultured as previously described for TAP experiments. However, in order to generate sufficient amounts of an alternatively dual tagged FHL1 protein for two different experimental conditions, 44 100 mm plates of cells were generated. Cells were transfected using calcium phosphate with pQE-TriSystem vectors encoding for full-length human FHL1 as a fusion protein with Strep-II and 8x histidine (His) tags. 48 hours later, cells were harvested and resuspended in 10mL of Lysis Buffer (250 mM sucrose, 50 mM Tris-HCl (pH 7.6), 1 mM MgCl<sub>2</sub>, 1 mM  $\beta$ -mercaptoethanol, 1mM PMSF, and 1x protease inhibitor). To generate a protein extract, the cells were homogenized on ice with 30 strokes using a loose-fitting pestle, followed by a 1 hour incubation on ice and centrifugation (8000 rpm, 20 minutes at 4°C). The supernatant was retained.

### **V.B Immobilization of FHL1 onto TALON® Metal Affinity Resin**

First, 80  $\mu$ L of a resin slurry was suspended in 1 mL of Lysis Buffer and centrifuged at 8000 rpm for 30 seconds at 4°C. Upon removal of the storage buffer, the resin was simultaneously washed and blocked by rotating twice for 20 minutes at 4°C in 1 mL of Lysis Buffer supplemented with 5 mM imidazole. Prepared resin was then rotated overnight at 4°C with the protein lysate described above, supplemented with 5 mM imidazole, which allows for sufficient binding between the resin and the 8xHis residues of tagged FHL1. The next day, four 15 minute washes were performed with 1 mL Wash Buffer (50 mM sodium phosphate, 300 mM NaCl, 0.05% Triton X-100, 0.1% CHAPS, 1 mM  $\beta$ -mercaptoethanol, 20 mM imidazole, 1mM PMSF, and 1x protease inhibitor), with centrifugation (4100 rpm, 3 minutes, 4°C). These stringent washes allowed for effective purification of tagged FHL1 alone.

### **V.C Preparation of Protein Lysate from Mice Ventricular Tissue**

**V.C.1 Maintenance of Animal Populations:** All mice, *Mus Musculus*, were maintained at the Division of Comparative Medicine, University of Toronto, including a population of Tg-PLN R9C mice. The transgenic mice express the PLN R9C mutant transgene under the control of the  $\alpha$ -cardiac myosin heavy chain promoter. Animals were maintained according to

guidelines set in place by the CCAC (Canadian Council of Animal Care) and protocols were approved by the Animal Care Committee at the University of Toronto.

**V.C.2 Generation of a Ventricular Protein Lysate:** Upon CO<sub>2</sub> asphyxiation euthanization, whole hearts were extracted from 16 weeks old wild type and transgenic female mice and washed in ice-cold 1x PBS. A total of two hearts were obtained for each condition. Ventricular tissues were then isolated and minced before homogenizing in 3 mL of ice-cold co-IP Lysis Buffer with a polytron homogenizer. Samples were then incubated on ice for 30 minutes before centrifugation at 2600 rpm for 15 minutes at 4°C. The resulting supernatant corresponded to the ventricular protein lysate.

#### **V.D Formation of FHL1 Interactions *In Vitro***

The resulting cardiac lysates (from wild type and transgenic mice) were then rotated overnight, at 4°C, with the one half of the resin immobilized FHL1 preparation. Next, five 10 minute washes were performed, all at 4°C, with 1 mL of Wash Buffer (25 mM Tris-Cl, 150 mM NaCl, pH 7.4). Final samples were recovered from the resin with two 30 minute elutions with 500µL of Elution Buffer (25 mM Tris-Cl, 300 mM NaCl, 500 mM imidazole). To concentrate the recovered protein, eluted samples were speed vacuumed at 45°C as required. The samples were analyzed by SDS-PAGE and silver staining.

## **VI. ALTERNATIVE DUAL TAGGING OF BAIT cDNAS**

### **VI.A Amplification of Destination Vector**

The pEF-DEST51 Gateway™ Destination Vector was purchased from Invitrogen (catalog number 12285-011) and provided as a lyophilized product. It was resuspended in 40uL of sterile water for a total concentration of 150ng/uL. To propagate pEF-DEST51 plasmids, a strain of *E. coli* cells resistant to the toxic effects of the *ccdB* gene were necessary. Since DH5- $\alpha$  cells could not be used, One Shot® *ccdB* Survival™ T1 Phage-Resistant Cells were purchased from Invitrogen (catalog number C7510-03). For transformation, a vial of cells was thawed on ice and 100 ng of pEF-DEST51 vector (~ 0.70 µL) was added and gently mixed by tapping. The cells were then incubated on ice for 30 minutes and then heat shocked for 30 seconds at 42°C without shaking. Following 2 minutes of incubation on ice, 250 µL of SOC medium, at room temperature, was added to the cells and shaken for 1 hour at 37°C. Next, the cells were

centrifuged for 1 minute at 14000 rpm and the pellet resuspended in enough SOC media to be plated onto LB agar plates with chloramphenicol (68 µg/mL) resistance. The plates were incubated overnight at 37°C. Transformed cells were grown in 250 mL of LB media with chloramphenicol (68 µg/mL) by inoculation and shaken at 37°C overnight. Amplified plasmids were isolated by maxi preparations.

## **VI.B Amplification of ORFeome Clones**

The cDNA for the potential interactors of interest were obtained from Open Biosystems' Human ORFeome Collection, version 1. The collection consisted of several 96-well microtiter plates containing live bacterial cultures of *E. coli* stored in LB media with an inert growth indicator, 8% glycerol, and spectinomycin (50 µg/mL). All cDNAs were provided in the pDONR223 Entry Vector. For each clone of interest, an inoculum was streaked onto LB agar plates with 50 µg/mL of spectinomycin and incubated overnight at 37°C. Individual colonies were grown 2 mL of sterile 2x YT media with 50 µg/mL of spectinomycin and the amplified clones were purified by the minipreparation method.

## **VI.C ORFeome Cloning**

**VI.C.1 Clonase Mediated Cloning:** To transfer the cDNA insert from the pDONR223 entry vector to the V5 epitope and 6x His (V5/6xHis) tags encoding pEF-DEST51 destination vector, an LR reaction was required. This was carried out using enzymes and reagents purchased from Invitrogen. Briefly, to perform the LR reaction, an 8 µL mixture was first prepared consisting of 1 µL of pEF-DEST51 destination vector (150 ng/µL), 5 µL of entry clone (20 ng/µL), and 3 µL of TE buffer (pH 8.0). The 5X solution of LR Clonase™ II enzyme mix was thawed on ice and briefly vortexed before adding 2 µL to the mixture, which were then incubated at 25°C for 1 hour. To terminate the reactions, 1 µL of Proteinase K solution was added and the samples incubated at 37°C for 10 minutes.

**VI.C.2 Amplification of cDNA Insert Containing pDONR223 Vectors:** DH5- $\alpha$  cells were transformed with the cloned products and plated on LB agar spectinomycin (50 µg/mL) plates overnight. Next, 2 mL of sterile 2x YT bacterial growth media with ampicillin (50 µg/mL) was inoculated with cells from individual colonies overnight. As a counterselection method, 2 mL of sterile 2x YT with chloramphenicol (68 µg/mL) resistance was inoculated from identical colonies. DNA was recovered via minipreparations, only from identical cultures

sets which exhibited growth in ampicillin conditions but not in chloramphenicol. To confirm insertion of the cDNA, nucleotide sequencing was performed by ACGT Corporation, using the generic BGH Reverse and T7 Forward Primers. To generate larger amounts DNA, of successfully cloned constructs, 250 mL of ampicillin (50 µg/mL) LB liquid media (BioShop) supplemented with 2% glucose was innocuated with transformed DH5- $\alpha$  cells and shaken for two days at 30°C.

## **VII. *IN-VIVO CO-IMMUNOPRECIPITATION FROM HEK-293 CELLS AND Tg-PLN R9C MICE***

### **VII.A Preparation of Protein Extracts from HEK-293 Cells and Tg-PLN R9C Mice**

HEK-293 cells were cultured as previously, except only 3 plates of cells were required for each co-immunoprecipitation (co-IP) experiment. Calcium phosphate method was used for co-transfections using equal amounts of FHL1-CBP/SBP and bait-V5/6xHis encoding plasmids. The cells were harvested and lysed in 1mL of ice cold co-IP Lysis Buffer (250 mM sucrose, 50 mM Tris-HCl (pH 7.6), 1 mM MgCl<sub>2</sub>, 1 mM DTT, 1 mM PMSF, and 1x protease inhibitor) by homogenization on ice with 30 strokes using a loose-fitting pestle. The lysate was then incubated on ice for 1 hour, with occasional brief vortexing, and subsequently centrifuged at 8000 rpm for 20 minutes at 4°C. For the preparation of a protein lysate from Tg-PLN R9C mice, ventricular tissue was isolated from 12 weeks old transgenic mice in the same manner described before. Lysates were also similarly prepared using 3 mL of co-IP Lysis Buffer.

### **VII.B Co-Immunoprecipitation**

**VII.B.1 Binding Antibody to Protein A/G-Agarose Resin:** To perform a co-IP experiment, the antibody-resin complexes were prepared first, whilst simultaneously blocked with bovine serum albumin (BSA). To do so, 50 µL of a Protein A/G-agarose resin slurry (Pierce) was incubated with 0.1% BSA (Sigma-Aldrich), 700 µL of Binding Buffer (25 mM Tris-Cl, 150 mM NaCl, pH 7.4), and 6-10 µL of the specific antibody for a minimum of 2 hours on a rotator at 4°C. Protein A/G-agarose beads without bound antibody and beads bound to donkey anti-goat (HRP-conjugated) secondary antibodies (Santa Cruz) served as negative controls.

**VII.B.2 Antibody Mediated Protein Pull Down:** The prepared protein extract was then added to the antibody-resin complex, which was collected by centrifugation (4100 rpm, 3 minutes), and supplemented with 0.1% Triton X-100 and 0.01 % BSA before incubation overnight on the rotator at 4°C. The next day, the samples were washed five times with 1mL of Binding Buffer for 10 minutes on the rotator at 4°C then centrifuged at 4100 rpm for 3 minutes. Finally, the purified samples were eluted with 100 µL of IgG Elution Buffer (Pierce) by rotating for at least 1 hour at 4°C. The eluted sample and resin were separated by centrifugation (8000 rpm, 2 minutes).

## **VIII. CO-IMMUNOFLUORESCENT SUBCELLULAR CO-LOCALIZATION ANALYSIS**

### **VIII.A Slide Preparations of Fixed Cultured Cells**

**VIII.A.1 Culturing C2C12 Mouse Myoblast Cells:** C2C12 myoblast cells were cultured in Growth Media in a 37°C, 5% CO<sub>2</sub>, humidified incubator. The Growth Media consisted of DMEM H21 media supplemented with 20% horse serum (Gibco), 10% fetal bovine serum, 1x MEM Non-Essential Amino Acids Solution, and 2.5µg/mL amphotericin-β. Stock cultures were maintained in 75 cm<sup>2</sup> cell culture flasks, in 12 mL of Growth Media. Culturing of HEK-293 cells was previously described

**VIII.A.2 Plating Slides of HEK-293 Cells and C2C12 Myoblasts:** Sterile glass cover slips were placed in individual wells of a 6-well cell culture plate and coated with warm gelatin (Sigam-Aldrich) and incubated at 37°C for 30 minutes with the lid on. An 80-100% confluent flask of HEK-293 cells was plated at a dilution of 1:18 to ensure 50-70% confluency of cells the next day for transfection. HEK-293 cells were grown in 3 mL of media. For plating C2C12 cells, a dilution of 1:50 was used instead. Transfection of cells was performed the next day using the calcium phosphate method, as previously described. Each well though was treated with only a third of the transfection solution used for one 100 mm plate.

**VIII.A.3 Fixing Slides of Transfected Cultured Cells:** 40-48 hours after transfection, following a 30 minute incubation in 2 mL of ice-cold 1x PBS at 4°C, the cells were fixed with 2 mL of 2% paraformaldehyde (made in 1x PBS, pH 7.4) for 30 minutes at 4°C. Two 1 mL washes were then performed with freshly prepared Permeabilization Buffer (0.2% Tween-20, 0.5% Triton X-100 in 1x PBS) at 4°C for 15 minutes each.

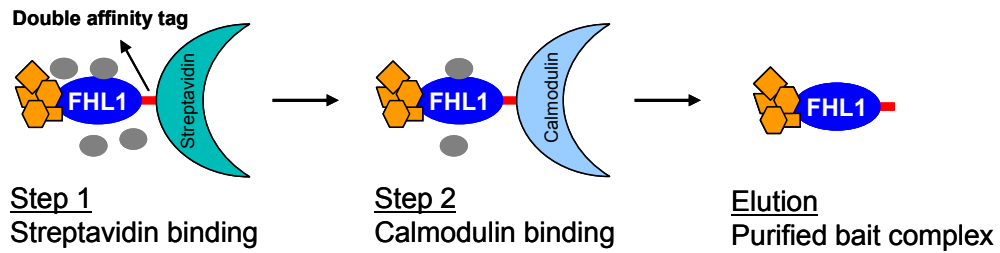
## **VIII.B Slide Preparations of Fixed Isolated Skeletal Soleus Muscle Fibers**

Skeletal slow twitch soleus muscle was kindly provided by Dr. Jeremy Simpson, from the University of Toronto. Muscle fibres were isolated from the hind limbs of adult female Spragley-Dawley rats upon euthanization via CO<sub>2</sub> asphyxiation. Immediately upon isolation, the tissue was incubated in excess ice-cold 1x PBS for 30 minutes before fixation in 2% paraformaldehyde for 30 minutes at 4°C. Two 1 mL washes were then performed, in 1.5 mL microcentrifuge tubes, with freshly prepared Permeabilization Buffer at 4°C for 15 minutes each.

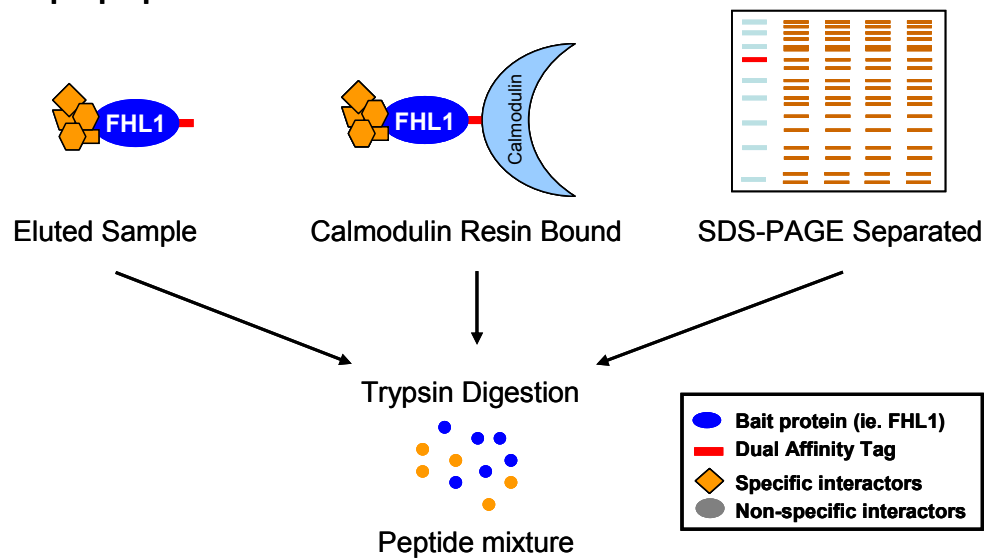
## **VIII.C Co-Immunofluorescent Staining of Fixed Tissue**

Upon paraformaldehyde fixation, washed tissues were then incubated in 1 mL of Blocking Buffer (5% FBS, 0.2% Tween-20, 0.5% Triton X-100 in 1x PBS) for 30 minutes at room temperature. For co-labeling, tissues were then treated with multiple primary antibodies diluted in 100 µL of Blocking Buffer, overnight at 4°C. This was followed by three 15 minute washes with 1 mL of Permeabilization Buffer at room temperature. Next, tissues were incubated in the dark for 1 hour at room temperature with fluorescent secondary antibodies diluted in 100 µL of Blocking Buffer. Subsequently, three 15 minute washes were performed with 1mL of 1x PBS in the dark at room temperature, before mounting in Fluoromount™ medium (Sigma). Dilutions for the various commercially available antibodies used are as such: anti-CBP tag (1:50; ICL), anti-V5 tag (1:200), anti-FHL1 (1:500, Aviva Systems Biology), anti-GSN (1:500), anti-ACTN1 (1:500), anti-RYR1 (1:500). The fluorescent Alexa 488 and Alexa 633 secondary antibodies, anti-mouse and -rabbit (Invitrogen), were diluted at 1:500 and 1:200, respectively.

### Phase 1: Double affinity purification



### Phase 2: Sample preparation



### Phase 3: MS analysis and protein identification

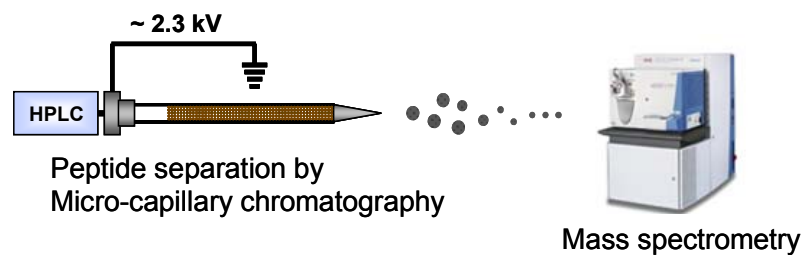


**Figure 7. Tandem Affinity Purification and Mass Spectrometry**

Illustration of the methodologies applied to identify protein interactions. Phase 1 consisted of TAP of dual tagged (SBP/CBP) FHL1 via binding resin immobilized streptavidin and calmodulin protein. Phase 2 involved in-solution, on-bead, or in-gel tryptic digestion of FHL1 and co-purified interacting proteins. To identify the proteins present in the peptide mixture, MS analysis was performed during Phase 3.

## CHAPTER THREE: RESULTS

### ***I. PURIFICATION OF FHL1 CONTAINING PROTEIN COMPLEXES***

Tandem affinity purification was initially developed to purify complex protein aggregates from yeast, such as ribosome, spliceosome, or transcription complexes [81]. This purification method, using a dual-affinity tagged protein of interest, can be combined with subsequent mass spectrometry analysis to identify the co-purified complexing proteins [71, 83]. Stratagene™ developed the Interplay® Mammalian TAP system for purification of fusion proteins from mammalian cells via a streptavidin binding peptide and calmodulin binding peptide. We anticipated that FHL1 could successfully be co-purified with interacting proteins. To distinguish technical artifacts inherent to the purification process, tag-control purifications were performed with two different proteins, DPYSL3 and RBP1, which were similarly tagged. DPYSL3 and RBP1, in conjunction with FHL1, were actually part of a larger project aimed at building a protein-protein interaction network encompassing several proteins found significantly upregulated in Tg-PLN R9C mice during disease. Both proteins were involved in the TAP optimization process and, considering their lack of actin and cytoskeleton associated GO terms, posed as good candidates for tag-controls.

#### **I.A Generation of FHL1-SBP/CBP Expression Constructs**

The full-length cDNAs purchased from OriGene contained a stop codon. In order to generate a C-terminally tagged protein by cloning into the pCTAP mammalian expression vector (Figure 8A), removal of the stop codon was necessary. Straightforward cloning proved to be problematic, necessitating additional steps shuttling the cDNA from one vector to another. Successful cloning of the cDNAs for FHL1 and both tag-controls into the pCTAP vector (Figure 8B) was achieved by: 1) PCR amplification of cDNAs using specific primers to omit the stop codon while introducing EcoRI and SalI restriction enzyme sites; 2) Topoisomerase I mediated cloning into Invitrogen's pCR®2.1-TOPO® vector; and 3) restriction enzyme digestion and insertion from pCR®2.1-TOPO® vectors into pCTAP vectors. To ensure cDNAs insertions were properly oriented and in frame with the tag sequences, nucleotide sequencing was performed using generic T3 Reverse and T7 Forward primers. Figure 8C demonstrates that the translated FHL1 protein sequence is in frame with the affinity tags and lacks an internal stop codon.

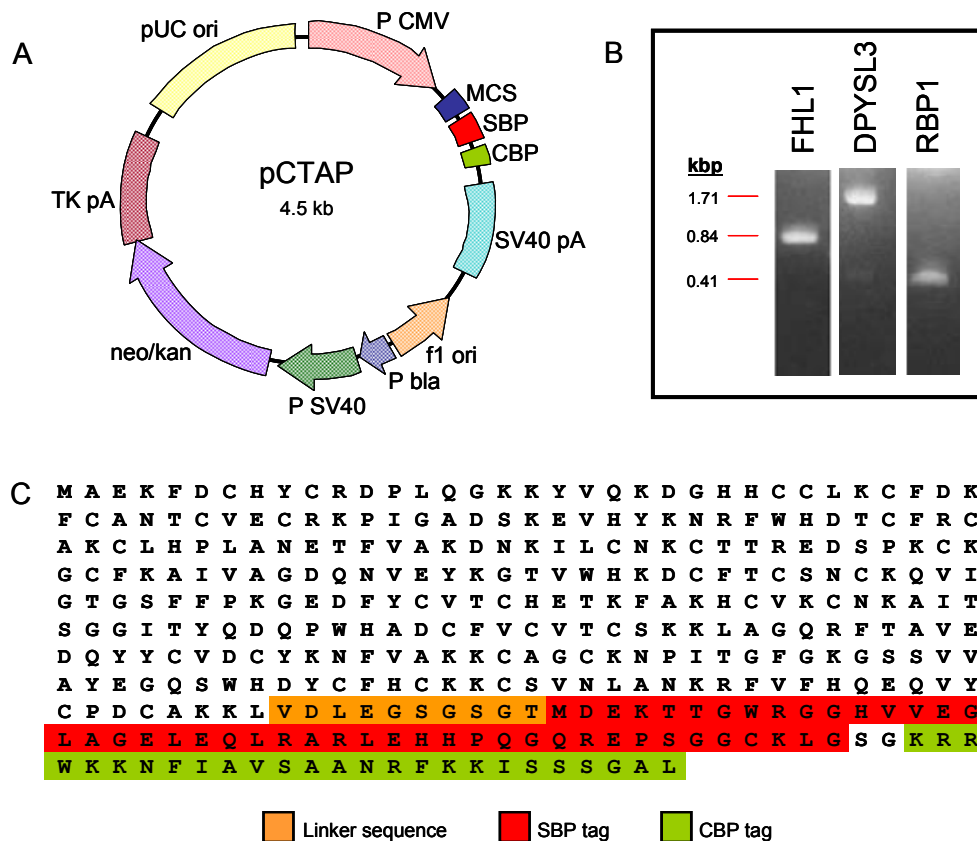


**Figure 8. Generation of FHL1-SBP/CBP Expression Constructs**

(A) Diagram representation of Stratagene's pCTAP vector, which was designed to encode for C-terminal tagging with both affinity tags, with expression in mammalian cells driven by the constitutively active CMV promoter. (B) Validation of cDNA insertion into the pCTAP vector for FHL1, DPYSL3, and RBP1. Plasmid samples were restriction enzyme digested (with EcoRI and Sall) and subjected to DNA gel electrophoresis. (C) Amino acid sequence of FHL1 in frame with the SBP and CBP tags. The protein sequence was determined using an on-line translation application (<http://ca.expasy.org/tools/dna.html>), derived from nucleotide sequencing results of FHL1.

## I.B Expression and Purification of Tagged Bait and Co-Purification of Potential Interactors

To assess for the expression of tagged baits, immunoblot analysis of a cell protein extract was not sufficient due to multiple background bands generated by the anti-CBP antibody (not shown). This issue, however, was resolved by analysis of purified samples (Figure 9). Furthermore, Figure 9 illustrates the efficiency of the applied TAP procedure. For instance, a considerable amount of tagged bait remained in the flowthrough following streptavidin bead binding, likely due to saturation of the volume of beads used. Some bait protein was also lost

during the subsequent washes, though progressively less with each additional wash. The washes were however a necessary component to improve the purity of the final product. In addition, analysis of the eluted beads revealed recovery of the bound bait was not 100%. These findings were similar for purifications using calmodulin resin. Regardless, a significant amount of the expressed recombinant protein could be purified and concentrated. In addition, the procedure proved to be applicable to a variety of proteins considering successful purification of FHL1 and the two tag control proteins (DPYSL3 and RBP1).

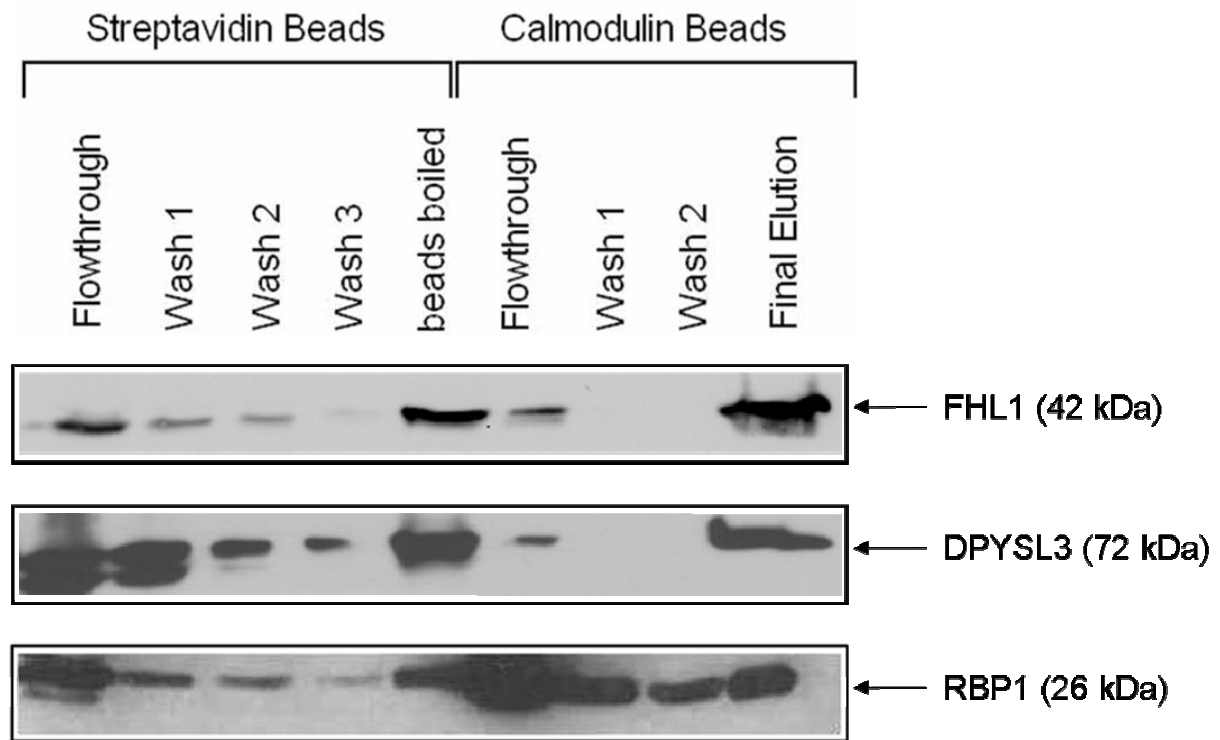


**Figure 9. Tandem Affinity Purification of SBP/CBP Tagged Proteins from HEK-293 Cells**

Two consecutive affinity purifications were performed utilizing the interactions between SBP and CBP tags with streptavidin and calmodulin proteins respectively. Each resin binding step was followed by multiple washes and elutions. The purification of FHL1 and tag-control proteins, DPYSL3 and RBP1, were validated by immunoblot analysis of fractions collected through the procedure. All proteins were detected with anti-CBP antibody (Santa Cruz).

### **I.C Co-Purification of Additional Proteins with FHL1**

Coomassie stain analysis of the same fractions from Figure 9 further revealed the efficiency of the TAP procedure (Figure 10A). Using the affinity binding parameters, the bait protein was removed from a very complex cell protein mixture, with washes further removing non-specific and weak interactions. However, FHL1 was not purified in isolation as shown in Figure 10B.

Compared to the cell lysate, the final purified sample is considerably less dense, but the presence of multiple proteins was evident in addition to the purification and concentration of the bait protein. Thus, the detected protein bands (black arrows) were representative of co-purified potential FHL1 interactors.

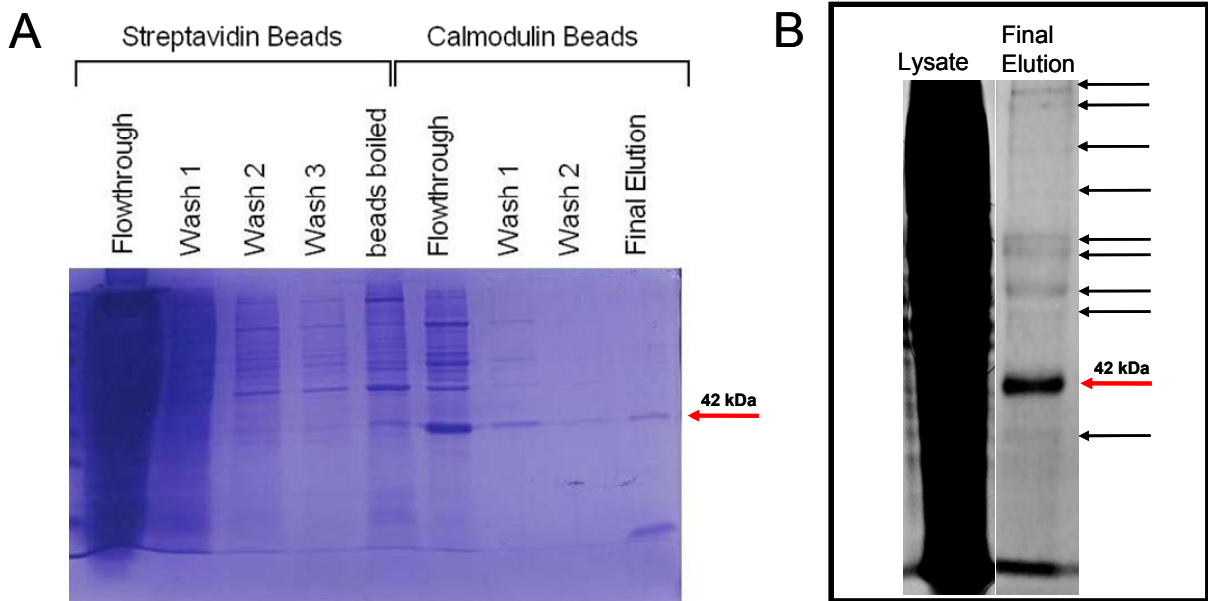


**Figure 10. Recovering Interacting Proteins with Purification of FHL1-SBP/CBP**

The application of two affinity purifications in tandem with gentle washes and small molecule elution conditions allowed for the clean isolation of FHL1 targeted complexes, and thus recovery of interacting protein partners. The efficient purification of FHL1-SBP/CBP and removal of non-specific interactors were evident by (A) coomassie staining of fractions collected throughout the TAP procedure and separated on a SDS-polyacrylamide gel. (B) Magnification of the cellular lysate and final elution lanes from a coomassie stained gel reveals the efficiency of the method. Black arrows indicate protein bands representative of potential FHL1 interacting proteins. The red arrow points to FHL1-SBP/CBP.

## II. IDENTIFICATION OF POTENTIAL FHL1 INTERACTING PROTEINS

### II.A Proteins Identified from FHL1 Purifications by Mass Spectrometry

A total of ten purifications were performed from HEK-293 cells and analyzed by MS. Of these, five were FHL1 purifications, with two negative control bead purifications and three tag control purifications. From the MS analysis, the generated collection of peptide tandem mass spectra was searched against the IPI protein sequence database to match the spectra to a protein. Since the resulting proteins were represented with different accession codes, to ensure

consistency and comparability, gene names were acquired for each protein and used henceforth for identification. For every experimental run, only proteins which were supported by at least two unique peptides were accepted for further consideration. Thus, when combined together, a total of 882 different proteins were identified from all ten purifications.

A variety of trypsin digestion methods were also applied to the purified samples in preparation for MS analysis. Depending on the method used, the pattern of protein detection and coverage varied. In general, in-solution trypsin digestion of eluted samples identified the greatest number of different proteins per experiment though the detection of the bait protein was weaker when compared to on-bead digestions. For instance, on average 233 proteins were detected from eluted FHL1 purifications samples compared to 187 proteins from on-bead digested samples. However, the respective average detection of FHL1 itself was 6 and 30 peptides. The differences in FHL1 detection was likely attributable to the significant amount of tagged protein remaining on calmodulin resin following elution, which could be avoided by directly digesting the protein while bound to the beads. However, performing on-bead tryptic digestion also resulted in digestion of the calmodulin protein crosslinked to the sepharose resin base. The sheer quantity of calmodulin masked the presence of lower abundant proteins, thus resulting in their poor detection. Nonetheless, at 93 proteins, the quantity of detected protein was lowest from in-gel digested samples, however with decent bait detection by comparison. Considering that immunoblot and silverstain analysis demonstrated similar purification efficiencies as all others, a significant amount of protein was likely lost during the multitude of steps involved with in-gel digestion and solid-phase extraction protocols. Figure 11A lists the unique peptide sequences used to identify FHL1 from each purification, while Figure 11B demonstrates the coverage the peptide sequences offered.

## **II.B Filtering and Comparing Subsets of Proteins Identified from Purifications**

Of the 882 proteins detected from all ten purifications, 628 were identified in any of the five FHL1 purifications. In order to identify potential FHL1 interactors of high confidence, the subsets of identified proteins were filtered and compared according to Figure 12. Figure 13A depicts the 882 co-purified and identified proteins via heatmap representation. First, non-specific interactors were removed. The major contaminating proteins external to the applied cell lysate were keratin proteins. Throughout the experimental process, all necessary steps were taken to minimize keratin contamination, including the use of filtered buffers and keratin free

tips, in addition to working in a laminar flow hood. Next, based solely on identical gene names, proteins found in negative control or tag control purifications were removed. Untransfected cells were used as negative controls to identify proteins with a capacity to bind non-specifically to the resin. To account for technical artifact proteins, inherent to the purification process, tag control purifications were performed. Following these eliminations, 442 proteins were identified as belonging uniquely to the FHL1 purifications (Figure 13B). Next, the filtered FHL1 MS datasets were compared to identify proteins present in multiple purifications, thereby strengthening confidence in the potential interactors. Aside from the bait FHL1 protein, 61 proteins were found in at least two FHL1 purification experiments (Figure 13C). Table 5 lists these 61 proteins and their corresponding total spectral counts detected during MS analysis of each purification. Eluted samples demonstrated the greatest homology in identified proteins, whereas reproducibility was lower for on-bead and in-gel digested samples (Figure 13C). The discrepancies observed could have been caused by reduced detection of co-purified proteins, from the latter two conditions, due to saturation of the mass spectrometers detection capacity by calmodulin and keratin proteins respectively.

**A**

NUMBER	UNIQUE PEPTIDE	FHL1 Purification Experiments				
		Run 1	Run 2	Run 3	Run 4	Run 5
1	KPIGADSK	x	x			
2	CAKCLHPLANETFVAK					x
3	CLHPLANETFVAK					x
4	AIVAGDQNVEYK	x	x	x	x	x
5	QVIGTGSFFPK				x	x
6	GEDFYCVTCHETK				x	
7	FTAVEDQYYCVDCYK		x	x	x	x
8	NPITGFGK	x	x			
9	GSSVVAYEGQSWHDYCFHCK		x	x	x	x
10	FV FHQEQVYCPDCAK	x	x	x	x	x

**B**

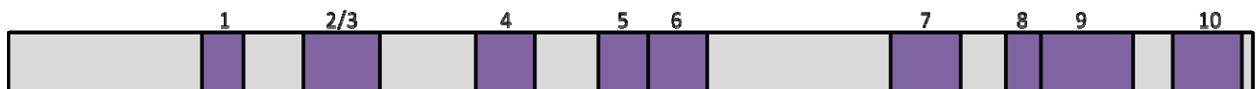


**Figure 11. Mass Spectrometry Detection of FHL1 (Isoform 1)**

To depict the specificity of FHL1 detection via mass spectrometry, (A) lists the unique peptides used to identify FHL1 during the various purifications. To visualize this coverage, (B) illustrates the location and length of each unique peptide sequence (purple boxes) relative to the complete sequence of FHL1 (gray bar, representative of 280 amino acids).

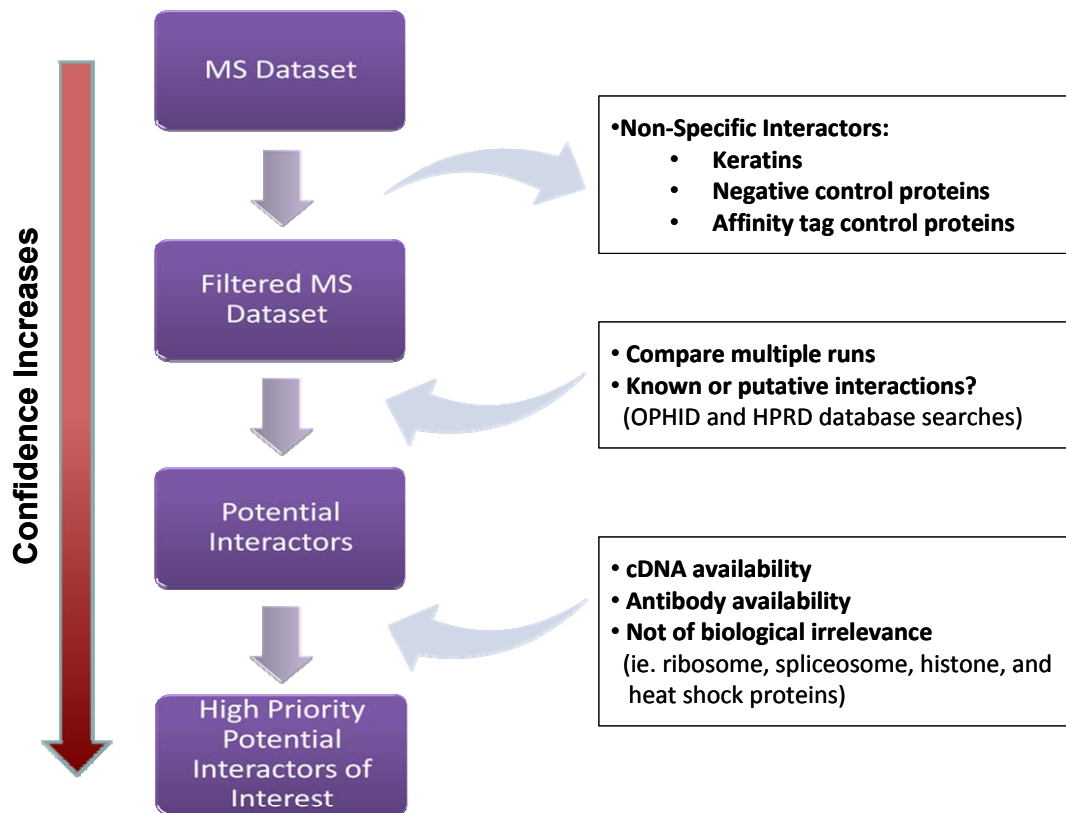


**Figure 12. Filtering and Comparing Mass Spectrometry Purification Data**

Multiple purification experiments were performed from HEK-293 cells (5 FHL1 repeats, 2 negative control repeats, and 3 tag-control repeats). First, to identify proteins detected uniquely in FHL1 purifications, non-specific interactors were removed from each FHL1 purification results, including keratins and proteins common to negative or tag-controls. Multiple filtered FHL1 datasets were compiled to identify repeatedly detected proteins and previously known or putative interactions. Currently known and putative FHL1 interactions were derived from OPHID (<http://ophid.utoronto.ca/>) and HPRD (<http://www.hprd.org/>) database searches, in addition to literature reviews. Potential interactors of high confidence were determined by frequency and strength of detection. Several factors contributed to the prioritization of potential interactors to pursue, including cDNA and antibody availability. Furthermore, proteins not of biological relevance and known common contaminants of purification procedures were reduced in importance, including ribosome and spliceosome components, histones and heat shock proteins.



**Table 5. 61 Potential FHL1 Interactors Found in Repetitive Experiments**

This table identifies the repeatedly detected 61 potential FHL1 interactors, ranked according to the number of purifications detected from (out of 5) and average intensity. Also provided is their corresponding total spectral counts detected during MS analysis of each purification.

GENE	PROTEIN NAME	# RUNS	Total Spectral Counts				
			Run 1	Run 2	Run 3	Run 4	Run 5
FHL1	Four and a half LIM domains protein 1	5	5	6	21	40	27
DHX9	ATP-dependent RNA helicase A	4	8	4	6	2	
DHX15	Nuclear DNA helicase II	4	7	3	2	3	
TUBA1B	Tubulin alpha-1B chain	3	66	67		40	
ACTN4	Non-muscle alpha-actinin 4	3	183	210		3	
MYH10	Myosin heavy chain, non-muscle IIB	3	41	32		3	
MYO18A	Myosin containing a PDZ domain	3	27	11		2	
SPTBN2	Spectrin, non-erythroid beta chain 2	3	2	6			11
DSP	Desmoplakin	3	3	3			31
PPP1R12A	Myosin phosphatase-targeting subunit 1	3	4	5			3
CSE1L	Cellular apoptosis susceptibility protein	3	2	10		2	
U2AF2	Splicing factor U2AF 65 kDa subunit	3	4	2		4	
BANF1	Barrier-to-autointegration factor	3	5	3		2	
HSP90AB1	Heat shock protein HSP 90-beta	3		5	2	3	
TUFM	Elongation factor Tu, mitochondrial	3	2	4		3	
DNAJA1	DnaJ homolog subfamily A member 1	3	2	4	2		
PRPF8	Pre-mRNA-processing-splicing factor 8	3	2	2		3	
DRG1	Developmentally-regulated GTP-binding protein 1	3	2	2		2	
RYR1	Ryanodine receptor 1	2			43	12	
ACTN1	Non-muscle alpha-actinin-1	2	52	40			
FLNB	Filamin-B	2	11	16			
PLS3	Plastin-3	2	11	13			
GSN	Gelsolin	2	19	16			
FLNA	Filamin-A	2	20	8			
MYO1D	Myosin-IId	2	8	10			
EFHD1	EF-hand domain-containing protein 1	2	7	9			
HIST1H2AD	Histone H2A type 1-D	2	13			4	
PRKDC	DNA-dependent protein kinase catalytic subunit	2	5	10			
PDLIM1	PDZ and LIM domain protein 1	2	7	7			
YBX2	Y-box-binding protein 2	2		7	7		
OBSCN	Obscurin	2			4	9	
GNB2L1	Receptor of activated protein kinase C 1	2	16	2			
LRP6	Low-density lipoprotein receptor-related protein 6	2	4	6			
EFHD2	EF-hand domain-containing protein D2	2	5	4			
DAK	Dihydroxyacetone kinase	2		5	4		
AHNAK	Neuroblast differentiation-associated protein AHNAK	2		4		5	
GCN1L1	Translational activator GCN1	2	3	7			
CALD1	Caldesmon	2	3	5			
SPECC1L	Cytospin-A	2	3	5			
JUP	Junction plakoglobin	2		3			5
DNAH5	Dynein heavy chain 5, axonemal	2			5	3	
HIST1H1C	Histone H1.2	2	2	7			
TPM3	Tropomyosin alpha-3 chain	2	4	3			
FASN	Fatty acid synthase	2	3	4			
TMOD2	Tropomodulin-2	2	3	4			
TCP1	T-complex protein 1 subunit alpha	2			2	6	
RCN2	Calcium-binding protein ERC-55	2	5	2			
LRP5	Low-density lipoprotein receptor-related protein 5	2		5	2		
MYBBP1A	Myb-binding protein 1A	2	3	3			
FLNC	Filamin-C	2	4	2			
APOB	Apolipoprotein B-100	2	2	4			
SF3B2	Splicing factor 3B subunit 2	2			2	4	
SERPINH1	Serpin H1	2	3	2			
KCNMA1	Calcium-activated potassium channel subunit alpha-1	2	2	3			
MYO18B	Myosin-XVIIIb	2	2		3		
HCRTR1	Orexin receptor type 1	2		2	3		
ZYX	Zyxin	2		2		3	
ALDH18A1	Delta-1-pyrroline-5-carboxylate synthetase	2	2	2			
MYO5A	Myosin-Va	2	2	2			
SIPA1	Signal-induced proliferation-associated protein 1	2	2	2			
XRCC6	ATP-dependent DNA helicase 2 subunit 1	2	2	2			
LYAR	Cell growth-regulating nucleolar protein	2			2	2	

## **II.C Prioritization of Potential Interactors**

The 61 potential interactors of interest were then prioritized to improve confidence and validate further experimental pursuit (Figure 13). Essentially, the proteins were first ordered in terms of frequency and strength of detection. Next, proteins belonging to families of common contaminants of purification procedures, and were also deemed to not be of biological relevance, were demoted. This included ribosomal, spliceosomal, histone, and heat shock associated proteins. For the purposes of this project, the availability of antibodies and cDNA clones in Open Biosystems ORFeome collection was also assessed.

## **II.D Screening for Known FHL1 Interacting Proteins**

To assess the validity of performing TAP in combination with MS, the 442 proteins detected uniquely in FHL1 purifications were screened to identify any known FHL1 interacting partners. As a result, one known and two putative FHL1 interactions were discovered amongst the 442 proteins, but were not able to make it past our strict filtering criteria. For instance, Talin, Protein 4.1, and HLA class I histocompatibility antigen, B-42  $\alpha$  are all known FHL1 interactors, but in my experiments I only found them in one experimental run, and thus these proteins did not make it into my shortlist (Table 5). The recently identified interactor, Titin, was discovered in multiple FHL1 purifications, but it was removed since I also found it in the DPYSL3 purification.

# ***III. CHARACTERIZATION OF THE 61 POTENTIAL FHL1 INTERACTING PROTEINS***

## **III.A Analysis of Overrepresented GO-Terms**

A GO-Term enrichment analysis was performed to determine which molecular functions and biological processes were overrepresented (Figures 14 and 15 respectively). Gene names corresponding to the 61 proteins found in multiple FHL1 purifications were inputted for analysis into the Gene Ontology for Functional Analysis (GOFFA) software. In general, terms associated with motility and transport, calcium ion and nucleotide binding, cell development and regulation, muscle processes, and particularly organization of and binding to actin cytoskeleton were common amongst the 61 proteins. When compared to GO-Terms associated with FHL1,

developmental processes with respect to differentiation and regulation of biological processes were common.

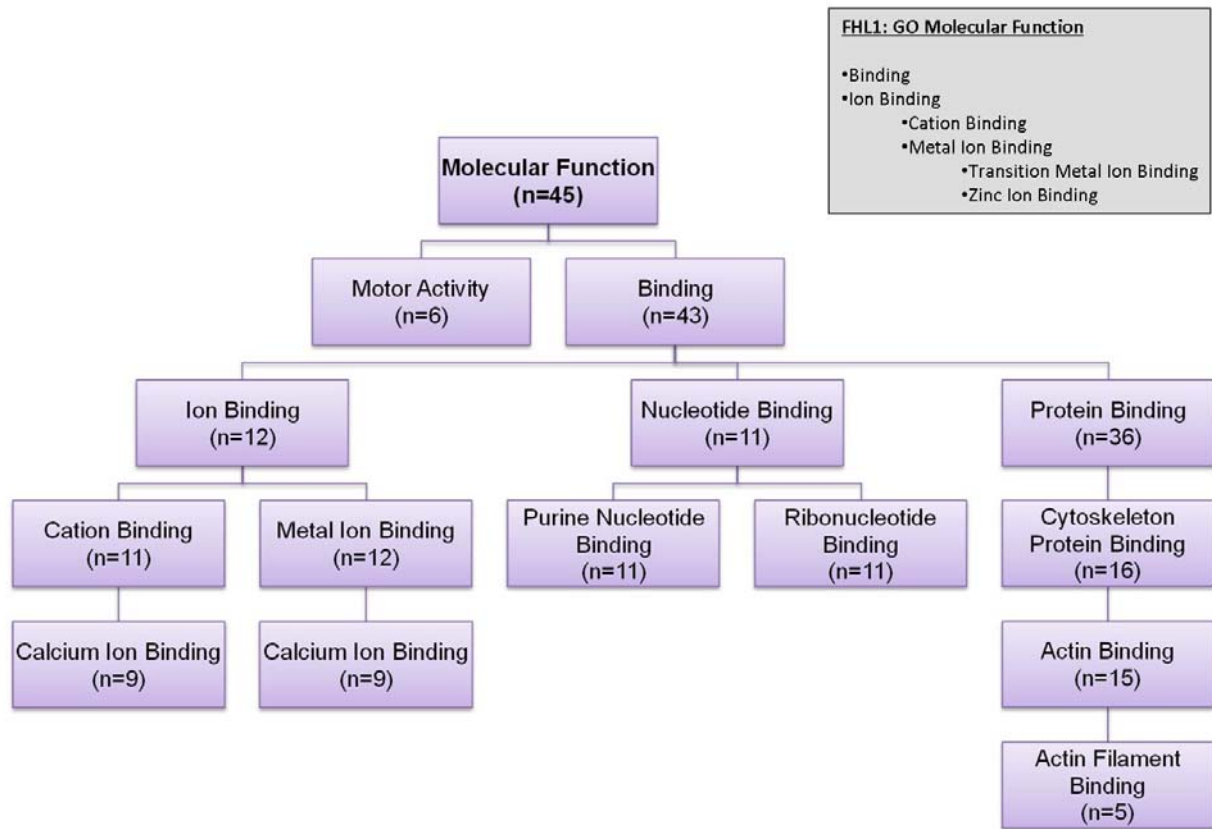


**Figure 14. Analysis of Overrepresented Molecular Functions Found Within the 61 Potential FHL1 Interactors**

GO-Term analysis of the 61 potential interactors of FHL1 was performed. Their gene name IDs were inputted into the GOFFA software to obtain overrepresented molecular functions ( $p \leq 0.05$ ), which are illustrated in a GO-tree format (for  $n \geq 5$ ). The number of proteins belonging to each category are indicated by 'n'. For comparison, molecular function GO-terms associated with FHL1 are listed in the inset.

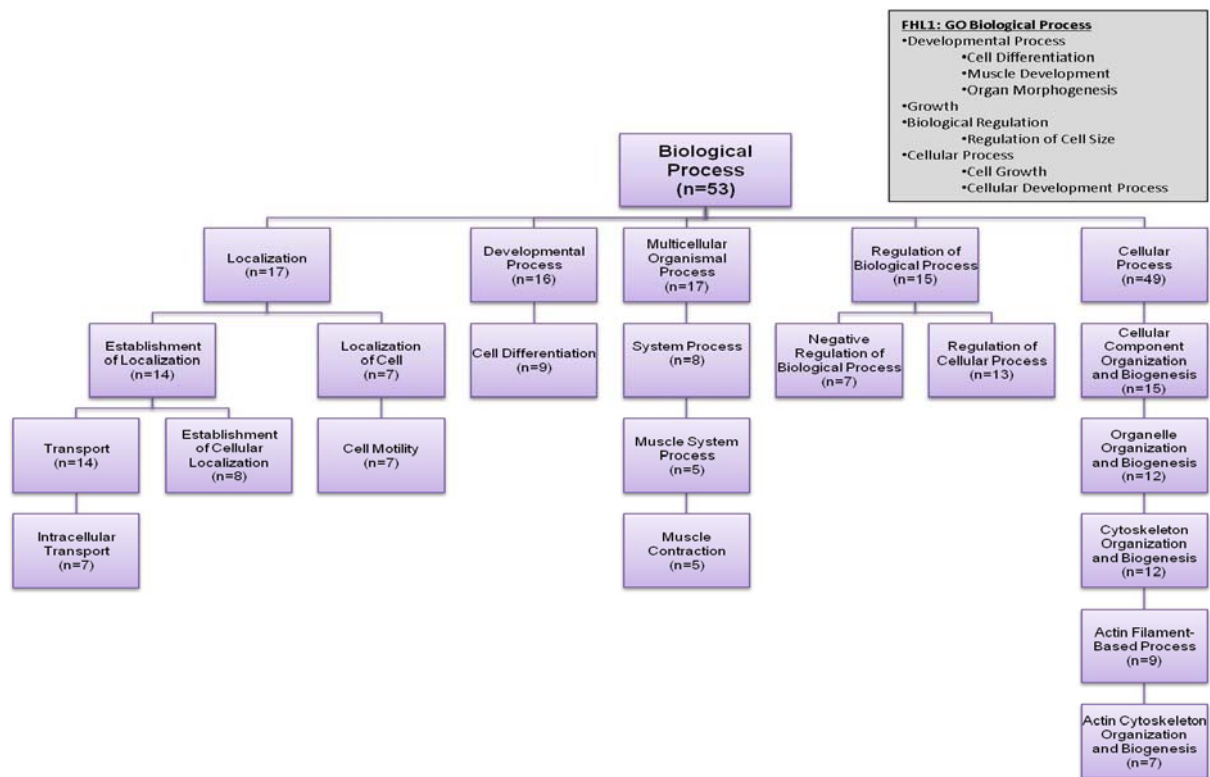


**Figure 15. Analysis of Overrepresented Biological Processes Found Within the 61 Potential FHL1 Interactors**

GO-Term analysis of the 61 potential interactors of FHL1 was performed using the GOFFA software to obtain overrepresented biological processes ( $p \leq 0.05$ ), which are illustrated in a pruned GO-tree format ( $n \geq 5$ ). The number of proteins belonging to each category are indicated by ‘n’. For comparison, molecular function GO-terms associated with FHL1 are listed in the inset.

### III.B Identification of Known Interactions

Under native conditions, TAP can purify multimeric protein complexes consisting of the tagged bait. The online STRING 8.1 database (<http://string.embl.de/>) was used to identify any previously described interactions amongst FHL1 and the 61 potential interactors, from human, mouse, and rat sources. The resulting protein-protein interaction network generated is depicted in Figure 16. The cluster of proteins consisting of LRP5, LRP6, APOB, and FASN, are all involved in lipid metabolism. The subset consisting of JUP, DSP, AHNAK, and PLS3 can be mapped to various cell adhesion structures. Furthermore, the filamin proteins interact and are involved in the MAPK signaling pathway. For the other two small protein clusters, one consisting of DNAH5, TUBA1B, HSP90AB1, and TCP1, and another composed of PRPF8,

U2AF2, DHX15, SF3B2, and DHX9, GO terms associated with nucleic acid binding was common to both, as well as association with metabolic processes, though with respect to proteins or nucleic acids respectively. Amongst the largest cluster of proteins, some of the overrepresented pathways include focal adhesion, tight junction, integrin signaling, and especially regulation of the actin cytoskeleton. Proteins not known to interact with any of the other candidates are represented as blue ovals, including FHL1. Thus, all 61 candidates represent potential novel interactions. All pathway analyses were performed using an application of GOFFA.

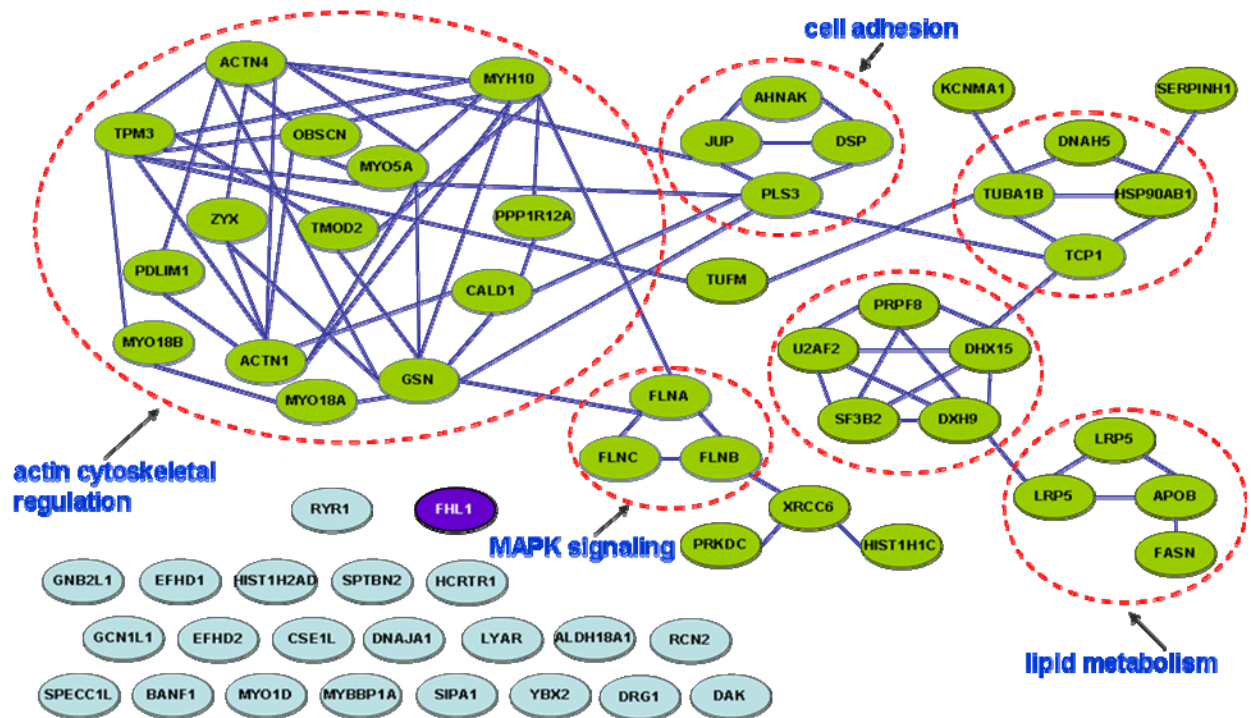


**Figure 16. Known Interactions Amongst FHL1 and the 61 Potential Interactors**

Protein-protein interaction network depicting previously defined interactions amongst the group of FHL1 and 61 potential interactors. Interactions were identified using the online STRING 8.1 database (<http://string.embl.de/>). The results obtained from human, mouse, and rat databases were compiled to generate the interaction network. Red broken line circles were used to highlight clusters of proteins with fairly high interaction connectivity, and labeled with the predominant pathway associated with the clustered proteins. Proteins not known to interact with any of the other 61 candidates are represented in blue, with FHL1 highlighted in purple.

## **IV. ASSOCIATION WITH DISEASE**

In cells, protein-protein interactions are vital for the mediation of function and form. In a diseased state, the cells' interactome becomes a disturbed network system with various interactions differentially regulated [117]. Some interactions demonstrate highly correlated co-expression patterns, such the components of the troponin complex in skeletal muscle [118, 119]. Such proteins usually fulfill specific functions within the cell [120]. Lower co-expression correlations are observed from more dynamic interactions which mediate global network connectivity, within the interactome [120]. Recently, Taylor and colleagues demonstrated that alterations in the coordinated co-expression of components in particular protein interaction networks, when comparing two breast cancer patient cohorts, could be associated with cancer prognosis. For instance, the general expression correlations between BRCA1 or SRC and their respective interacting partners was misregulated in tumours obtained from patients who died of disease [120]. In the Tg-PLN R9C mouse model of DCM, FHL1 was identified as one of the most significantly elevated proteins during disease [113]. Correlations in expression may be detected from FHL1 interactors which mediate specific cellular functions. Whereas, lower co-expression correlations may be observed from interactions which mediate communication between different pathways [120].

### **IV.A Lysate Differences**

To determine visually if differences existed between FHL1 interactions in normal and diseased states, pull down assays were performed using resin immobilized FHL1 treated with cardiac lysates from wild type or Tg-PLN R9C mice. Differences between both conditions could definitely be visualized by silver stain analysis of elution samples (Figure 17). In general, there were more bands present in the wild type conditions which were missing from the diseased state, than the inverse. In either case, arrows in Figure 17 represent the presence of a band not visible in the alternate condition. Thus, during disease, certain interactions are lost whilst novel ones are formed, or simply altered in predominance.

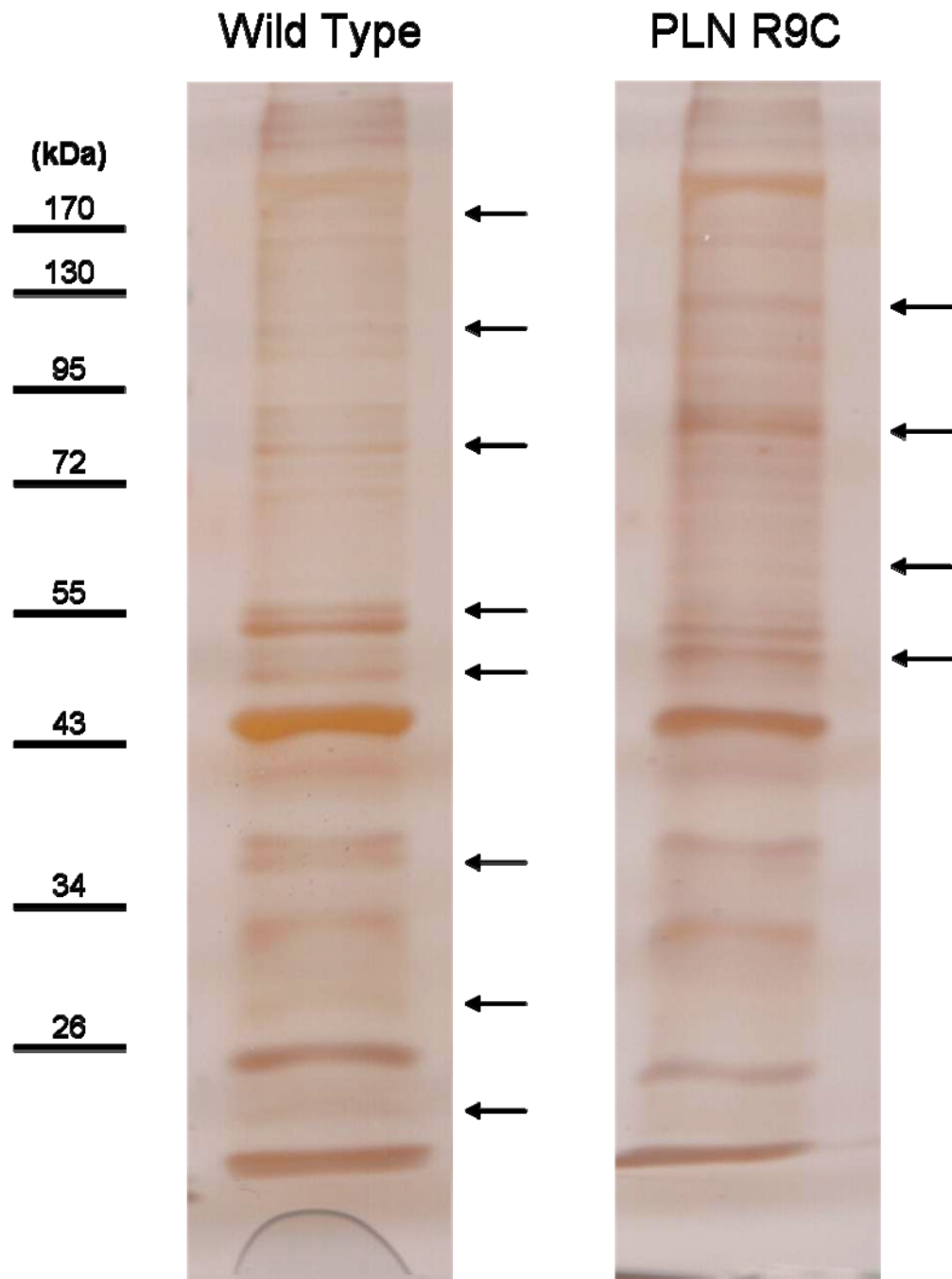


**Figure 17. Differences in Pull-Down Assays from Wild Type and PLN R9C mice**

To identify if differences existed in FHL1 interactions in wild type mice compared to Tg-PLN R9C mice, ventricular protein lysates were incubated with 8xHis/StrepII tagged FHL1 immobilized on metallic TALON® resin. Final purified samples were eluted and separated by SDS-PAGE and visualized by silver staining technique. Arrows indicate protein bands present in one sample and not detected in the other.

## IV.B Microarray Study

Previously, a large collaborative microarray profile study was performed to identify differentially expressed genes in Tg-PLN R9C mice, compared to wild type mice [113]. A global mRNA profiling was performed using full-genome array chips [113]. Since 8, 16, and 24 weeks were deemed to be representative of early, mid, and late stage DCM respectively, transcript levels were assessed at all three time points. The microarray database was thus screened to determine if any of the 61 potential FHL1 interactors demonstrated altered expression during disease (Figure 18A). From the average fold expression graph, ratios greater than 1.2 and less than 0.8 were chosen to be representative of upregulation and downregulation of mRNA levels respectively. 11 candidates demonstrated increased transcript levels, particularly EFHD2, ZYX, MYO5A, and FLNA, and FLNC (Figure 18B). These five also displayed drastic increases during the late stages of disease, similar to FHL1. Figure 18C identifies the candidates which, on average, did not report large variations in transcript levels throughout disease. Meanwhile, three potential interactors progressively declined during disease development (Figure 18D). RYR1 in particular declined dramatically, with large differences occurring by early stages. However, expression profiles for 19 candidates (DHX9, TUBA1B, MYH10, SPTBN2, DSP, CSE1L, DRG1, PLS3, MYO1D, PDLIM1, OBSCN, DAK, HIST1H1C, RCN2, MYBBP1A, APOB, SF3B2, MYO18B, and LYAR) were not available. For these candidates, the results from a comparative proteomics study, performed in parallel to the microarray study, was consulted. Nine of these proteins were detected via MS: PLS3, PDLIM1, CSE1L, DHX9, MYO1D, DAK, HIST1H1C, RCN2, and APOB. A minimum average of two fold change throughout disease was detected for PLS3, PDLIM1, CSE1L, and HIST1H1C.

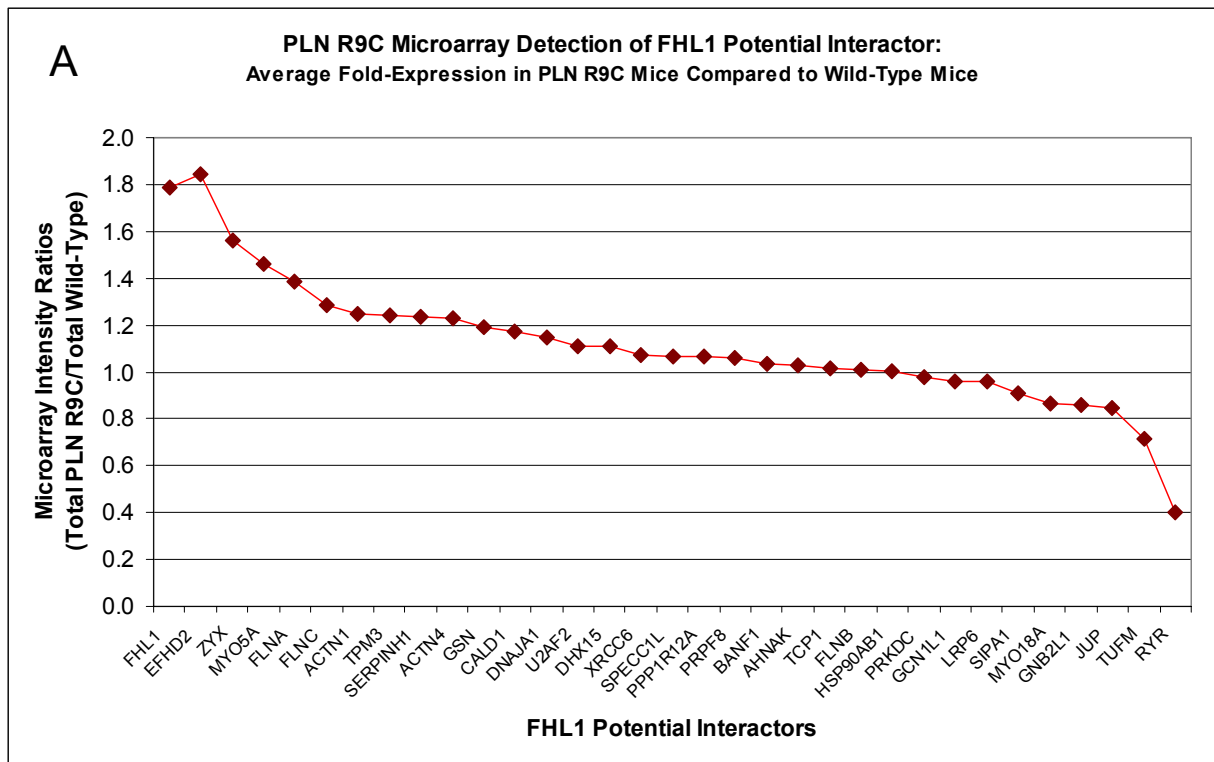
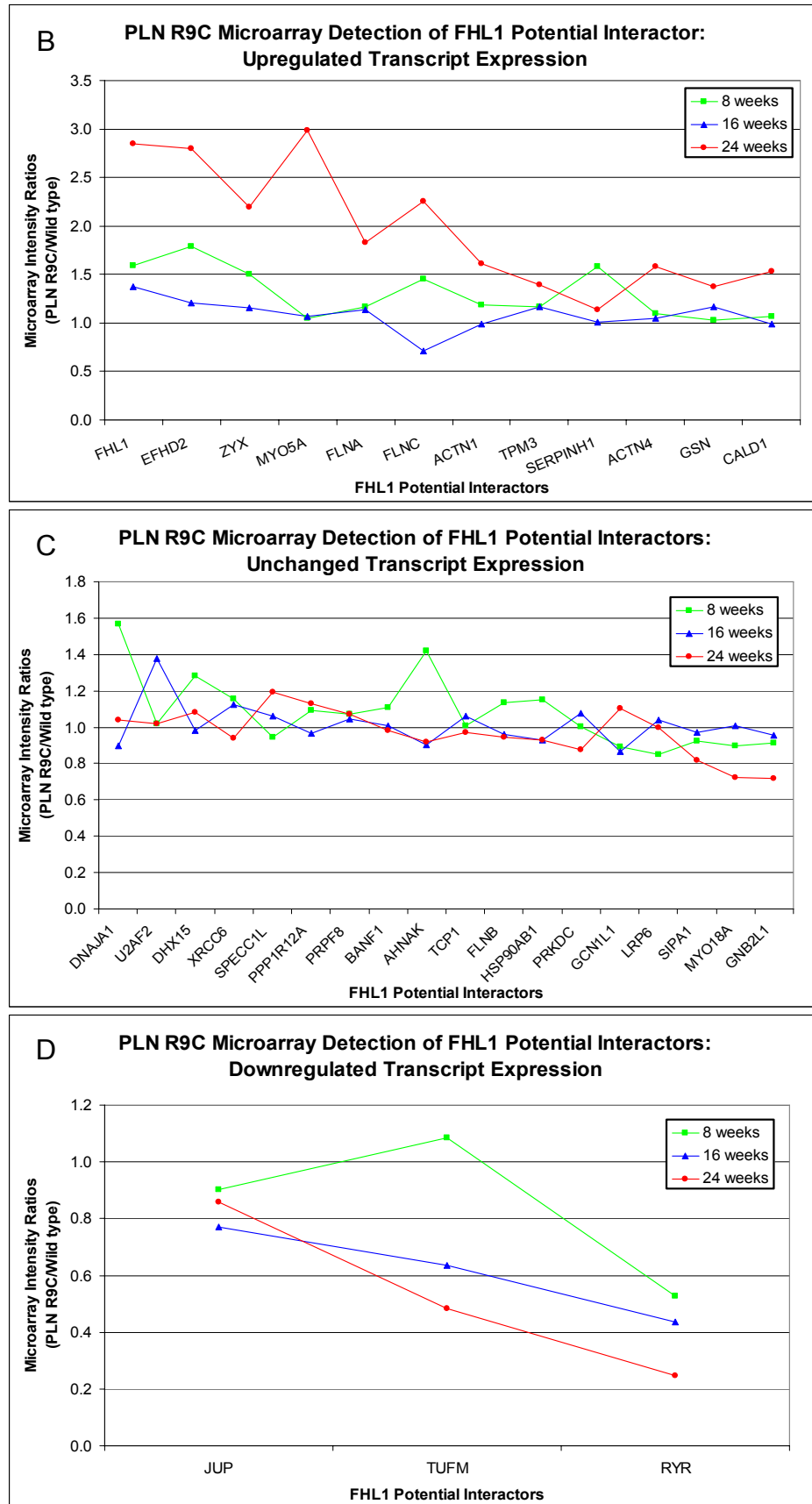


**Figure 18. Correlations in mRNA Transcript Levels of FHL1 and Potential Interactors in Tg-PLN R9C Mice**

To identify patterns in expression between FHL1 and the potential interactors in PLN R9C mice, results from a previous microarray study of PLN R9C mice was assessed [113]. Transcript levels were available at all three time points (8, 16, and 24 weeks) for 33 homologous genes. **(A)** The average fold-difference in transcript levels from wild-type to PLN R9C mice are depicted for all 33 genes. Intensity ratios of 1.2 and greater were chosen to be representative of increased expression, whereas 0.8 and below indicated downregulation of transcript levels. Thus, ratios between 1.2 and 0.8 were deemed to not show a general difference between wild-type and PLN R9C mice. **(B)** In addition to FHL1, 11 genes demonstrated an upregulation in mRNA transcript expression throughout disease progression in the PLN R9C mice when compared to age-matched wild-type mice. **(C)** Of the 33 genes, 18 were not found to be differentially expressed between the wild-type and transgenic mice throughout disease progression. **(D)** Finally, 3 genes were identified to be downregulated at the mRNA level in diseased mice compared to the wild-type.

Figure 18 B-D. Correlations in mRNA Transcript Levels of FHL1 and Potential Interactors in Tg-PLN R9C Mice



## **V. VALIDATION OF INTERACTIONS**

61 proteins were identified from multiple FHL1 purifications as potential interactors. Considering FHL1's association with the actin cytoskeleton, and its upregulation during cardiomyopathy where major cytoskeletal remodeling occurs, we were interested in validating FHL1 interactions with several proteins involved with regulation of the actin cytoskeleton (Figure 16). In addition, interaction validation was also attempted with a  $\text{Ca}^{2+}$  channel of particular interest in our lab. The most commonly used techniques for interaction validation tend to be co-IP and immunodetion, which were also used here.

### **V.A In HEK-293 Cells**

Since the cDNA for PDLIM1 was available in the Human ORFeome library, it was alternatively tagged using the Gateway® cloning technology. This recombination technology allows for cDNAs to be swapped from one vector to another, without restriction enzymes. Instead, Clonase enzymes are used, which recognizes specific nucleotide attachment sites flanking the cDNA sequence and mediates the transfer into a desired vector containing another attachment site sequence. To avoid significant overexpression, the pEF-DEST51 expression was chosen for its human elongation factor 1 $\alpha$  promoter, which exhibits weaker activity than the CMV promoter. The interaction between FHL1 and PDLIM1 was verified by co-IP experiments performed from HEK-293 cells (Figure 19). In addition to the detection of PDLIM1 in FHL1 pull downs, reciprocal IPs using PDLIM1 as the bait also co-purified FHL1. Since neither protein was detected in the protein A/G resin or immunoglobulin control IPs, the possibility of non-specific binding was voided. Furthermore, the specificity of the procedure and interaction was supported by the negative control results, where an interaction was not detected between FHL1 and RBP-J. RBP-J was chosen as a negative control for its specific interaction with the FHL1 spliced variants containing a RBP-J binding domain, which is absent in the FHL1A isoform used here.

RYR1 is predominantly a skeletal muscle protein, vital to the calcium cycling pathway in muscle cells as the major calcium release channel of the SR [121]. To ensure proper identification via MS, the mapped MS spectra was screened to identify the unique peptides sequences used for identification and the coverage they offered (Figure 20). Considering the approximate 65% sequence homology between RYR1 and its isoforms (RYR2 and RYR3), and the detection of unique peptides distributed throughout the full sequence, the MS detection was

considered genuine. However, the specific spliced variants of RYR1 could not be distinguished since the unique peptide sequences were common to each one (Figure 20A).

Next, to validate the interaction between FHL1 and RYR1, several methods were attempted. RYR1 is a fairly large protein at approximately 565 kDa, and existing as a functional tetrameric complex within the cell, it presents many challenges with respect to solubility and purification [121]. Thus, when initial FHL1 co-IP experiments from HEK-293 cells failed to co-purify RYR1, it was attributed to either issues in solubility, strength of interaction, expression levels of RYR1 protein, or possibility of non-interaction. In order to eliminate the first possibility, the experiment was repeated using the Lysis Buffer provided in Stratagene's TAP kit, which was successful in solubilizing RYR1 during the FHL1 purifications. Unfortunately, the buffer proved to be incompatible for the co-IP procedure since the FHL1 bait could not be purified even though it was expressed. Finally, a pull down assay was performed from HEK-293 cells transiently expressing FHL1-SBP/CBP, using the streptavidin bead affinity for the SBP tag, with Stratagene's Lysis Buffer. Immunoblot detection verified the presence of RYR1 in the purified sample with FHL1, detected as a characteristic double band. Both FHL1 and RYR1 were absent from the control purification (Figure 21A). When the presence of GSN was detected from purified samples in parallel, a significant enrichment was apparent in FHL1 samples while minute amounts were detected in the control (Figure 21B). This suggests a two-step purification is ideal for certain interactions. Furthermore, these experiments validated their MS identification.

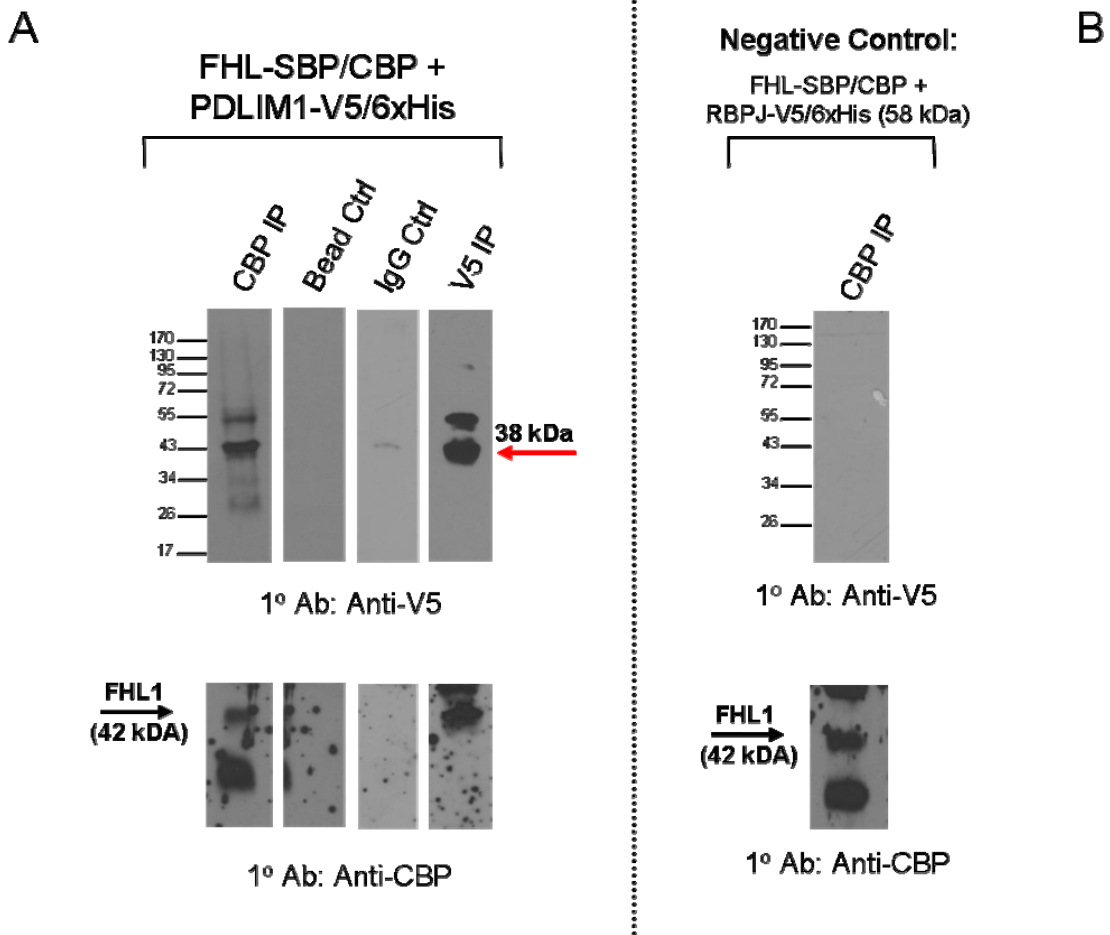


**Figure 19. Co-immunoprecipitation Validation of FHL1 Interactions from HEK-293 Cells**

Immunoblot analysis of co-IPs performed from HEK-293 cells co-transfected with FHL1-SBP/CBP and (A) PDLIM1-V5/6xHis or (B) RBPJ-V5/6xHis. FHL-SBP/CBP was co-immunoprecipitated with anti-CBP antibody, while reciprocal co-IPs for PDLIM1-V5/6xHis was performed with anti-V5 antibody. Co-immunoprecipitations performed using unconjugated protein A/G-agarose resin and resin bound to anti-goat IgG secondary antibody served as controls. Samples were immunoblotted with anti-CBP or anti-V5 antibody to detect tagged FHL1 or prey (PDLIM1 or RBP-J) respectively. RBP-J served as a negative control since full-length FHL1 lacks an RBP-J binding domain, which is present in alternative isoforms of FHL1 (KyoT2 and KyoT3) to mediate an interaction.

A

Number	Unique Peptide	FHL1 Purifications		Ryanodine Receptor 1		
		Run 3	Run 4	Isoform 1	Isoform 2	Isoform 3
1	VGDDIILVSVSSER	x		x	x	x
2	WYFEFEAVTTGEMR	x		x	x	x
3	DDPEIILNTTTYYSVR	x		x	x	x
4	AAASLDTATFSTTEMALALNR	x		x	x	x
5	WMDISQEFIAHLEAVVSSGR	x		x	x	x
6	SKLDEDYLYMAYADIMAK	x	x	x	x	x
7	QMVDMLVESSSNVEMILK	x	x	x	x	x
8	DIGFNVAVLLTNLSEHVPHDPR	x		x	x	x

B

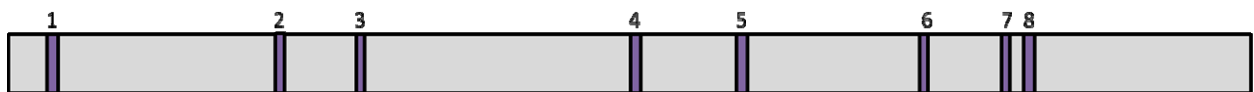


**Figure 20. Mass Spectrometry Detection of Ryanodine Receptor 1**

To depict the specificity of RYR1 detection via mass spectrometry, (A) lists the unique peptides used to identify RYR1 during the various purifications. For isoform specificity, the presence of the particular peptide in known isoforms is denoted by 'x'. To visualize the coverage offered by unique peptide sequences, (B) illustrates the location and length of each unique peptide sequence (purple boxes) relative to the complete sequence of RYR1 (gray bar, representative of 5033 amino acids).

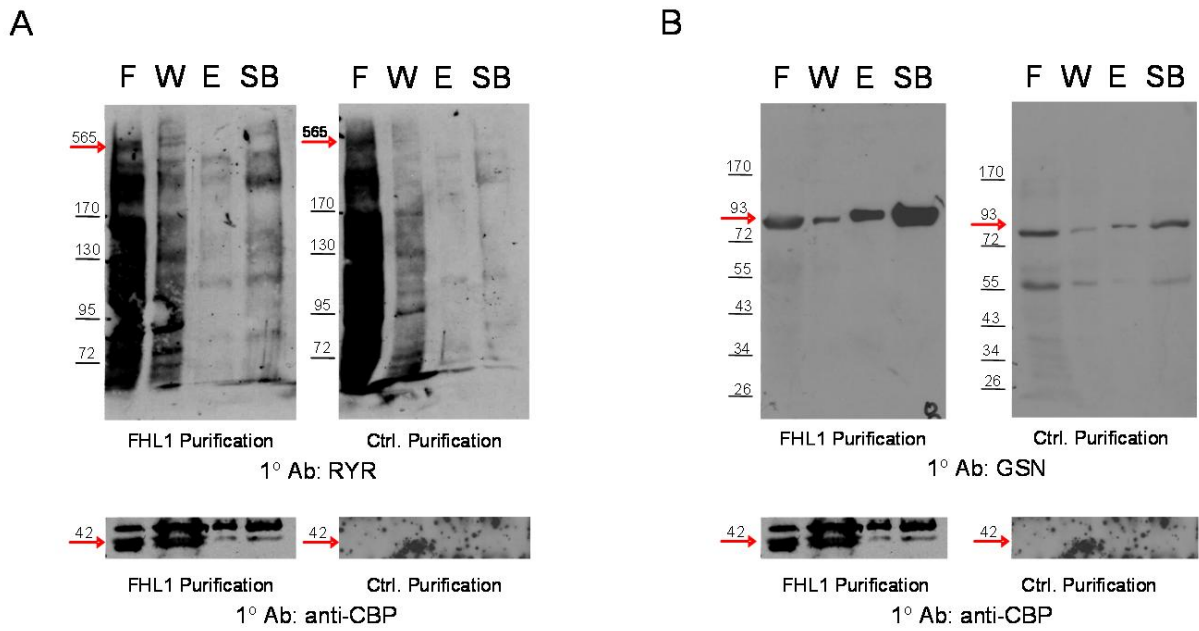


**Figure 21. Validation of Interactions by Streptavidin Affinity Purification from HEK-293 Cells**

One-step streptavidin affinity purifications were performed from HEK-293 cells expressing FHL1-SBP/CBP. FHL1-SBP/CBP containing protein complexes were pulled-down under native conditions via the SBP tag interaction with streptavidin. To reduce background noise, five gentle washes were performed. In parallel, control purifications were performed with untransfected cells. The flowthrough (F), first wash (W), elution (E), and eluted streptavidin bead (SB) fractions collected throughout the process were either heated at 65°C (A) or boiled (B) and separated on an SDS-polyacrylamide gel. Immunoblot analysis was performed to detect endogenous (A) ryanodine receptor, and (B) gelsolin. For each set, the purification of FHL1-SBP/CBP was validated by immunoblotting with the anti-CBP antibody (Santa Cruz).

## V.B In Diseased Hearts

Since FHL1 is abundantly expressed in muscle, and especially elevated in diseased hearts of Tg-PLN R9C mice, FHL1 co-IP experiments were performed using ventricular tissue from Tg-PLN R9C mice at mid-stage DCM. This would avoid issues related to overexpression of bait protein and allow for studying endogenous interactions, particularly from the diseased model. Necessary controls were implemented to eliminate non-specific interactions intrinsic to the procedure itself. Immunoblotting revealed FHL1 could be effectively recovered from a ventricular lysate. Furthermore, co-purifications of GSN and ACTN1 were also detected, which were not present in either the protein A/G resin or immunoglobulin controls (Figure 22 A, B, C). Unfortunately, reciprocal co-IP experiments were not successful due to antibody incompatibility issues. In Figure 22A, FHL1 is detected as the lower molecular weight band at 32 kDa. The prominent bands at approximately 55 kDa are likely protein A/G stripped from the agarose resin

upon boiling in loading buffer. Reactions with the immunoglobulin chains of the antibody probes used during immunoblotting likely caused for their presence to be detected.

To determine the specific isoforms of GSN and ACTN1 detected during the original FHL1 TAP experiments, the unique peptide sequences used in their identifications were assessed (Figure 23 and 24, respectively). However, the specific spliced variant could not be distinguished for either GSN or ACTN1 since the unique peptide sequences were common to all their respective isoforms.

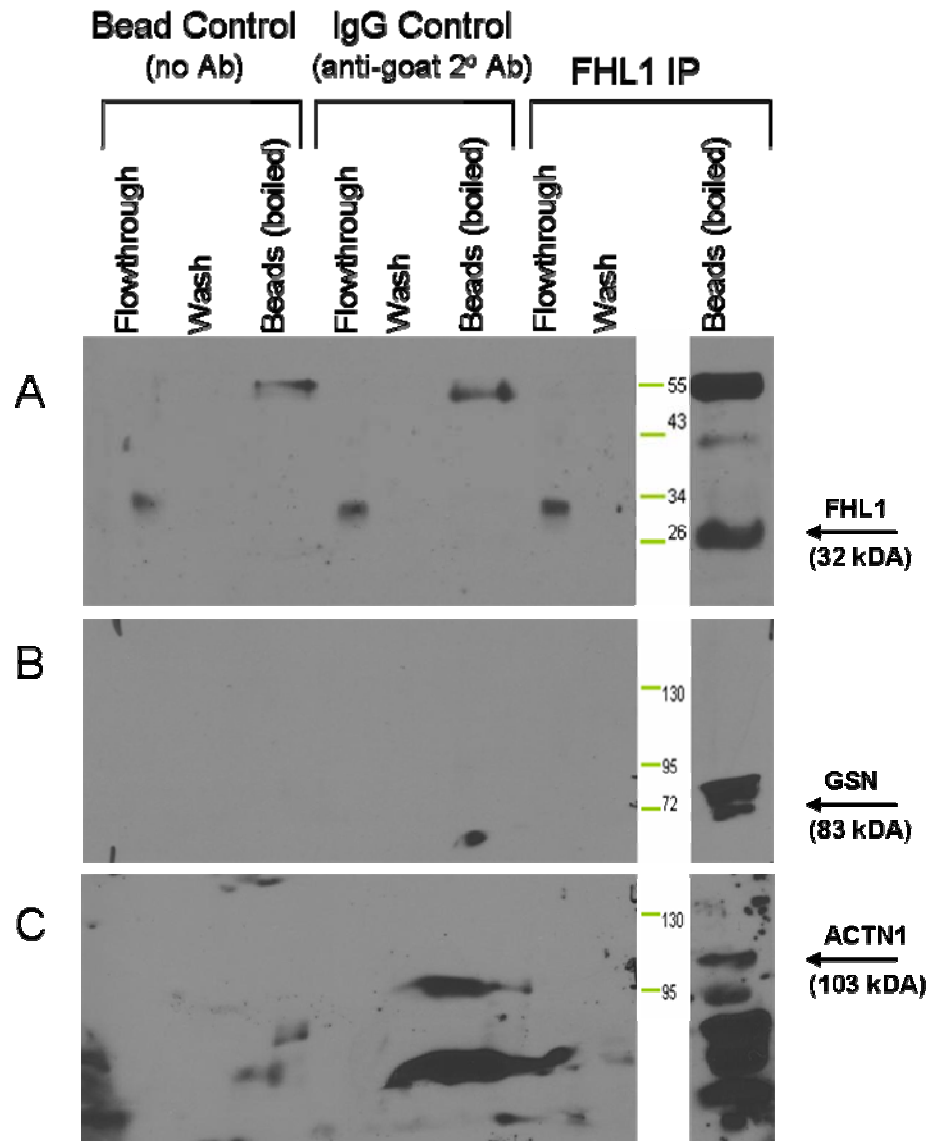


**Figure 22. Co-immunoprecipitation Validation of FHL1 Interactions from PLN R9C Mice Ventricles**  
 Immunoblot analysis of FHL1 co-immunoprecipitations performed from PLN R9C ventricular tissue. Co-immunoprecipitations performed using unconjugated protein A/G-agarose resin and resin bound to anti-goat IgG secondary antibody served as controls. Immunoblotting was performed to detect for endogenous (A) FHL1, (B) GSN, and (C) ACTN1.

**A**

Number	Unique Peptide	FHL1 Purifications		Gelsolin	
		Run 1	Run 2	Isoform 1	Isoform 2
1	AQPVQVAEGSEPDGFWEALGGK	x		x	x
2	DPDQTDGLGLSYLSSHIANVER	x	x	x	x
3	FDLVPVPTNLYGDFFTGDAYVILK	x	x	x	x
4	EPGLQIWR		x	x	x
5	GGVASGFK		x	x	x
6	YIETDPANR		x	x	x

**B**



**Figure 23. Mass Spectrometry Detection of Gelsolin**

To depict the specificity of GSN detection via mass spectrometry, **(A)** lists the unique peptides used to identify GSN during the various purifications. For isoform specificity, the presence of the particular peptide in known isoforms is denoted by ‘x’. To visualize the coverage offered by unique peptide sequences, **(B)** illustrates the location and length of each unique peptide sequence (purple boxes) relative to the complete sequence of GSN (gray bar, representative of 731 amino acids).

A

Number	Unique Peptides	FHL1 Purifications		Alpha Actinin 1		
		Run 1	Run 2	Isoform A	Isoform B	Isoform C
1	KAGTQIENIEEDFR		x	x	x	x
2	LLEVISGER	x	x	x	x	x
3	LVSIGAEIIVDGNVK	x	x	x	x	x
4	NVNIQNFHISWK		x	x	x	x
5	KDDPLTNLNTAFDVAEK	x	x	x	x	x
6	DDPLTNLNTAFDVAEK	x	x	x	x	x
7	MLDAEDIVGTARPDEK	x		x	x	x
8	VLAVNQENEQLMEDYEK		x	x	x	x
9	VPENTMHAMQQK		x	x	x	x
10	QKDYETATLSEIK		x	x	x	x
11	DYETATLSEIK		x	x	x	x
12	CQKICDQWDNLGALTQK	x		x	x	x
13	ATLPDADKER		x	x	x	x
14	LAILGIHNEVSK	x	x	x	x	x
15	DQALTEEHAR		x	x	x	x
16	GISQEQMNEFR		x	x	x	x
17	DHSGTLGPEEFK		x	x	x	
18	ETADTDTADQVMASFK	x		x	x	x
19	NYITMDELRL	x	x	x	x	x

B

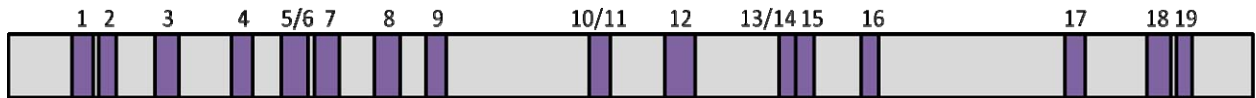


**Figure 24. Mass Spectrometry Detection of Alpha Actinin 1 (Isoform 1)**

To depict the specificity of ACTN1 detection via mass spectrometry, (A) lists the unique peptides used to identify ACTN1 during the various purifications. For isoform specificity, the presence of the particular peptide in known isoforms is denoted by ‘x’. To visualize the coverage offered by unique peptides sequences, (B) illustrates the location and length of each unique peptide sequence (purple boxes) relative to the complete sequence of ACTN1 (gray bar, representative of 892 amino acids)

## **VI. SUBCELLULAR LOCALIZATION**

In order for proteins to interact, either directly or indirectly, they must be in close proximity within the cell. Although interacting proteins can possess different overall subcellular expression patterns, they must share some co-residence. Immunofluorescence (IF) studies allow for visualization of the subcellular localization of proteins, and regions of co-expression. Co-localization thus strengthens validation of *in vivo* interactions.

### **VI.A HEK-293 Cells**

Since TAP of FHL1 interactions were initially isolated from HEK-293 cells, co-IF stainings were first performed in HEK-293 cells. In cultured cells, FHL1 localizes diffusely to both the cytoplasmic and nuclear compartments, predominantly in the former. A similar pattern has been identified from other non-muscle cultured cells, with FHL1 also associating with actin stress fibers and focal adhesion complexes in the cytoplasm [11]. Here, cytoplasmic co-localization was evident between FHL1 and the proteins associated with actin filaments and stress fiber structures, PDLIM1, GSN, and ACTN1 (Figures 25, 26, and 27 respectively). Higher magnification demonstrates partial co-localization within the cytoplasm, with varying degrees of overlay amongst them. Of these, greatest overlap was seen between FHL1 and PDLIM1, which may be due to overexpression of both candidates (Figure 25). A distinct region of partial co-localization was also evident between FHL1 and GSN by the intracellular surface of the cytoplasmic membrane, where both proteins have previously been identified (Figure 26, lower panel) [11, 122]. In addition to the cytoplasm, nuclear co-localization was also evident for FHL1 and PDLIM1, albeit at lower intensities, probably due to decreased nuclear expression in general (Figure 25). Although ACTN1 was also detected in the nucleus, significant co-localization was not apparent, supporting site specific association.

In contrast to the actin associated proteins, RYR1 is specifically localized to the endoplasmic reticulum membrane [106]. Thus the co-localization between FHL1 and RYR1 is along the extensive endoplasmic reticulum network (Figure 28A). In HEK-293 cells co-expressing tagged FHL1 and only the cytosolic fraction of RYR1, upon deletion of the transmembrane domain, an association is still preserved (Figure 28B). This suggests the normal interaction is likely along the external surface of the endoplasmic reticulum, between FHL1 and the cytosolic portion of RYR1. The bead-like features in Figure 28B is possibly due to loss of anchorage of RYR1 to the endoplasmic reticulum membrane.

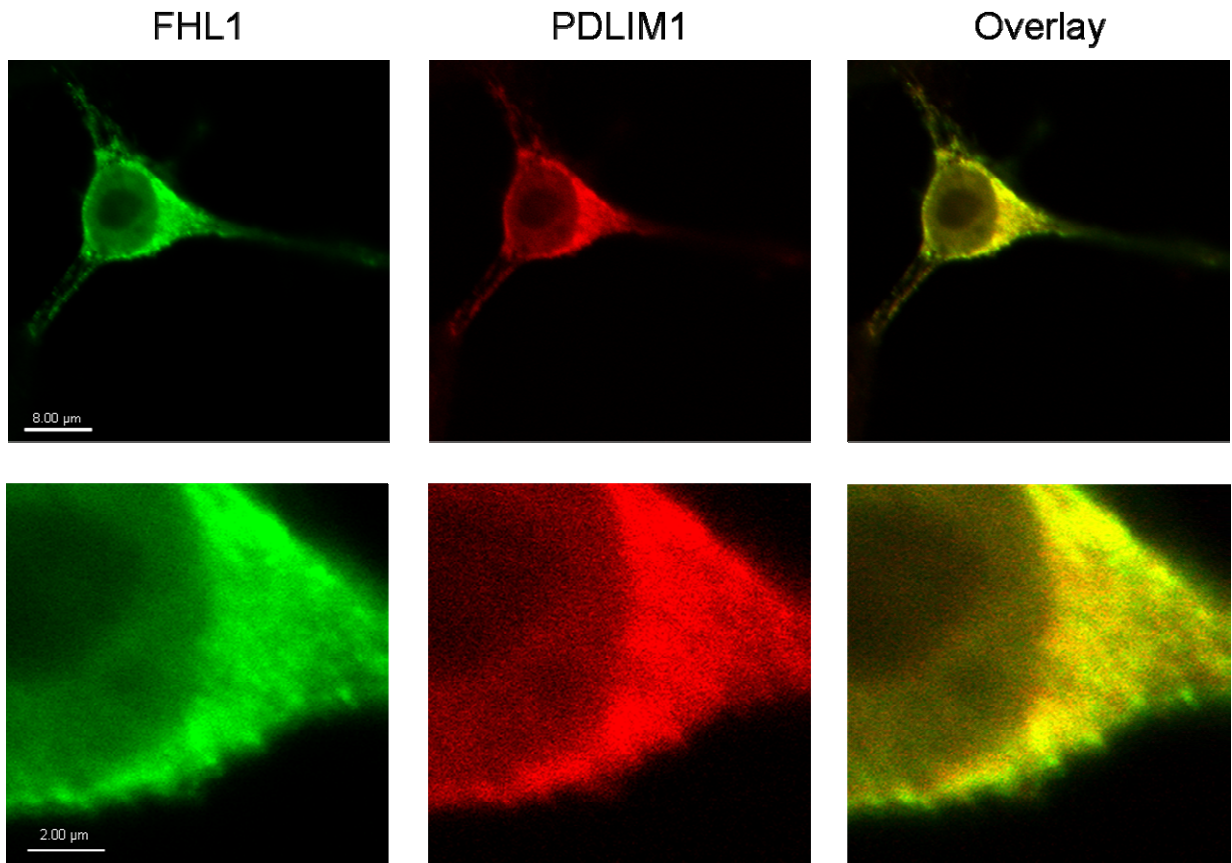


**Figure 25. Subcellular Co-localization of FHL1 and PDLIM1 in HEK-293 Cells**

Immunofluorescent analysis of subcellular distribution of FHL1 and PDLIM1 in transfected HEK-293 cells. FHL1 was detected with anti-CBP antibody and labeled green, whilst PDLIM1 was detected using anti-V5 antibody and labeled red. Regions of overlap are represented by yellow. The bottom panel illustrates the co-localization at a higher magnification.

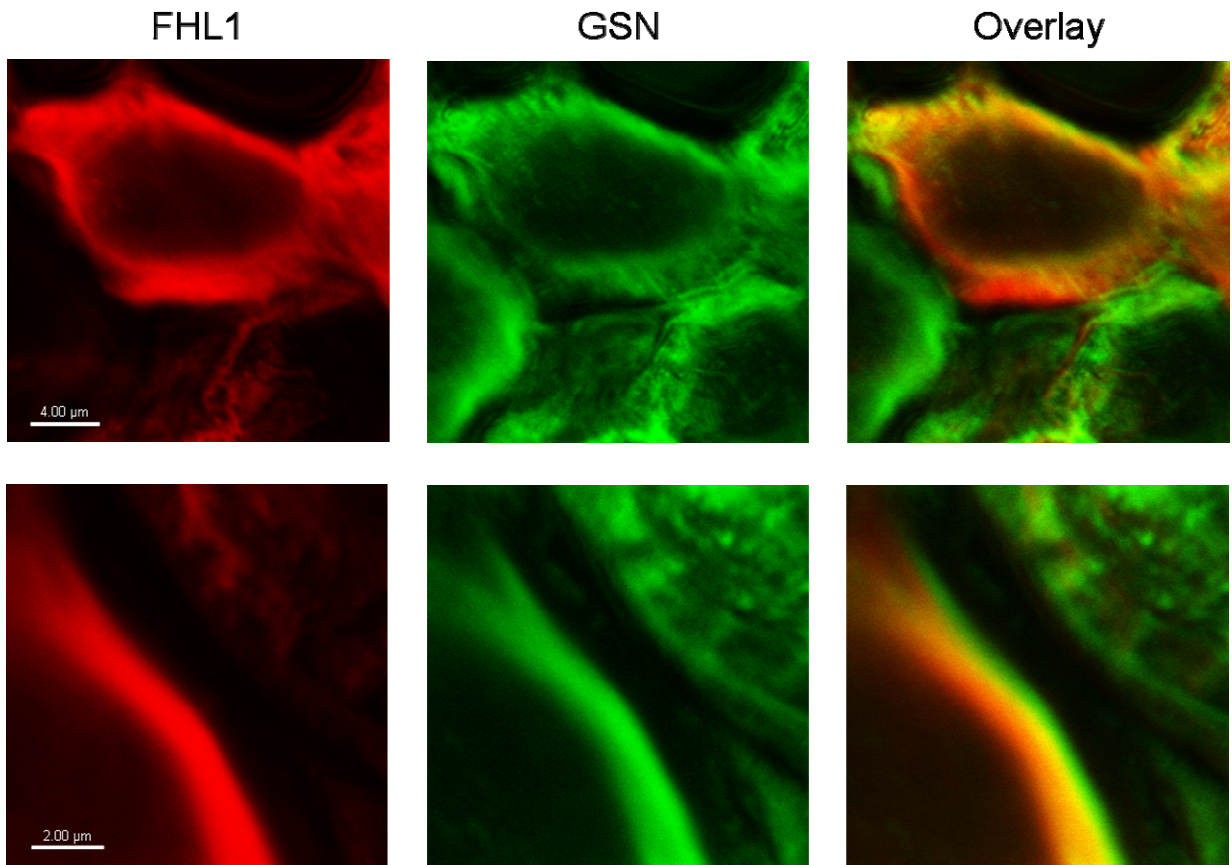


**Figure 26. Subcellular Co-localization of FHL1 and GSN in HEK-293 Cells**

Immunofluorescent analysis of subcellular distribution of FHL1 and GSN in HEK-293 cells. FHL1 was detected with anti-CBP antibody and labeled red, whilst endogenous GSN was labeled green. Regions of overlap are represented by yellow. The bottom panel illustrates the co-localization at a higher magnification.

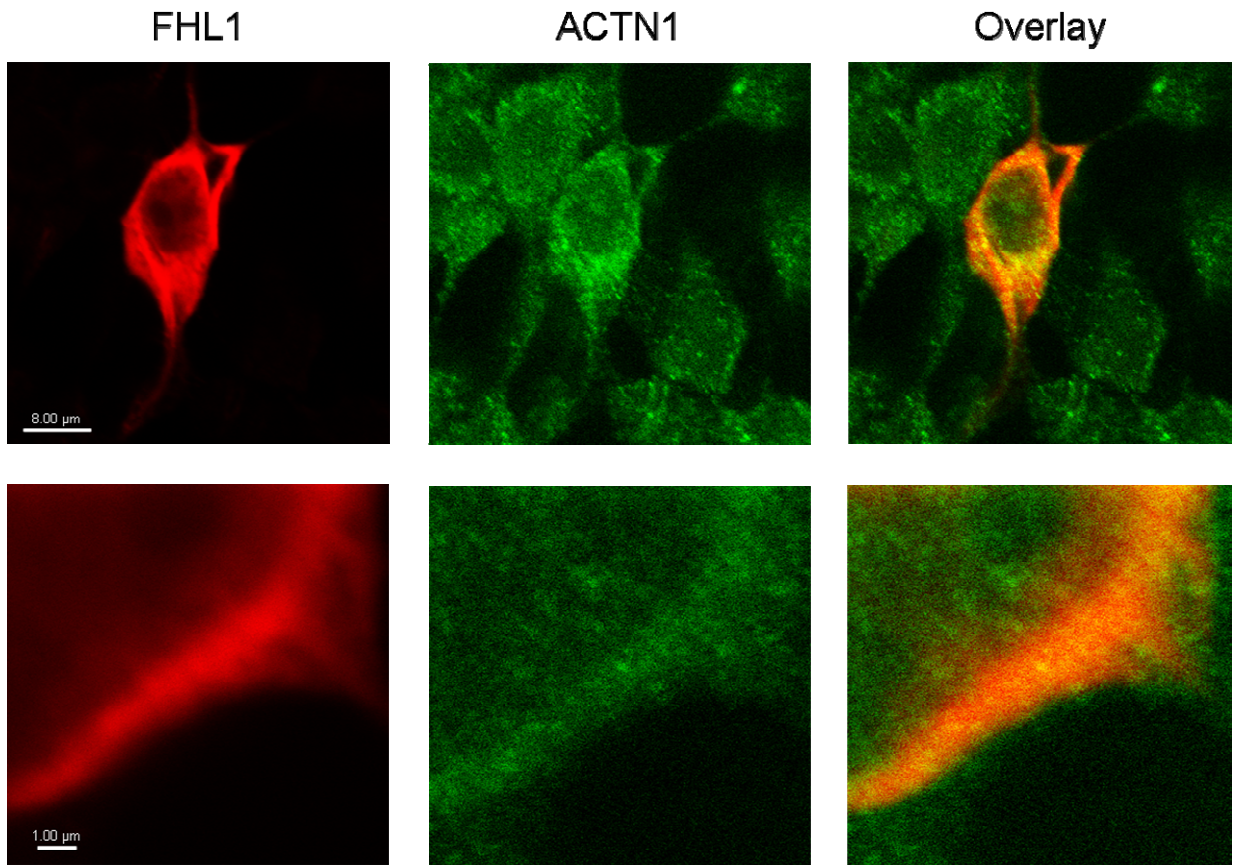


**Figure 27. Subcellular Co-localization of FHL1 and ACTN1 in HEK-293 Cells**

Immunofluorescent analysis of subcellular distribution of FHL1 and ACTN1 in HEK-293 cells. FHL1 was detected with anti-CBP antibody and labeled red, whilst endogenous ACTN1 was labeled green. Regions of overlap are represented by yellow. The bottom panel illustrates the co-localization at a higher magnification.

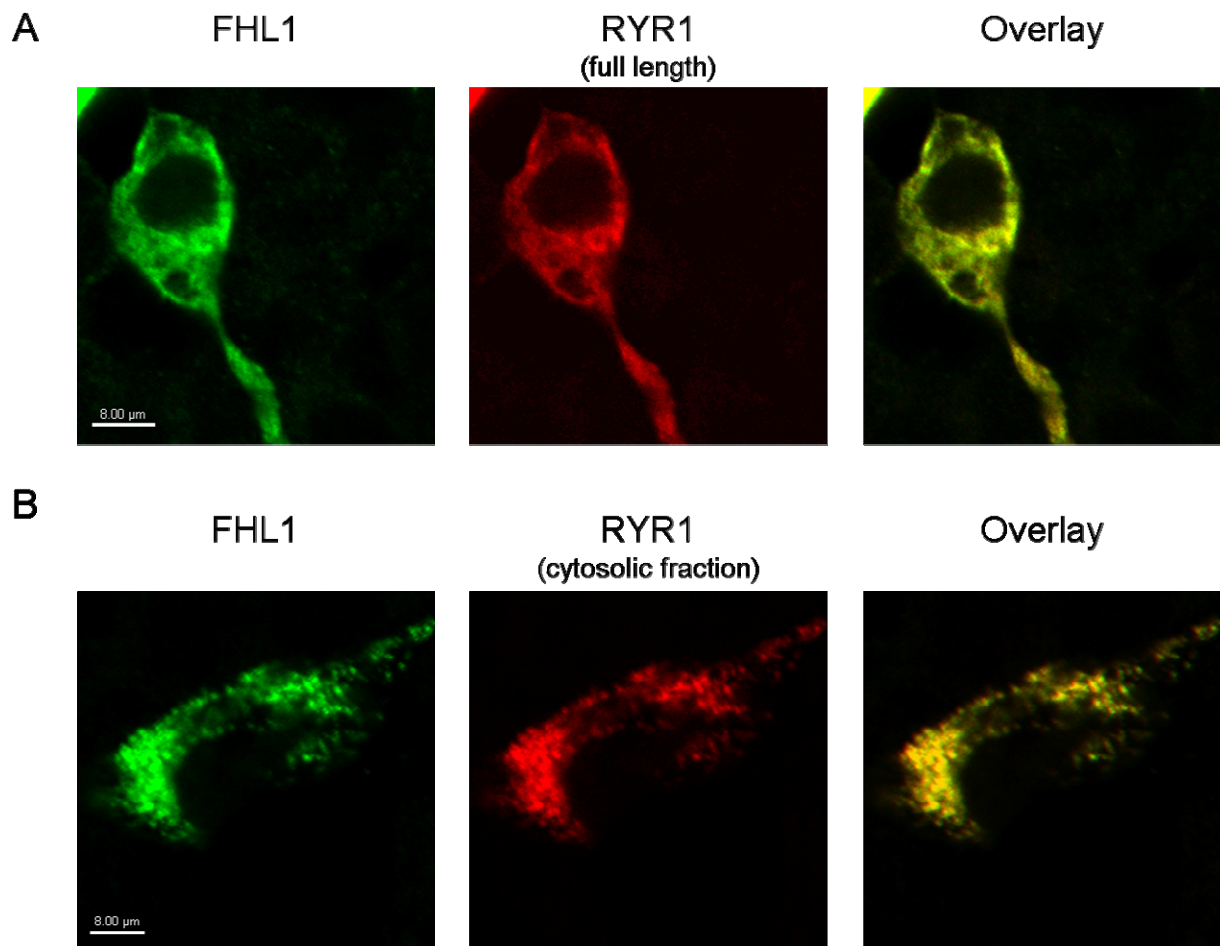


**Figure 28. Subcellular Co-localization of FHL1 and RYR1 in HEK-293 Cells**

Immunofluorescent analysis of subcellular distribution of FHL1 and RYR1 in transfected HEK-293 cells. (A) FHL1 was detected with anti-CBP antibody and labeled green, whilst transfected full length RYR1 was detected using anti-RYR antibody and labeled red. (B) Cells were co-transfected with SBP/CBP tagged FHL1 and 8xHis/StrepII tagged RYR1 lacking the transmembrane domains. The cytosolic fragment of RYR1 was detected using anti-RYR antibody and labeled red. Regions of overlap are represented by yellow in the third column.

## VI.B Skeletal Muscle

In skeletal muscle, where it is most abundant, FHL1 is localized at the I-band, encompassing the Z-line, and transiently at the M-line where it extends partially into the C-zone of the A-band. The resulting transverse banding pattern is of alternating thick and thin bands, corresponding to the I-band and the center of the A-band respectively [52]. Co-localization in muscles systems was assessed by co-IF studies using isolated rat soleus skeletal muscle fibers.

In Figure 29, the typical FHL1 alternating thick and thin banding pattern is evident. GSN staining also produced an alternating banding pattern, differing in intensities rather than thickness. When overlaid with the FHL1 IF-staining, the brighter bands of GSN corresponded with the thin FHL1 bands at the middle of the A-band. However, the fainter bands of GSN co-localized with the FHL1 at the thick I-band regions. In contrast, FHL1 and ACTN1 co-localization spanned the full range of the I-band (Figure 30). Here, the thin intervening band of FHL1 present at the M-line was absent, supporting previous findings of its transient localization pattern [52]. Unlike GSN and ACTN1, in skeletal muscle RYR1 is retained in the SR membrane, at the terminal cisternae of the A-I junctions [123]. During confocal microscopy studies, RYR1 can be resolved as double rows of dot-like immunosignals, with each spot representing a single triad structure [124]. In skeletal muscle co-stained with FHL1 and RYR1, a particular co-localization pattern was evident (Figure 31). Partial co-localization was observed, but only at one of the RYR1 double rows and consistently on the same side throughout the longitudinal section. Endogenous co-localization between PDLIM1 and FHL1 in skeletal muscle was not similarly studied due to a lack of antibody availability. Instead, to assess the colocalization in muscle systems, C2C12 cells were transiently transfected to express tagged FHL1 and PDLIM1 proteins (Figure 32). Similar to HEK-293 cells, FHL1 was diffusely present throughout the myoblast sarcoplasm, with weaker expression in the nucleus. Although PDLIM1 exhibited a similar pattern as in HEK-293 cells, in myoblasts it did not display differences in expression intensities in the sarcoplasm compared to the nucleus. Thus, the resulting co-localization was more prominent in the sarcoplasm. Multiple attempts to identify the expression patterns in differentiated C2C12 myotubes, however, were unsuccessful. Shortly upon cell fusion, and before sufficient differentiation was achieved, C2C12 myotubes persistently peeled off from the gelatin coated glass slides. Cells did not fare much better on plastic slides either. Thus, the PDLIM1 and FHL1 co-localization in striated muscle could not be properly assessed.

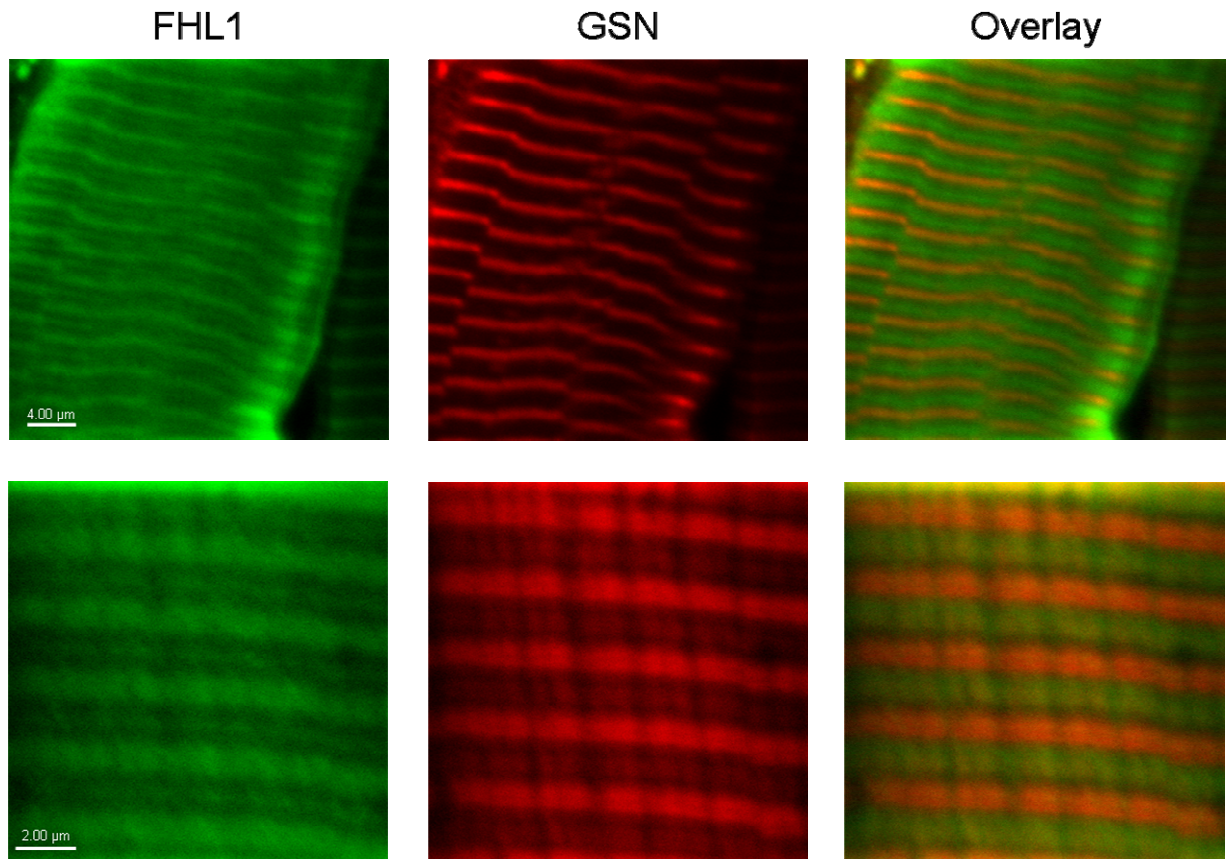


**Figure 29. Subcellular Co-localization of FHL1 and GSN in Skeletal Muscle**

Immunofluorescent analysis of subcellular distribution of endogenous FHL1 and GSN in rat soleus skeletal muscle. FHL1 was detected labeled green (first column), whilst GSN was alternatively labeled red (middle column). Regions of overlap are represented by yellow in the third column. The bottom panel illustrates the co-localization at a higher magnification.

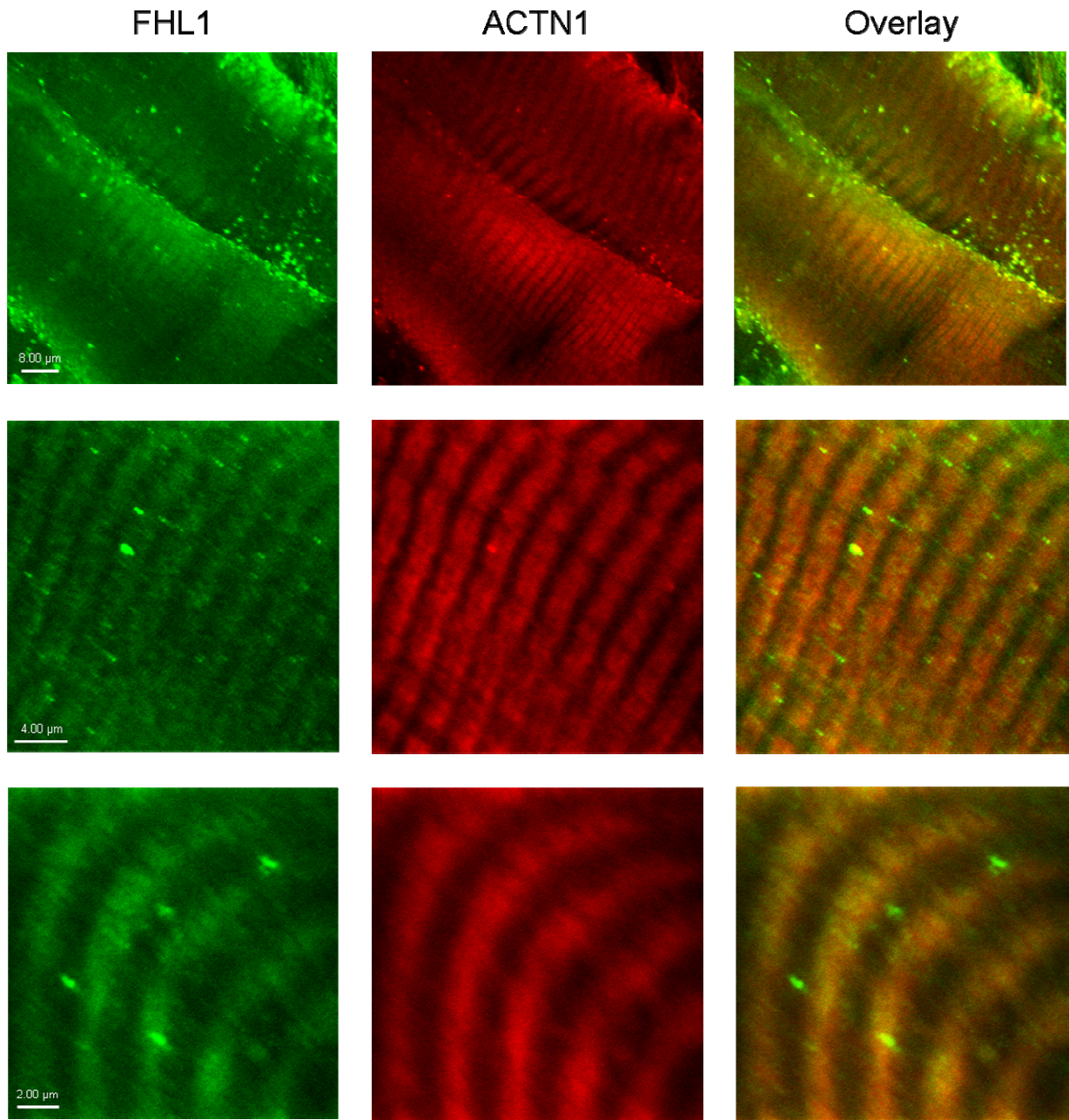


**Figure 30. Subcellular Co-localization of FHL1 and ACTN1 in Skeletal Muscle**

Immunofluorescent analysis of subcellular distribution of endogenous FHL1 and ACTN1 in rat soleus skeletal muscle. FHL1 was detected labeled green (first column), whilst ACTN1 was alternatively labeled red (middle column). Regions of overlap are represented by yellow in the third column. The bottom two panels illustrate the co-localization at a higher magnification.

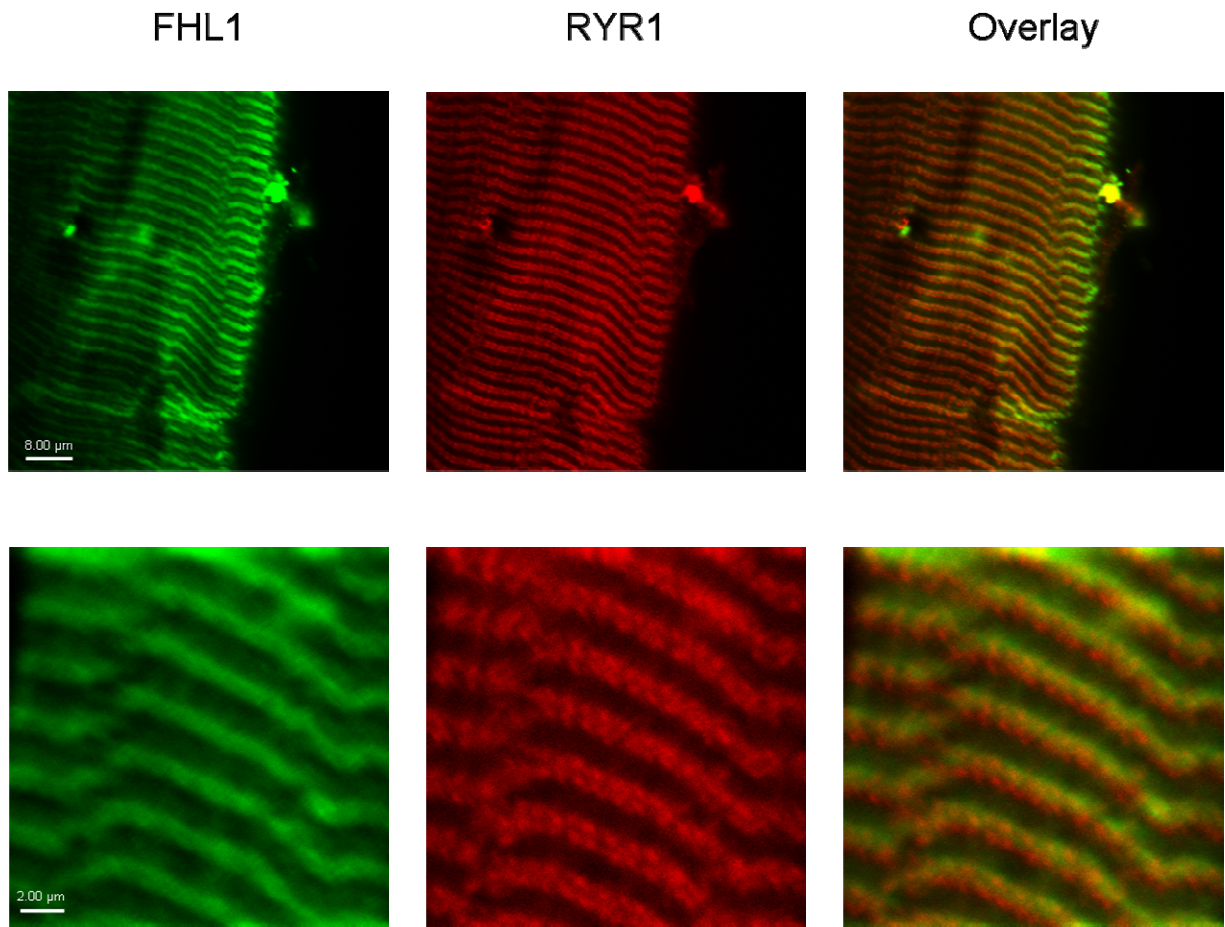


**Figure 31. Subcellular Co-localization of FHL1 and RYR1 in Skeletal Muscle**

Immunofluorescent analysis of subcellular distribution of endogenous FHL1 and RYR1 in rat soleus skeletal muscle. FHL1 was detected labeled green (first column), whilst RYR1 was alternatively labeled red (middle column). Regions of overlap are represented by yellow in the third column. The bottom panel illustrates the co-localization at a higher magnification.

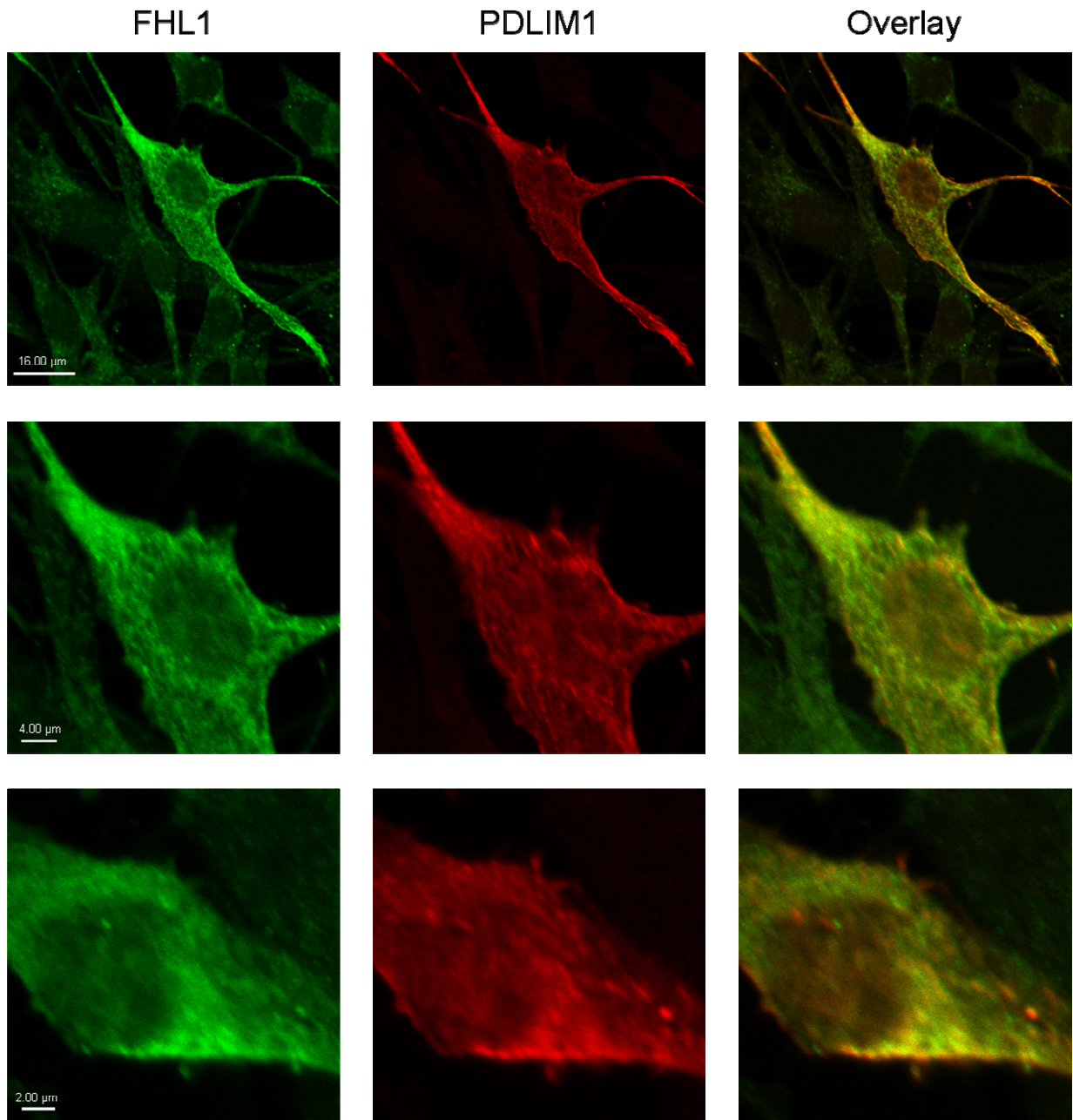


**Figure 32. Subcellular Co-localization of FHL1 and PDLIM1 in C2C12 Myoblasts**

Immunofluorescent analysis of subcellular distribution of FHL1 and PDLIM1 in transfected C2C12 myoblasts. FHL1 was detected with anti-CBP antibody and labeled green, whilst PDLIM1 was detected using anti-V5 antibody and labeled red. Regions of overlap are represented by yellow in the third column. The bottom two panels illustrate the co-localization at a higher magnification.

## CHAPTER FOUR: CONCLUSIONS

In general, the aim of my thesis was to identify novel interacting partners of FHL1. From the results obtained during the course of this project, a number of conclusions can be made.

- SBP/CBP dual affinity tagged FHL1 can be aptly purified and concentrated from HEK-293 cells;
- TAP allows for co-purification of interacting proteins with the tagged protein of interest, as witnessed by coomassie staining of protein gels and MS analysis of purified samples;
- a total of 882 proteins were identified via MS analysis of ten affinity purified samples
- 628 different proteins were identified from five FHL1 purifications, of which 442 were unique to FHL1 purifications;
- 61 proteins were identified uniquely in multiple FHL1 purifications;
- four proteins were validated as novel interacting partners of FHL1: PDLIM1, RYR1, GSN, and ACTN1;
- shared subcellular localization existed between FHL1 and the four novel interacting proteins, in both HEK-293 cells and skeletal muscle.

## CHAPTER FIVE: DISCUSSION

### ***I. PURIFYING PROTEIN COMPLEXES***

To identify novel FHL1 protein interactions, the TAP method was applied in HEK-293 cells. This particular method was chosen for its efficiency, potential for high-throughput applications, and capacity for purifying protein complexes from *in vivo* systems [71, 83]. Since its conception in yeast, TAP has performed efficiently from various organisms. However, successful application to higher eukaryotic organisms, particularly mammalian cells, has continued to face several limitations. Requirement of large sample quantities, overall low yield of bait and interacting proteins, and endogenous protein competition for interactors are some of the common issues faced [83-87].

For the purification of FHL1 containing protein complexes from mammalian cells, HEK-293 cells proved to be a worthy contender. Although FHL1 was known to express predominantly in skeletal muscle tissue, most available research demonstrated its association with the cytoskeleton, particularly the actin stress fibers, which are ideally studied from non-muscle cells [75]. Since endogenous expression of FHL1 is also present in HEK-293 cells, concerns regarding ectopic expression were alleviated [55]. Furthermore, due to its relatively high transfection efficiency, HEK-293 cells also reduced the amount of starting cells necessary when compared to C2C12 myoblasts, almost by one half. However, due to the CMV promoter driven plasmid transcription, concerns of overexpression consequences persisted, replacing concerns of endogenous FHL1 competing for interactors. Unfortunately, multiple attempts to generate stable cell lines with moderate FHL1 expression in order to resolve this issue were unsuccessful.

Considering the purification itself, the recovery and concentration of bait protein from the cell lysate was satisfactory. However, the recovery of SBP/CBP dual tagged bait bound to either the streptavidin or calmodulin resin proved to be difficult. In order to retrieve a decent proportion of the bound protein, multiple lengthy elutions were necessary. Suboptimal protein recovery also resulted in complications to the ideal tryptic digestion method for subsequent MS analysis, hence the comparison between in-solution, on-bead, and in-gel digestion. Each method proved to possess particular benefits and disadvantages. For instance, in-solution digestion identified the greatest number of different proteins, although with low detection of FHL1 due to poor recovery from calmodulin resin. In comparison, on-bead digestion identified

the greatest amount of bait protein, however ideal detection of co-purified proteins was masked by saturation of the mass spectrometers capacity by large amounts of digested calmodulin peptides. In-gel digestion, however, proved to be the weakest method for detecting co-purified proteins. Although boiling protein bound resin in loading dye is sufficient to sever affinity interactions, tryptic digestion or recovery of peptides from resolved SDS-PAGE gels was insufficient, or a significant amount of protein was lost during the many steps involved with in-gel digestion and solid-phase extraction procedures.

The effectiveness and reproducibility of the TAP method, however, must also be considered and was best demonstrated visually by heatmap representation (Figure 13). Of the 882 total proteins identified, almost one half were eliminated by their presence in the control purifications. However, approximately 65% of those proteins were only present in tag control purifications and were possibly specific interactors of DPYSL3 or RBP1. The remaining 35% of contaminant proteins were thus intrinsic to the TAP procedure and abundantly present, which contributed to saturating the mass spectrometers detection capacity. Particularly predominant were actin, acetyl-CoA carboxylase, myosin, and ribosome proteins. Certain proteins were also enriched depending on the trypsin digestion method used, such as calmodulin for on-bead digestion and keratins for in-gel digestion. Furthermore, reproducibility was also considerably low. Although approximately one half of the total detected proteins were uniquely isolated from FHL1 purifications, only 14% were identified in multiple experiments. A number of factors could explain this disparity. For instance, if large multimeric FHL1 containing complexes were routinely isolated, different protein components may have been differentially detected during the various experiments. This would also explain the presence of ribosomal and spliceosomal components, which are common contaminating proteins. Since specific gene names were used during the initial filtering steps, specific components not repeatedly detected were allowed to proceed to the next level. Furthermore, GO term analysis revealed a significant proportion of the proteins were membrane-bound, particularly nuclear membrane, and components of nuclear processes (ie. gene expression, DNA polymerization). Membrane proteins and nuclear proteins are often the most difficult to purify from cell systems [125, 126]. Considering the non-stringent, native conditions used for TAP, the transient appearance of these proteins may be caused by technical incompatibilities. In general, consistent identification of weak or transient interactions can be challenging and is obviously a weakness of my approach.

During the course of this project, several alternative affinity tags and methods were employed for the purification of protein complexes. For instance, and although data is not

shown, TAP was performed from HEK-293 cells for baits dual tagged with 8x His residues and a short Strep-II tag, using their affinity properties to Ni-NTA and Strep-Tactin® resin respectively. First, these affinity tags were significantly smaller than the SBP/CBP tags (approximately 2 kDa versus 10 kDa), thus reducing concerns for potential conformational changes. Second, while retrieval of tagged proteins from the cell lysate was similar to the SBP/CBP system, the recovery of bait protein bound to affinity resin was more efficient. However, this particular TAP system was rejected due to its significantly high background proteins, particularly ribosomal and spliceosomal components. Alternatively, when endogenously expressed FHL1 was immunoprecipitated from rabbit skeletal muscle lysate and analysed by MS to identify the co-purified proteins, the immunoglobulin proteins proved to be a major concern by saturating the mass spectrometers detection capacity. In fact, contrary to the strong signal detected during immunoblot analysis, a total of only three spectra were identified for FHL, which was also lower than the 5-40 spectra detected from TAP experiments. The use of an acidic (pH 2.4) elution buffer was sufficient to release the immunoglobulin-protein A/G interactions initially used for resin immobilization of the primary antibody. Interestingly, the pull down assay performed using immobilized tagged FHL1 treated with a muscle lysate appeared to be both successful and sensitive, as depicted by silver stain analysis (Figure 17). For greater specificity of binding the 8xHis tag on FHL1, the newer TALON® metal affinity resin, precharged with cobalt, were used instead of Ni-NTA beads. Distinct differences were visible between wild type and Tg-PLN R9C lysate conditions, and although protein interactions were formed *in vitro*, this method might be worth consideration for any future purification experiments, although an improved in-gel digestion or alternative MS compatible elution methods would be required.

Regardless, a possible 61 FHL1 protein interactions were identified using TAP from HEK-293 cells. GO-term analysis of these proteins revealed many were involved in biological processes which were rationally plausible for FHL1 involvement, such as organization and binding of the actin cytoskeleton, motility, intracellular transport, cell development and regulation, and muscle processes. Furthermore, many interactions were previously identified between proteins from the group of 61, which could form the basis for in-direct FHL1 interactions within larger multimeric protein complexes. These interacting proteins could be mapped to pathways involving regulation of the actin cytoskeleton, cell-cell signaling, fatty acid metabolism, MAPK and Wnt signaling, and focal adhesion, tight junction, and integrin signaling. Thus, a variety of techniques are available for identifying novel protein interactions,

each with their own set of pros and cons. However, the applied TAP method was successful in identifying 61 potential interactors, which can be mapped to a broad range of cellular processes.

## **II. ASSOCIATION WITH HEART FAILURE**

### **II.A Validity of Studying the Tg-PLN R9C Model**

The PLN R9C mutation was originally characterized from a large American family, demonstrating an autosomal dominant inheritance of an early-onset and rapidly progressive form of DCM [112]. The transgenic mouse model of this mutation remarkably recapitulated the phenotype [112, 113]. Prior to this model, most studies of DCM utilized a selection of mutations identified in sarcomeric or cytoskeletal proteins, such as dystrophin, desmin, taffazin, lamin A/C, titin, actin, troponin T, and B-myosin heavy chain. Disease was thought to result from impaired force production or transmission [106]. In contrast, the PLN R9C mutation resulted in DCM by disruption of the normal calcium cycling, which is a prominent feature of failing cardiomyocytes [112]. Thus, the Tg-PLN R9C model was a good candidate for further studies in heart failure and DCM.

### **II.B Reliability of the Profiling Studies of the Tg-PLN R9C Model**

Although much progress has been made towards understanding the underlying mechanisms leading to heart failure, further identification and knowledge is required of the major protein candidates associated with disease. For these purposes, Gramolini *et al.* performed both large scale proteomics and microarray assessments of the Tg-PLN R9C model to characterize the key molecular candidates involved in disease, particularly at the earliest stages prior to clinical presentation [113].

For the proteomics study, homogenized ventricular samples were fractionated into their cytosolic, mitochondrial, and microsomal portions and analysed separately, while the abundant contractile proteins were excluded. This alleviated saturation of the mass spectrometer's detection capacity by components of the contractile machinery and allowed for better coverage of the proteins present in each fraction, at higher sensitivity to their relative proportions [113]. Following this, a total of 12,847,690 spectra were acquired from the multiple samples analysed, which could be mapped with high confidence to 6190 proteins in the heart, of which 593 demonstrated statistically significant differential abundance. Furthermore, with additional

stringent statistical analysis, the proteins were ranked to obtain a subset of the 40 most differentially expressed [113].

Meanwhile, microarray profiling was performed in parallel, using full-genome array chips. To assess the reliability of the techniques, comparative analyses were performed with the proteomic and mRNA expression patterns. An excellent correspondence was detected between both global profiles [113]. Of the 593 protein candidates which exhibited differential expression in the diseased model compared to wild type, only 16 were deemed to be significantly non-correlated, none of which belonged to the subset of top ranked 40 proteins. The differences identified between both data sets could reflect post-transcriptional regulation [113]. Thus, considering the strong correlations between the proteomic and microarray studies, and the inherently better sensitivity and identification properties offered by microarray analysis, assessing the expression patterns in disease for the 61 potential FHL1 interactors using the microarray dataset proved to be a valid choice.

## **II.C Four and a half LIM domain protein 1**

FHL1 was identified from the list of top ranked 40 proteins as one of the four most upregulated, with changes occurring early in disease. Similarly, FHL1 was also detected upregulated during comparative gene expression profiling of transgenic mice overexpressing Gs-alpha, with respect to control littermates [127]. Similar to observations in Tg-PLN R9C mice, a 2-3 fold increase in FHL1 transcript level was detected even at the earliest time points tested, although alterations in expression were not detected for either FHL2 or FHL3 [127]. Furthermore, FHL1 overexpression was detected at various time points from three additional mouse models of cardiomyopathy, with enhanced  $\beta$ -adrenergic receptor (AR) signaling. In all three mice models, overexpressing  $\beta$ 1-AR,  $\beta$ 2-AR, or PKA, FHL1 was upregulated by the early stages of disease, and continued to increase with disease progression. Thus, FHL1 was upregulated in all four mouse models with chronic stimulation of the  $\beta$ -AR signaling pathway [127]. Since differential expression could be detected before disease onset, with continued increase throughout disease, it was suggested FHL1 could participate in the transition of phenotype between early and late stages, and thus contributes to the development of cardiomyopathy [127].

In contrast, the opposite expression profile was detected for FHL1 from human DCM hearts. Using high-density oligonucleotide arrays, Yang *et al.* quantified the expression levels of approximately 7000 genes in non-failing and failing human hearts with a diagnosis of end-

stage ischemic and DCM [128]. In diseased hearts, FHL1 was found to be downregulated at both the mRNA and protein level [128]. Thus, the contradictory FHL1 expression profiles from DCM in mice and humans might be a consequence of the inherent physiological differences between the species. This has always posed a concern when findings from one species are adapted to another. Alternatively, the discrepancies could also be explained by differences in experimental technicalities (such as probe sets, methodologies, etc.), specificities of detection, or the conditions of the hearts obtained from patients of end-stage disease. However, FHL1 has consistently been identified as a strong candidate for overexpression in human cardiac hypertrophy, from three different large-scale gene expression profiling studies [129-131]. Thus continued study of FHL1 with respect to heart failure is warranted, especially since HCM and DCM do share common pathways in disease development [132].

## **II.D $\alpha$ -Actinin-1**

Similar to FHL1, ACTN1 was also present in the list of top ranked 40 proteins identified from the proteomic assessment of Tg-PLN R9C mice [113]. It was recently also reported to be 2.2-fold greatly expressed in idiopathic DCM human hearts, although the differential expression was specific for female patients [133]. Analogous to this, talin, a recently identified interactor of FHL1, was also detected amongst the 40 most differentially expressed proteins in Tg-PLN R9C mice [75, 113]. Thus, FHL1 interacts with multiple proteins significantly upregulated in disease.

## **II.E Gelsolin**

In the PLN R9C microarray study, GSN mRNA levels were detected to slowly increase throughout disease, culminating in an approximately 1.5 fold increase by end-stage DCM. More drastic changes, however, have been detected in alternative mice models of DCM. For instance, in TOT and racET models, GSN proteins levels were 3 and 2 folds higher, respectively. Similarly, in a racET model of HCM, a 4 fold increase was detected [128]. Furthermore, GSN transcript levels were significantly elevated in hearts explanted from human patients of end-stage ischemic and dilated cardiomyopathy [128]. In mice subjected to myocardial infarction, elevated GSN was detected and determined to regulate the ensuing cardiac remodeling [134]. GSN contribution to the increased apoptosis was mediated by interaction with hypoxia-inducible factor-1 $\alpha$  and deoxyribonuclease I [134]. Thus, GSN could mediate similar effects in the Tg-PLN R9C mice, where significant apoptosis was detected.

## **II.F PDZ-LIM Protein 1**

PDLIM1 mRNA was not identified from the microarray study, though it was identified via proteomics where an approximately two fold average difference was detected in Tg-PLN R9C mice during disease. To date PDLIM1 has not been associated with any cardiovascular disease, as determined by PubMed searches. However, in general, PDLIM1 is a poorly annotated protein and disease associations may yet be discovered.

## **II.G Ryanodine Receptor 1**

Unlike the other three FHL1 interacting candidates described, RYR1 mRNA was actually found to decrease during disease. In fact, it was only one of three candidates from the 61 potential FHL1 interactors found to be negatively regulated. Furthermore, it was found to be significantly lower early in DCM development, with continued decrease throughout disease progression. Northern blot analysis of human cardiac samples from patients with ICM or DCM have also shown a significant reduction in transcript levels (28-31%) [135, 136]. However, the association between RYR1 and disease may not only translate into lower protein expression, but also alterations in proper function, possibly involving disturbed excitation-contraction coupling in the failing heart as well as aberrant release of SR calcium. In failing hearts, these effects were considered attributable to PKA mediated hyperphosphorylation of RYR [121].

## **III. INTERACTIONS WITH FHL1**

### **III.A $\alpha$ -Actinin-1**

$\alpha$ -Actinins are ubiquitously expressed actin-filament cross-linking proteins, belonging to a highly conserved family of actin-binding proteins, the spectrin superfamily. There are four  $\alpha$ -actinin encoding genes, whose expressed products can be grouped into two distinct classes: muscle and non-muscle isoforms, which are calcium insensitive and sensitive respectively. ACTN1 belongs to the latter group and is crucial to the extensive actin stress fiber subcellular structure [137]. Stress fibers consist of bundles of actin filaments, approximately 10-30, held together by the crosslinking protein ACTN1 and randomly oriented [138]. In muscle systems, the contractile sarcomeric structures are deemed the equivalent of the actin stress fiber network in non-muscle cells [137, 138].

The interaction between ACTN1 and FHL1 may be mapped to biomechanical stress induced responses in cells. FHL1 was previously identified as a component of the stress sensor

complex at the sarcomeric I-band, where it interacts with the MAPK cascade components, Raf1, MEK2, and ERK2, at the N2B region of titin in cardiomyocytes [53]. Though the precise mechanisms are not known, FHL1 mediates a connection between the muscle stretch sensor and downstream responses by titin and MAPK components [53]. Similarly, in human intestinal epithelial cells, ACTN1 has also been associated with deformation strain-induced cytoskeletal signaling. An intact cytoskeleton was determined to be required for strain-induced phosphorylation of ERK1/2, as well as a microtubule network capable of undergoing rearrangement [139]. In fact, siRNA-mediated knockdown experiments demonstrated a specific requirement for the non-muscle ACTN1 for strain-induced mechanotransduction and phosphorylation of ERK1/2, as opposed to non-muscle ACTN4 [139]. Apart from the structural role of ACTN1, its ability to function as a scaffolding protein and interaction with ERK1/2 could explain its involvement [139]. Furthermore, ERK2 is a common interactor of both FHL1 and ACTN1 proteins, all involved in biomechanical stress response. Thus the functions and interactions of ACTN1 in epithelial cells may be adapted to muscle cells, or conversely, those of FHL1 may be applied to non-muscle cells, considering IF co-localization of both proteins in both cell systems (Figures 27 and 30).

### **III.B Gelsolin**

The transcribed GSN gene products consists of a cytoplasmic and secreted plasma isoforms, of which the former was likely identified here as an interactor of FHL1 [140]. Within the cell, the multifunctional cytoplasmic GSN has been best described for its role in actin filament turnover [140, 141]. Structurally, the cytoplasmic GSN is composed of six GSN-like domains and exists in a globular conformation in the absence of calcium. In the presence of calcium, the structure is relaxed allowing for the formation of a calcium binding domain coordinated by actin and the fourth GSN-like domain. In its activate form, GSN binds to and severs two adjacent actin filaments, with GSN remaining bound to the newly formed barbed ends of one of the resulting shorter filaments [140, 141]. Subsequent binding of GSN to phosphatidylinositol lipids results in uncapping actin filaments, which exposes the barbed ends for polymerization. Within the cell, phosphatidylinositol 3,4 or 4,5-bisphosphate are two isoforms capable of inhibiting the actin severing activity of GSN and inducing dissociation from actin [140, 141].

Considering the actin filament remodeling properties of GSN, the phenotype of myoblast cells overexpressing FHL1, and the overrepresented biological GO term amongst the group of

61 potential interactors, FHL1 may participate in cell motility functions with GSN. Multiple factors contribute to the general properties of the cytoskeleton, including filament length, flexibility, concentration and presence of crosslinks. Proteins capable of modifying any of these parameters are potential candidates for regulating cellular morphology and functions, such as cell shape and motility [140]. Both GSN and FHL1 demonstrated co-localization in HEK-293 cells in this study (Figure 26), and previously along actin stress fibers [75, 141].

In cultured fibroblasts, overexpression of GSN resulted in increased motility, whereas osteoclasts isolated from GSN null mice exhibited decreased motility [142]. These osteoclasts failed to form podosomes, cell adhesion structures, which affected their normal and osteopontin-induced motile properties [143]. Furthermore, delayed retraction was observed of filopodia from neuronal growth cones from GSN null mice. Neuronal growth cones are highly motile structures, and since the formation of filopodia appeared unaffected, which is mainly dependent on adseverin function, GSN could be held accountable for the retraction process [143]. Similarly, in  $\alpha 5\beta 1$ -integrin activated myoblasts, overexpression of FHL1 promoted cell spreading and migration while inhibiting cell adhesion [50]. In differentiated muscle cells, overexpression of FHL1 resulted in significant branching with multiple major cytoplasmic protrusions from the cell body. GSN and FHL1 are possibly components of the normal, regulated, cell motility processes, as opposed to pathological migration. In accordance with this, both GSN and FHL1 have repeatedly been detected downregulated in a variety of tumours, particularly in invasive cases, such as colon, breast, and pancreatic cancers [60, 62, 144-147]. A disturbed cytoskeleton is characteristic of transformed cells [145].

### **III.C PDZ-LIM Protein 1**

PDLIM1 belongs to the family of PDZ-LIM proteins, whereby each member possesses an N-terminal PDZ domain and one to three LIM domains at the C-terminal. PDLIM1 contains only one LIM domain, but both the PDZ and LIM domains are common multifunctional protein-protein interaction motifs [148, 149]. In non-muscular cells, PDLIM1 has been localized to stress fibers via interaction with ACTN1 by its PDZ domain [148, 149]. Moreover, PDLIM1 is actually essential for the assembly of stress fibers as well for the maturation of focal complexes into focal adhesions. As determined from a trophoblast-derived choriocarcinoma cell line, RNAi mediated suppression of PDLIM1 resulted in a loss of stress fibers, with localization of actin filaments and  $\alpha$ -actinin at the cells periphery [150]. Studies from resting platelets

suggested PDLIM1 and ACTN1 actually formed a complex in the cytosol first, before translocating to the F-actin rich cytoskeleton [148].

Of the four described novel FHL1 interactors, PDLIM1 is the least characterized. However, based on knowledge obtained from other PDZ-LIM proteins, the relationship PDLIM1 maintains with FHL1 is possibly as an adaptor protein. Many PDZ-LIM proteins function as adaptor proteins mediating a connection between signaling molecules and the actin cytoskeleton, usually binding kinases at their LIM domains [148, 150]. For instance, Cypher binds ACTN2 at the Z-line via its PDZ domain, while simultaneously recruiting protein kinase C via its LIM domain [151]. Similarly, another member, Enigma interacts with  $\beta$ -tropomyosin through its PDZ domain and with receptor tyrosine kinases at its LIM domain [152]. When co-expressed in U2OS osteosarcoma cells, PDLIM1 itself interacts with the normally nuclear Clik1 kinase via its LIM domain, and causes relocalization to the actin stress fibers [153]. Thus, PDLIM1 might also target FHL1 to the actin stress fibers, possibly via a LIM-LIM domains interaction. LIM-LIM domain interactions have been described, for instance, between two LIM only proteins such as muscle LIM protein and CRP [154]. LIM-LIM domain interactions likely also mediates the interaction between FHL1 and FHL2, since both proteins possess only LIM domains [74]. Furthermore, PDLIM1 may even be responsible for shuttling FHL1 out of the nucleus, similar to Clik1 [153]. PDLIM1 and FHL1 co-IF studies performed for this project demonstrated nuclear co-localization in HEK-293 cells and C2C12 myoblasts. However, in differentiated myotubes, FHL1 is absent from the nucleus [11]. Since the FHL1A isoform lacks a known nuclear export signal, an alternative mechanism must exist to ensure its relocalization from the nucleus upon cell differentiation. Perhaps PDLIM1 acts to target FHL1 to the sarcomeric and cytoskeletal elements.

### **III.D Ryanodine Receptor 1**

Three RYR isoforms have been identified in mammals. RYR1 is predominantly found in skeletal muscle, whilst RYR2 is the cardiac specific isoform. In contrast, RYR3 was first cloned from rabbit brain samples. Encoded from different genes, all three RYRs share a high sequence identity (66-70%) [155]. The functional ryanodine receptor is a massive tetrameric  $\text{Ca}^{2+}$  channel, with each monomer containing an excess of 5000 amino acids and weighing approximately 565 kDa [155]. Approximately 90% of the polypeptide sequence comprises the cytoplasmic domain, while the remaining 10% accounts for the transmembrane and channel domain [155]. In skeletal muscle, RYR1 forms the foot structure associating the junctional

terminal cisternae of the SR with the transverse tubule [124]. Muscle contraction is initiated by activation of the RYR1 through a physical interaction with the surface membrane L-type  $\text{Ca}^{2+}$  channel, dihydropyridine receptor, located in the T-tubular membrane where it is directly opposed to RYR1 serving as a 'voltage sensor' to detect action potentials [121].

In contrast to the actin filament associated novel FHL1 interactors described above, RYR1 is a large transmembrane  $\text{Ca}^{2+}$  release channel. Considering the association between FHL1 and the cytoskeleton, and the scaffolding properties of LIM proteins, it is plausible FHL1 functions to anchor the channel to the underlying cytoskeleton. However, a regulatory function is possible, either directly or by recruiting other regulatory proteins to its LIM domains, thereby functioning as an adaptor protein.

Cytoskeletal proteins include an array of proteins which underlie and interact with cell membrane elements. In mouse T-lymphoma cells, RYR was identified from internal  $\text{Ca}^{2+}$  storage vesicles, and an interaction was described with I-ankyrin [156]. Ankyrin is a membrane-associated cytoskeletal protein which also demonstrated a capacity to regulate internal  $\text{Ca}^{2+}$  release during lymphocyte activation. It also effectively prevented the binding and  $\text{Ca}^{2+}$  release inhibitions by ryanodine [156]. Furthermore, in cultured neuronal cells, disruption of the actin cytoskeleton resulted in diminished RYR-mediated  $\text{Ca}^{2+}$  release. Disassembly of the actin cytoskeleton was caused by treatment with cytochalasin D, which inhibits actin polymerization [157]. Moreover, an interaction has previously been described between FHL1 and another ion channel protein, KCNA5. Patch clamp experiments demonstrated a functional role for FHL1, whereby KCNA5 activity was modified by increased  $\text{K}^+$  current density, altered channel gatings, and enhanced slow inactivation [55].

Similarly, FHL2 was also discovered to interact with a pore-forming  $\text{K}^+$  channel subunit, human ether-a-go-go-related gene (HERG) [158]. HERG contributes to the rapidly activating delayed rectifier potassium current ( $\text{I}_{\text{Kr}}$ ), which is vital for action potential repolarization in myocardium. When coexpressed in cells, FHL2 significantly amplified the HERG current amplitude and accelerated the deactivation rate of the tail currents [158]. FHL2 may also be involved in repolarization of cardiac cells via its interaction with the  $\beta$ -subunit minK of voltage-gated  $\text{K}^+$  channels encoding the delayed rectifier current  $\text{I}_{\text{Ks}}$  [159]. Thus, FHL1 protein may mediate a structural connection between RYR1 and the cytoskeleton, in addition to regulating electrophysiology.

## CHAPTER SIX: LIMITATIONS

The current study applied the TAP method to identify FHL1 interactions from HEK-293 cells. However, considering FHL1 is predominantly expressed in skeletal muscle and upregulated in cardiomyopathies, interactions would ideally have been identified from muscle cells. However, poor transfection efficiencies and purification from C2C12 skeletal muscle cells inhibited further immediate TAP studies. Furthermore, concerns regarding the transient overexpression of FHL1 in cells could not be appeased. Multiple attempts at generating stably expressing cell lines were unsuccessful.

Another limitation to the entire process was the loss of interacting proteins at various stages. First, transient and weak interactions were inherently lost during the TAP procedure with multiple washes and insufficient elution efficiencies. Interacting proteins were also lost during the tryptic digestion process and solid-phase extraction. In addition, low abundant proteins are often overlooked during MS analysis, masked by the presence of more abundantly present proteins. Without at least two unique spectras, these proteins would have failed to make the minimum requirements for further consideration.

With respect to MS identification, however, absolute resolution between highly homologous proteins is a challenge. For instance, although GSN was identified via MS, whether the cytoplasmic or secreted isoform was detected could not be absolutely determined. Specific identity might only be achieved by increased peptide coverage, identifying unique isoform specific peptides if available. Furthermore, an ideal trypsin digestion method was not available for preparing samples for MS analysis, with in-solution, on-bead, and in-gel digestion methods each presenting with various limitations. In-gel digestion was especially challenging, which prevented proper analysis of the purified samples obtained from immobilized FHL1 pull down assays, comparing wild type and Tg-PLN R9C lysates. During the TAP optimization process, buffer compatibility with the mass spectrometer posed a continued limitation.

Considering the validation of protein interactions, an alternative method is necessary to strengthen the association between FHL1 and RYR1. In addition, negative controls and reciprocal co-IPs would be ideal for validation of an interaction between FHL1 and both GSN and ACTN1. For PDLIM1, however, purchase of a primary antibody is warranted for validation of the subcellular co-localization in skeletal muscle. It would also avoid the need to overexpress tagged proteins in cultured cells for co-IP validation of interactions and confocal imaging, which would alleviate concerns of false positive interactions and mislocalization.

## CHAPTER SEVEN: FUTURE DIRECTIONS

In the present study, 61 potential FHL1 interactions were identified, with validation of only four. Similar to PDLIM1, cDNAs for 22 additional candidates were cloned into the V5/6xHis tag encoding vector. For generating a larger FHL1 interaction network, validation of interactions can be systematically performed using the generic co-IP method. Alternatively, Invitrogen's ProtoArray™ Human Protein Microarray could be screened to identify additional novel interactions, while simultaneously verifying interactions with the 61 potential interactors.

For the four proteins where a novel interaction with FHL1 was established, characterization of the interaction is warranted. Since different LIM domains mediate different interactions and are considered capable of establishing subcellular localization, interaction domain analysis may be valid. In addition, the kinetics of binding affinities can also be assessed. For instance, Biacore™ sensor chips can be prepared with immobilized FHL1 and subjected to an analyte solution consisting of an interacting protein. The automated Biacore™ system can then provide details regarding, for instance, the interaction kinetics (ie. association and dissociation), affinity constants, and concentration dependencies.

Furthermore, functional studies would be incredibly insightful. For electrophysiological modifications caused by FHL1, recordings from caffeine assays could be performed from cultured CHO ovarian cells transfected to express FHL1 and RYR1. Endogenous expression of either protein was barely, if at all, detectable from CHO cells [55, 160]. Considering the association of FHL1, ACTN1 and GSN with the cytoskeleton and cell migration, one approach would be wound assays with fibroblasts [161]. Numerous conditions could be tested, with siRNA mediated knockdown of various protein combinations. To determine if PDLIM1 participates in translocation of FHL1 during differentiation, co-IF studies can be performed from differentiated C2C12 skeletal muscles cells with siRNA mediated knockdown of PDLIM1. Also, co-localization studies are outstanding for FHL1 and PDLIM1 from skeletal muscle fibers.

Aside from studies revolving around these interactions, other studies involving FHL1 can be performed. For instance, FHL1 interacted with SMAD proteins to regulate TGF- $\beta$ -responsive gene transcription, independent of the TGF- $\beta$  signaling pathway (Figure 5). However, SMAD4 interacts with various transcription factors to regulate gene expression. Chromatin IP assays coupled to MS could be performed to identify the presence of additional transcription factors in the FHL1/SMAD protein complex. Alternatively, microarray analysis could be performed to identify additional gene targets of FHL1.

## REFERENCES

1. Lee, S.M., et al., *Chromosomal mapping, tissue distribution and cDNA sequence of four-and-a-half LIM domain protein 1 (FHL1)*. Gene, 1998. **216**(1): p. 163-70.
2. Morgan, M.J. and A.J. Madgwick, *The LIM proteins FHL1 and FHL3 are expressed differently in skeletal muscle*. Biochem Biophys Res Commun, 1999. **255**(2): p. 245-50.
3. Newman, A.P., et al., *The lin-11 LIM domain transcription factor is necessary for morphogenesis of C. elegans uterine cells*. Development, 1999. **126**(23): p. 5319-26.
4. Gupta, B.P., M. Wang, and P.W. Sternberg, *The C. elegans LIM homeobox gene lin-11 specifies multiple cell fates during vulval development*. Development, 2003. **130**(12): p. 2589-601.
5. Pfaff, S.L., et al., *Requirement for LIM homeobox gene Isll in motor neuron generation reveals a motor neuron-dependent step in interneuron differentiation*. Cell, 1996. **84**(2): p. 309-20.
6. Way, J.C. and M. Chalfie, *mec-3, a homeobox-containing gene that specifies differentiation of the touch receptor neurons in C. elegans*. Cell, 1988. **54**(1): p. 5-16.
7. Morgan, M.J., et al., *The developmental regulation of a novel muscle LIM-protein*. Biochem Biophys Res Commun, 1995. **212**(3): p. 840-6.
8. Morgan, M.J. and A.J. Madgwick, *Slim defines a novel family of LIM-proteins expressed in skeletal muscle*. Biochem Biophys Res Commun, 1996. **225**(2): p. 632-8.
9. Kadmas, J.L. and M.C. Beckerle, *The LIM domain: from the cytoskeleton to the nucleus*. Nat Rev Mol Cell Biol, 2004. **5**(11): p. 920-31.
10. Zheng, Q. and Y. Zhao, *The diverse biofunctions of LIM domain proteins: determined by subcellular localization and protein-protein interaction*. Biol Cell, 2007. **99**(9): p. 489-502.
11. Brown, S., et al., *Characterization of two isoforms of the skeletal muscle LIM protein 1, SLIM1. Localization of SLIM1 at focal adhesions and the isoform slimmer in the nucleus of myoblasts and cytoplasm of myotubes suggests distinct roles in the cytoskeleton and in nuclear-cytoplasmic communication*. J Biol Chem, 1999. **274**(38): p. 27083-91.
12. Labouesse, M. and E. Georges-Labouesse, *Cell adhesion: parallels between vertebrate and invertebrate focal adhesions*. Curr Biol, 2003. **13**(13): p. R528-30.
13. Pomies, P., H.A. Louis, and M.C. Beckerle, *CRP1, a LIM domain protein implicated in muscle differentiation, interacts with alpha-actinin*. J Cell Biol, 1997. **139**(1): p. 157-68.
14. Schmeichel, K.L. and M.C. Beckerle, *LIM domains of cysteine-rich protein 1 (CRP1) are essential for its zyxin-binding function*. Biochem J, 1998. **331** ( Pt 3): p. 885-92.
15. Chang, D.F., et al., *Cysteine-rich LIM-only proteins CRP1 and CRP2 are potent smooth muscle differentiation cofactors*. Dev Cell, 2003. **4**(1): p. 107-18.
16. Chan, K.K., et al., *Molecular cloning and characterization of FHL2, a novel LIM domain protein preferentially expressed in human heart*. Gene, 1998. **210**(2): p. 345-50.
17. Morgan, M.J. and S.A. Whawell, *The structure of the human LIM protein ACT gene and its expression in tumor cell lines*. Biochem Biophys Res Commun, 2000. **273**(2): p. 776-83.
18. Johannessen, M., et al., *The multifunctional roles of the four-and-a-half-LIM only protein FHL2*. Cell Mol Life Sci, 2006. **63**(3): p. 268-84.
19. Greene, W.K., et al., *Genomic structure, tissue expression and chromosomal location of the LIM-only gene, SLIM1*. Gene, 1999. **232**(2): p. 203-7.

20. Fimia, G.M., D. De Cesare, and P. Sassone-Corsi, *A family of LIM-only transcriptional coactivators: tissue-specific expression and selective activation of CREB and CREM*. Mol Cell Biol, 2000. **20**(22): p. 8613-22.
21. Morgan, M.J. and A.J. Madgwick, *The fourth member of the FHL family of LIM proteins is expressed exclusively in the testis*. Biochem Biophys Res Commun, 1999. **255**(2): p. 251-5.
22. Kleiber, K., K. Strebhardt, and B.T. Martin, *The biological relevance of FHL2 in tumour cells and its role as a putative cancer target*. Anticancer Res, 2007. **27**(1A): p. 55-61.
23. Chu, P.H., et al., *Expression patterns of FHL/SLIM family members suggest important functional roles in skeletal muscle and cardiovascular system*. Mech Dev, 2000. **95**(1-2): p. 259-65.
24. Kong, Y., et al., *Cardiac-specific LIM protein FHL2 modifies the hypertrophic response to beta-adrenergic stimulation*. Circulation, 2001. **103**(22): p. 2731-8.
25. Chu, P.H., et al., *FHL2 (SLIM3) is not essential for cardiac development and function*. Mol Cell Biol, 2000. **20**(20): p. 7460-2.
26. Purcell, N.H., et al., *Extracellular signal-regulated kinase 2 interacts with and is negatively regulated by the LIM-only protein FHL2 in cardiomyocytes*. Mol Cell Biol, 2004. **24**(3): p. 1081-95.
27. Krishnamurthy, G., et al., *Developmental evolution of the delayed rectifier current IKs in canine heart appears dependent on the beta subunit minK*. Heart Rhythm, 2004. **1**(6): p. 704-11.
28. Bovill, E., et al., *Reduction of four-and-a-half LIM-protein 2 expression occurs in human left ventricular failure and leads to altered localization and reduced activity of metabolic enzymes*. J Thorac Cardiovasc Surg, 2009. **137**(4): p. 853-61.
29. Arimura, T., et al., *Structural analysis of four and half LIM protein-2 in dilated cardiomyopathy*. Biochem Biophys Res Commun, 2007. **357**(1): p. 162-7.
30. Neuman, N.A., et al., *The four-and-a-half LIM domain protein 2 regulates vascular smooth muscle phenotype and vascular tone*. J Biol Chem, 2009. **284**(19): p. 13202-12.
31. Philippar, U., et al., *The SRF target gene Fhl2 antagonizes RhoA/MAL-dependent activation of SRF*. Mol Cell, 2004. **16**(6): p. 867-80.
32. Hinson, J.S., et al., *Regulation of myocardin factor protein stability by the LIM-only protein FHL2*. Am J Physiol Heart Circ Physiol, 2008. **295**(3): p. H1067-H1075.
33. Li, H.Y., et al., *Protein-protein interaction of FHL3 with FHL2 and visualization of their interaction by green fluorescent proteins (GFP) two-fusion fluorescence resonance energy transfer (FRET)*. J Cell Biochem, 2001. **80**(3): p. 293-303.
34. Coghill, I.D., et al., *FHL3 is an actin-binding protein that regulates alpha-actinin-mediated actin bundling: FHL3 localizes to actin stress fibers and enhances cell spreading and stress fiber disassembly*. J Biol Chem, 2003. **278**(26): p. 24139-52.
35. Cottle, D.L., et al., *FHL3 binds MyoD and negatively regulates myotube formation*. J Cell Sci, 2007. **120**(Pt 8): p. 1423-35.
36. Meeson, A.P., et al., *Sox15 and Fhl3 transcriptionally coactivate Foxk1 and regulate myogenic progenitor cells*. Embo J, 2007. **26**(7): p. 1902-12.
37. Turner, J., et al., *The LIM protein FHL3 binds basic Kruppel-like factor/Kruppel-like factor 3 and its co-repressor C-terminal-binding protein 2*. J Biol Chem, 2003. **278**(15): p. 12786-95.
38. Takahashi, K., C. Matsumoto, and C. Ra, *FHL3 negatively regulates human high-affinity IgE receptor beta-chain gene expression by acting as a transcriptional co-repressor of MZF-1*. Biochem J, 2005. **386**(Pt 1): p. 191-200.

39. Fimia, G.M., D. De Cesare, and P. Sassone-Corsi, *CBP-independent activation of CREM and CREB by the LIM-only protein ACT*. Nature, 1999. **398**(6723): p. 165-9.
40. Fimia, G.M., et al., *Transcriptional cascades during spermatogenesis: pivotal role of CREM and ACT*. Mol Cell Endocrinol, 2001. **179**(1-2): p. 17-23.
41. De Cesare, D., G.M. Fimia, and P. Sassone-Corsi, *Signaling routes to CREM and CREB: plasticity in transcriptional activation*. Trends Biochem Sci, 1999. **24**(7): p. 281-5.
42. Taniguchi, Y., et al., *LIM protein KyoT2 negatively regulates transcription by association with the RBP-J DNA-binding protein*. Mol Cell Biol, 1998. **18**(1): p. 644-54.
43. Lee, S.M., et al., *Characterization of a brain-specific nuclear LIM domain protein (FHL1B) which is an alternatively spliced variant of FHL1*. Gene, 1999. **237**(1): p. 253-63.
44. Ng, E.K., et al., *Characterization of tissue-specific LIM domain protein (FHL1C) which is an alternatively spliced isoform of a human LIM-only protein (FHL1)*. J Cell Biochem, 2001. **82**(1): p. 1-10.
45. Liang, L., et al., *KyoT3, an isoform of murine FHL1, associates with the transcription factor RBP-J and represses the RBP-J-mediated transactivation*. Biochim Biophys Acta, 2008. **1779**(12): p. 805-10.
46. High, F.A. and J.A. Epstein, *The multifaceted role of Notch in cardiac development and disease*. Nat Rev Genet, 2008. **9**(1): p. 49-61.
47. Qin, H., et al., *RING1 inhibits transactivation of RBP-J by Notch through interaction with LIM protein KyoT2*. Nucleic Acids Res, 2004. **32**(4): p. 1492-501.
48. Qin, H., et al., *The PcG protein HPC2 inhibits RBP-J-mediated transcription by interacting with LIM protein KyoT2*. FEBS Lett, 2005. **579**(5): p. 1220-6.
49. Wang, J., et al., *The transcriptional repression activity of KyoT2 on the Notch/RBP-J pathway is regulated by PIAS1-catalyzed SUMOylation*. J Mol Biol, 2007. **370**(1): p. 27-38.
50. Robinson, P.A., et al., *Skeletal muscle LIM protein 1 regulates integrin-mediated myoblast adhesion, spreading, and migration*. Am J Physiol Cell Physiol, 2003. **284**(3): p. C681-95.
51. McGrath, M.J., et al., *Skeletal muscle LIM protein 1 (SLIM1/FHL1) induces alpha 5 beta 1-integrin-dependent myocyte elongation*. Am J Physiol Cell Physiol, 2003. **285**(6): p. C1513-26.
52. McGrath, M.J., et al., *Four and a half LIM protein 1 binds myosin-binding protein C and regulates myosin filament formation and sarcomere assembly*. J Biol Chem, 2006. **281**(11): p. 7666-83.
53. Sheikh, F., et al., *An FHL1-containing complex within the cardiomyocyte sarcomere mediates hypertrophic biomechanical stress responses in mice*. J Clin Invest, 2008. **118**(12): p. 3870-80.
54. Cowling, B.S., et al., *Identification of FHL1 as a regulator of skeletal muscle mass: implications for human myopathy*. J Cell Biol, 2008. **183**(6): p. 1033-48.
55. Yang, Z., et al., *Four and a half LIM protein 1: a partner for KCNA5 in human atrium*. Cardiovasc Res, 2008. **78**(3): p. 449-57.
56. Bhattacharjee, A., et al., *Classification of human lung carcinomas by mRNA expression profiling reveals distinct adenocarcinoma subclasses*. Proc Natl Acad Sci U S A, 2001. **98**(24): p. 13790-5.
57. Jiang, F., et al., *Genomic profiles in stage I primary non small cell lung cancer using comparative genomic hybridization analysis of cDNA microarrays*. Neoplasia, 2004. **6**(5): p. 623-35.

58. Fryknas, M., et al., *Molecular markers for discrimination of benign and malignant follicular thyroid tumors*. *Tumour Biol*, 2006. **27**(4): p. 211-20.
59. Shen, Y., et al., *SRC uses Cas to suppress Fhl1 in order to promote nonanchored growth and migration of tumor cells*. *Cancer Res*, 2006. **66**(3): p. 1543-52.
60. Sakashita, K., et al., *Clinical significance of loss of Fhl1 expression in human gastric cancer*. *Ann Surg Oncol*, 2008. **15**(8): p. 2293-300.
61. Finley, D.J., et al., *Molecular profiling distinguishes papillary carcinoma from benign thyroid nodules*. *J Clin Endocrinol Metab*, 2004. **89**(7): p. 3214-23.
62. Li, X., et al., *Coordinate suppression of Sdpr and Fhl1 expression in tumors of the breast, kidney, and prostate*. *Cancer Sci*, 2008. **99**(7): p. 1326-33.
63. Ding, L., et al., *Human four-and-a-half LIM family members suppress tumor cell growth through a TGF-beta-like signaling pathway*. *J Clin Invest*, 2009. **119**(2): p. 349-61.
64. Quinzii, C.M., et al., *X-linked dominant scapulooperoneal myopathy is due to a mutation in the gene encoding four-and-a-half-LIM protein 1*. *Am J Hum Genet*, 2008. **82**(1): p. 208-13.
65. Windpassinger, C., et al., *An X-linked myopathy with postural muscle atrophy and generalized hypertrophy, termed XMPMA, is caused by mutations in FHL1*. *Am J Hum Genet*, 2008. **82**(1): p. 88-99.
66. Schessl, J., et al., *Proteomic identification of FHL1 as the protein mutated in human reducing body myopathy*. *J Clin Invest*, 2008. **118**(3): p. 904-12.
67. Schessl, J., et al., *Clinical, histological and genetic characterization of reducing body myopathy caused by mutations in FHL1*. *Brain*, 2009. **132**(Pt 2): p. 452-64.
68. Shalaby, S., et al., *Novel FHL1 mutations in fatal and benign reducing body myopathy*. *Neurology*, 2009. **72**(4): p. 375-6.
69. Shalaby, S., et al., *Rigid spine syndrome caused by a novel mutation in four-and-a-half LIM domain 1 gene (FHL1)*. *Neuromuscul Disord*, 2008. **18**(12): p. 959-61.
70. Bauer, A. and B. Kuster, *Affinity purification-mass spectrometry. Powerful tools for the characterization of protein complexes*. *Eur J Biochem*, 2003. **270**(4): p. 570-8.
71. Zhu, H., M. Bilgin, and M. Snyder, *Proteomics*. *Annu Rev Biochem*, 2003. **72**: p. 783-812.
72. Guan, H. and E. Kiss-Toth, *Advanced technologies for studies on protein interactomes*. *Adv Biochem Eng Biotechnol*, 2008. **110**: p. 1-24.
73. Ewing, R.M., et al., *Large-scale mapping of human protein-protein interactions by mass spectrometry*. *Mol Syst Biol*, 2007. **3**: p. 89.
74. Lange, S., et al., *Subcellular targeting of metabolic enzymes to titin in heart muscle may be mediated by DRAL/FHL-2*. *J Cell Sci*, 2002. **115**(Pt 24): p. 4925-36.
75. Kwapiszewska, G., et al., *Fhl-1, a new key protein in pulmonary hypertension*. *Circulation*, 2008. **118**(11): p. 1183-94.
76. Foster, L.J., et al., *Insulin-dependent interactions of proteins with GLUT4 revealed through stable isotope labeling by amino acids in cell culture (SILAC)*. *J Proteome Res*, 2006. **5**(1): p. 64-75.
77. Koegl, M. and P. Uetz, *Improving yeast two-hybrid screening systems*. *Brief Funct Genomic Proteomic*, 2007. **6**(4): p. 302-12.
78. Goehler, H., et al., *A protein interaction network links GIT1, an enhancer of huntingtin aggregation, to Huntington's disease*. *Mol Cell*, 2004. **15**(6): p. 853-65.
79. Hall, D.A., J. Ptacek, and M. Snyder, *Protein microarray technology*. *Mech Ageing Dev*, 2007. **128**(1): p. 161-7.
80. Ramachandran, N., et al., *Self-assembling protein microarrays*. *Science*, 2004. **305**(5680): p. 86-90.

81. Rigaut, G., et al., *A generic protein purification method for protein complex characterization and proteome exploration*. Nat Biotechnol, 1999. **17**(10): p. 1030-2.
82. Abu-Farha, M., F. Elisma, and D. Figeys, *Identification of protein-protein interactions by mass spectrometry coupled techniques*. Adv Biochem Eng Biotechnol, 2008. **110**: p. 67-80.
83. Giannone, R.J., et al., *Dual-tagging system for the affinity purification of mammalian protein complexes*. Biotechniques, 2007. **43**(3): p. 296, 298, 300 passim.
84. Yang, P., H.M. Sampson, and H.M. Krause, *A modified tandem affinity purification strategy identifies cofactors of the Drosophila nuclear receptor dHNF4*. Proteomics, 2006. **6**(3): p. 927-35.
85. Chang, I.F., et al., *Proteomic profiling of tandem affinity purified 14-3-3 protein complexes in Arabidopsis thaliana*. Proteomics, 2009. **9**(11): p. 2967-85.
86. Drakas, R., M. Prisco, and R. Baserga, *A modified tandem affinity purification tag technique for the purification of protein complexes in mammalian cells*. Proteomics, 2005. **5**(1): p. 132-7.
87. Burckstummer, T., et al., *An efficient tandem affinity purification procedure for interaction proteomics in mammalian cells*. Nat Methods, 2006. **3**(12): p. 1013-9.
88. Rosamond, W., et al., *Heart disease and stroke statistics--2007 update: a report from the American Heart Association Statistics Committee and Stroke Statistics Subcommittee*. Circulation, 2007. **115**(5): p. e69-171.
89. Mosterd, A. and A.W. Hoes, *Clinical epidemiology of heart failure*. Heart, 2007. **93**(9): p. 1137-46.
90. Gupta, S., B. Das, and S. Sen, *Cardiac hypertrophy: mechanisms and therapeutic opportunities*. Antioxid Redox Signal, 2007. **9**(6): p. 623-52.
91. Heineke, J. and J.D. Molkentin, *Regulation of cardiac hypertrophy by intracellular signalling pathways*. Nat Rev Mol Cell Biol, 2006. **7**(8): p. 589-600.
92. Clerk, A., et al., *Signaling pathways mediating cardiac myocyte gene expression in physiological and stress responses*. J Cell Physiol, 2007. **212**(2): p. 311-22.
93. Molkentin, J.D. and G.W. Dorn, 2nd, *Cytoplasmic signaling pathways that regulate cardiac hypertrophy*. Annu Rev Physiol, 2001. **63**: p. 391-426.
94. Dostal, D.E., et al., *Molecular mechanisms of angiotensin II in modulating cardiac function: intracardiac effects and signal transduction pathways*. J Mol Cell Cardiol, 1997. **29**(11): p. 2893-902.
95. Struthers, A.D., *Pathophysiology of heart failure following myocardial infarction*. Heart, 2005. **91 Suppl 2**: p. ii14-6; discussion ii31, ii43-8.
96. Teerlink, J.R., *Reversal of left ventricular remodeling: role of the endothelin pathway*. J Card Fail, 2002. **8**(6 Suppl): p. S494-9.
97. Penna, C., et al., *Effect of endothelins on the cardiovascular system*. J Cardiovasc Med (Hagerstown), 2006. **7**(9): p. 645-52.
98. Hasper, D., et al., *Systemic inflammation in patients with heart failure*. Eur Heart J, 1998. **19**(5): p. 761-5.
99. Bozkurt, B., et al., *Pathophysiologically relevant concentrations of tumor necrosis factor-alpha promote progressive left ventricular dysfunction and remodeling in rats*. Circulation, 1998. **97**(14): p. 1382-91.
100. Janczewski, A.M., et al., *Morphological and functional changes in cardiac myocytes isolated from mice overexpressing TNF-alpha*. Am J Physiol Heart Circ Physiol, 2003. **284**(3): p. H960-9.

101. Oral, H., et al., *Myocardial proinflammatory cytokine expression and left ventricular remodeling in patients with chronic mitral regurgitation*. *Circulation*, 2003. **107**(6): p. 831-7.
102. Ventura-Clapier, R., A. Garnier, and V. Veksler, *Energy metabolism in heart failure*. *J Physiol*, 2004. **555**(Pt 1): p. 1-13.
103. Tomaselli, G.F. and E. Marban, *Electrophysiological remodeling in hypertrophy and heart failure*. *Cardiovasc Res*, 1999. **42**(2): p. 270-83.
104. Furukawa, T. and J. Kurokawa, *Potassium channel remodeling in cardiac hypertrophy*. *J Mol Cell Cardiol*, 2006. **41**(5): p. 753-61.
105. Hill, J.A., *Electrical remodeling in cardiac hypertrophy*. *Trends Cardiovasc Med*, 2003. **13**(8): p. 316-22.
106. MacLennan, D.H. and E.G. Kranias, *Phospholamban: a crucial regulator of cardiac contractility*. *Nat Rev Mol Cell Biol*, 2003. **4**(7): p. 566-77.
107. Marks, A.R., *Novel therapy for heart failure and exercise-induced ventricular tachycardia based on 'fixing' the leak in ryanodine receptors*. *Novartis Found Symp*, 2006. **274**: p. 132-47; discussion 147-55, 272-6.
108. Tada, M. and T. Toyofuku, *Molecular regulation of phospholamban function and expression*. *Trends Cardiovasc Med*, 1998. **8**(8): p. 330-40.
109. Minamisawa, S., et al., *Mutation of the phospholamban promoter associated with hypertrophic cardiomyopathy*. *Biochem Biophys Res Commun*, 2003. **304**(1): p. 1-4.
110. Haghighi, K., et al., *Human phospholamban null results in lethal dilated cardiomyopathy revealing a critical difference between mouse and human*. *J Clin Invest*, 2003. **111**(6): p. 869-76.
111. Haghighi, K., et al., *A mutation in the human phospholamban gene, deleting arginine 14, results in lethal, hereditary cardiomyopathy*. *Proc Natl Acad Sci U S A*, 2006. **103**(5): p. 1388-93.
112. Schmitt, J.P., et al., *Dilated cardiomyopathy and heart failure caused by a mutation in phospholamban*. *Science*, 2003. **299**(5611): p. 1410-3.
113. Gramolini, A.O., et al., *Comparative proteomics profiling of a phospholamban mutant mouse model of dilated cardiomyopathy reveals progressive intracellular stress responses*. *Mol Cell Proteomics*, 2008. **7**(3): p. 519-33.
114. Shevchenko, A., et al., *In-gel digestion for mass spectrometric characterization of proteins and proteomes*. *Nat Protoc*, 2006. **1**(6): p. 2856-60.
115. Gortzak-Uzan, L., et al., *A proteome resource of ovarian cancer ascites: integrated proteomic and bioinformatic analyses to identify putative biomarkers*. *J Proteome Res*, 2008. **7**(1): p. 339-51.
116. Sodek, K.L., et al., *Identification of pathways associated with invasive behavior by ovarian cancer cells using multidimensional protein identification technology (MudPIT)*. *Mol Biosyst*, 2008. **4**(7): p. 762-73.
117. Wu, Z.K., et al., *Revealing Disease Related Interactions by Correlation Analysis*. *Optimization and Systems Biology, Proceedings*, 2008. **9**: p. 341-349
- 405.
118. Brotto, M.A., et al., *Coupled expression of troponin T and troponin I isoforms in single skeletal muscle fibers correlates with contractility*. *Am J Physiol Cell Physiol*, 2006. **290**(2): p. C567-76.
119. Metzler, H., et al., *Perioperative myocardial cell injury: the role of troponins*. *Br J Anaesth*, 1997. **78**(4): p. 386-90.
120. Taylor, I.W., et al., *Dynamic modularity in protein interaction networks predicts breast cancer outcome*. *Nat Biotechnol*, 2009. **27**(2): p. 199-204.

121. Marks, A.R., *Ryanodine receptors/calcium release channels in heart failure and sudden cardiac death*. J Mol Cell Cardiol, 2001. **33**(4): p. 615-24.
122. Hartwig, J.H., K.A. Chambers, and T.P. Stossel, *Association of gelsolin with actin filaments and cell membranes of macrophages and platelets*. J Cell Biol, 1989. **108**(2): p. 467-79.
123. Takekura, H., B.E. Flucher, and C. Franzini-Armstrong, *Sequential docking, molecular differentiation, and positioning of T-Tubule/SR junctions in developing mouse skeletal muscle*. Dev Biol, 2001. **239**(2): p. 204-14.
124. Salanova, M., et al., *Ryanodine receptor type-1 (RyR1) expression and protein S-nitrosylation pattern in human soleus myofibres following bed rest and exercise countermeasure*. Histochem Cell Biol, 2008. **130**(1): p. 105-18.
125. Byrne, B., *Expression, purification, and crystallisation of membrane proteins*. Evolving Methods for Macromolecular Crystallography, 2007. **245**: p. 11-23
- 191.
126. Huq, M.D. and L.N. Wei, *Post-translational modification of nuclear co-repressor receptor-interacting protein 140 by acetylation*. Mol Cell Proteomics, 2005. **4**(7): p. 975-83.
127. Gaussin, V., et al., *Common genomic response in different mouse models of beta-adrenergic-induced cardiomyopathy*. Circulation, 2003. **108**(23): p. 2926-33.
128. Yang, J., et al., *Decreased SLIM1 expression and increased gelsolin expression in failing human hearts measured by high-density oligonucleotide arrays*. Circulation, 2000. **102**(25): p. 3046-52.
129. Hwang, D.M., et al., *A genome-based resource for molecular cardiovascular medicine: toward a compendium of cardiovascular genes*. Circulation, 1997. **96**(12): p. 4146-203.
130. Hwang, D.M., et al., *Identification of differentially expressed genes in cardiac hypertrophy by analysis of expressed sequence tags*. Genomics, 2000. **66**(1): p. 1-14.
131. Lim, D.S., R. Roberts, and A.J. Marian, *Expression profiling of cardiac genes in human hypertrophic cardiomyopathy: insight into the pathogenesis of phenotypes*. J Am Coll Cardiol, 2001. **38**(4): p. 1175-80.
132. Towbin, J.A. and N.E. Bowles, *The failing heart*. Nature, 2002. **415**(6868): p. 227-33.
133. Haddad, G.E., et al., *Human cardiac-specific cDNA array for idiopathic dilated cardiomyopathy: sex-related differences*. Physiol Genomics, 2008. **33**(2): p. 267-77.
134. Li, G.H., et al., *Gelsolin regulates cardiac remodeling after myocardial infarction through DNase I-mediated apoptosis*. Circ Res, 2009. **104**(7): p. 896-904.
135. Brillantes, A.M., et al., *Differences in cardiac calcium release channel (ryanodine receptor) expression in myocardium from patients with end-stage heart failure caused by ischemic versus dilated cardiomyopathy*. Circ Res, 1992. **71**(1): p. 18-26.
136. Go, L.O., et al., *Differential regulation of two types of intracellular calcium release channels during end-stage heart failure*. J Clin Invest, 1995. **95**(2): p. 888-94.
137. Sjoblom, B., A. Salmazo, and K. Djinojic-Carugo, *Alpha-actinin structure and regulation*. Cell Mol Life Sci, 2008. **65**(17): p. 2688-701.
138. Pellegrin, S. and H. Mellor, *Actin stress fibres*. J Cell Sci, 2007. **120**(Pt 20): p. 3491-9.
139. Craig, D.H., J. Zhang, and M.D. Basson, *Cytoskeletal signaling by way of alpha-actinin-1 mediates ERK1/2 activation by repetitive deformation in human Caco2 intestinal epithelial cells*. Am J Surg, 2007. **194**(5): p. 618-22.
140. Silacci, P., et al., *Gelsolin superfamily proteins: key regulators of cellular functions*. Cell Mol Life Sci, 2004. **61**(19-20): p. 2614-23.
141. Arora, P.D., P.A. Janmey, and C.A. McCulloch, *A role for gelsolin in stress fiber-dependent cell contraction*. Exp Cell Res, 1999. **250**(1): p. 155-67.

142. Chellaiah, M., et al., *Gelsolin deficiency blocks podosome assembly and produces increased bone mass and strength*. J Cell Biol, 2000. **148**(4): p. 665-78.
143. Lu, M., et al., *Delayed retraction of filopodia in gelsolin null mice*. J Cell Biol, 1997. **138**(6): p. 1279-87.
144. Gay, F., et al., *In colon carcinogenesis, the cytoskeletal protein gelsolin is down-regulated during the transition from adenoma to carcinoma*. Hum Pathol, 2008. **39**(10): p. 1420-30.
145. Ni, X.G., et al., *The ubiquitin-proteasome pathway mediates gelsolin protein downregulation in pancreatic cancer*. Mol Med, 2008. **14**(9-10): p. 582-9.
146. Walsh, N., et al., *Aldehyde dehydrogenase 1A1 and gelsolin identified as novel invasion-modulating factors in conditioned medium of pancreatic cancer cells*. J Proteomics, 2008. **71**(5): p. 561-71.
147. Liu, J., et al., *Concurrent down-regulation of Egr-1 and gelsolin in the majority of human breast cancer cells*. Cancer Genomics Proteomics, 2007. **4**(6): p. 377-85.
148. Bauer, K., et al., *Human CLP36, a PDZ-domain and LIM-domain protein, binds to alpha-actinin-1 and associates with actin filaments and stress fibers in activated platelets and endothelial cells*. Blood, 2000. **96**(13): p. 4236-45.
149. Vallenius, T., K. Luukko, and T.P. Makela, *CLP-36 PDZ-LIM protein associates with nonmuscle alpha-actinin-1 and alpha-actinin-4*. J Biol Chem, 2000. **275**(15): p. 11100-5.
150. Tamura, N., et al., *The PDZ-LIM protein CLP36 is required for actin stress fiber formation and focal adhesion assembly in BeWo cells*. Biochem Biophys Res Commun, 2007. **364**(3): p. 589-94.
151. Zhou, Q., et al., *Cypher, a striated muscle-restricted PDZ and LIM domain-containing protein, binds to alpha-actinin-2 and protein kinase C*. J Biol Chem, 1999. **274**(28): p. 19807-13.
152. Wu, R., et al., *Specificity of LIM domain interactions with receptor tyrosine kinases*. J Biol Chem, 1996. **271**(27): p. 15934-41.
153. Vallenius, T. and T.P. Makela, *Clik1: a novel kinase targeted to actin stress fibers by the CLP-36 PDZ-LIM protein*. J Cell Sci, 2002. **115**(Pt 10): p. 2067-73.
154. Arber, S. and P. Caroni, *Specificity of single LIM motifs in targeting and LIM/LIM interactions in situ*. Genes Dev, 1996. **10**(3): p. 289-300.
155. Yano, M., *Ryanodine receptor as a new therapeutic target of heart failure and lethal arrhythmia*. Circ J, 2008. **72**(4): p. 509-14.
156. Bourguignon, L.Y., et al., *Ryanodine receptor-ankyrin interaction regulates internal Ca<sup>2+</sup> release in mouse T-lymphoma cells*. J Biol Chem, 1995. **270**(30): p. 17917-22.
157. Bose, D.D. and D.W. Thomas, *The actin cytoskeleton differentially regulates NG115-401L cell ryanodine receptor and inositol 1,4,5-trisphosphate receptor induced calcium signaling pathways*. Biochem Biophys Res Commun, 2009. **379**(2): p. 594-9.
158. Lin, J., et al., *The four and a half LIM domain protein 2 interacts with and regulates the HERG channel*. Febs J, 2008. **275**(18): p. 4531-9.
159. Kupersmidt, S., et al., *Cardiac-enriched LIM domain protein fh12 is required to generate I(Ks) in a heterologous system*. Cardiovasc Res, 2002. **56**(1): p. 93-103.
160. Bhat, M.B., et al., *Caffeine-induced release of intracellular Ca<sup>2+</sup> from Chinese hamster ovary cells expressing skeletal muscle ryanodine receptor. Effects on full-length and carboxyl-terminal portion of Ca<sup>2+</sup> release channels*. J Gen Physiol, 1997. **110**(6): p. 749-62.
161. Rodriguez, L.G., X. Wu, and J.L. Guan, *Wound-healing assay*. Methods Mol Biol, 2005. **294**: p. 23-9.